Laser Tweezers for Moving Live Dissociated Neurons

Thesis by

Gang Chow

In Partial Fulfillment of the Requirements
for the Degree of

Doctor of Philosophy

California Institute of Technology

Pasadena, California

2008

(Defended October 17, 2007)

Acknowledgements

I would like to thank my wife, Pauline, for her support over the years. Also, I would like to thank my parents, and my brother, Dr. Benjamin Chow, for his encouragement and lead.

I would like to thank my advisor, Professor Jerry Pine, for his advice, guidance, and support over the years. Also, thanks to Professor Guruswami Ravichandran and Professor Mory Gharib for their help and advice. Thanks to my mentor, Dr. Harvey Kasdan, for spending many hours going over and correcting my thesis. Also, I would like to thank Angela Tooker for fabricating and providing the neurochips, Sheri Mckinney for preparing the neurons, and John Ericson for his wonderful company. Finally, I would like to thank Linda Scott for all her administrative support.

Abstract

A laser tweezers system for transporting dissociated neurons into small "cages" on a culture dish was constructed, and it was studied extensively.

The system consists of an inverted microscope, a 1064 nm or 980 nm laser module, a beam expander, a motorized mechanical stage, a CCD camera, and steering mirrors. A laser beam is generated by the IR laser module, and the beam is expanded by the beam expander to match the size of the back aperture of the objective. The beam is then steered into the objective where it is focused to a point. The system uses this single, tightly focused laser beam to trap a neuron. Once a neuron is trapped and lifted, the mechanical stage is moved to locate the neuron above its destination. The system will know the location of the neurocages and will automatically move neurons to their destination.

Newly dissociated neurons will attach to most substrate surfaces eagerly, and the lifting of a neuron is impossible when it is attached to the surface. Many possible surfaces were investigated, and it was discovered that the surface can best be made "non-sticky" for more than an hour, by coating the surface with Poly-2-hydroxyethyl methacrylate (PolyHEMA). The neural survival at different laser intensities, exposure times, and wavelengths were studied. The results show that neural survival depends strongly on laser wavelengths, and a 980 nm laser is less damaging than a 1064 nm laser.

For 980 nm, perfect survival after irradiation is independent of laser power up to our maximum of 130 mW for exposure time up to 4 minutes. At 17 mW, almost all neurons can be lifted off a PolyHEMA substrate. The maximum speed for moving a neuron through the medium at different laser intensities was studied, and was 250 um/s at 100 mW for 980 nm. The studies have shown that a laser tweezers system is suitable for transporting live dissociated neurons over millimeter distance in less than a minute. The neural survival in neurocages on glass substrate was then studied. The survival and growth over time for neurons loaded into cages was found to be no different than for that of a control culture.

Table of Contents

List of Figures

List of Tables

CHAPTER 1
Introduction

The central nervous system is a complex network of more than 100 billion neurons—the basic functional unit of the nervous system—each with an average of 1,000 synaptic connections to other neurons in the system, and all with the ability to communicate with each other by using electrical signals. Incoming signals enter the neuron through synapses on neuronal dendrites, and output signals leave the neuron through a single axon which branches out to other parts of the nervous system. Neurons are arranged into differently organized neural networks that perform various functions of the nervous system. Thus, neural networks and their pattern of connections have undergone extensive research in an attempt to try to understand them. Unfortunately, it is very difficult to study these networks *in vivo* because of their complexity and inaccessibility in living animals. Therefore, many of these studies have been done *in vitro*.

Multi-electrode arrays (MEAs) are one of the standard electrophysiological techniques used to study electrical interactions among neurons in an *in vitro* culture. Unlike the traditional patch clamp technique, MEAs can record from and stimulate many neurons simultaneously, and they are well-suited for long-term experiments because they are non-destructive. Most MEAs are two-dimensional electrode arrays on glass substrates on which a cultured neural network can grow (Thomas, 1972; Pine, 1980;

Meister, 1994; Jimbo, 1996; Gross, 1997; Morefield, 2000). MEAs have many electrodes that are in electrical contact with a cultured neural network. MEAs can be used to record cell responses when external stimuli are applied, or to record activity of the network. Recent experiments in electrophysiology using MEAs have made significant contributions to our understanding of brain functions (Taketani et al., 2006).

Our lab is interested in the development and plasticity of small neural networks. We want to study the network connectivity at a given time by stimulating one neuron in a network and observing the responses of all the others. However, traditional MEAs are not suitable for our research. In an MEA, an electrode can stimulate or record from many nearby neurons; therefore, it lacks the one-to-one correspondence between neurons and electrodes that we are looking for. To cope with this problem, a "neurochip" was developed (Maher, 1999; He, 2003; Meng, 2003).

Neurocages are micromachined structures that are used to trap neurons in close proximity to extracellular electrodes. The neurocages shown in schematically in green in Figure 1.1, trap a neuron above an extracellular electrode. The cage electrode can be utilized to stimulate or record from a neuron in a network non-destructively. The neuron is loaded into the cage through the hole at the top and adheres to the substrate. The neurites grow out through six tunnels that are too small for neurons to escape through. The cartoon in Figure 1.1 shows that the neurite of one neuron forms a synapse with the neurite of an adjacent neuron. A scanning electron micrograph of a neurocage is shown in Figure 1.2. It consists of a chimney, five anchors, six tunnels and an electrode. The cage is fixed onto the glass substrate by five inverted mushroom shaped anchors. A layer of Parylene-C is used to insulate the electrodes and the electrode leads. The current

neurochip design has an array of sixteen cages, on a silicon substrate, shown in Figure 1.3. The neurocages are 110 um apart and allow neurons to grow neurites, connect, and form a neural network. Jon Erickson in our lab has successfully moved dissociated neurons into neurocages by lifting and carrying them with a pipette. Loaded neurons have exhibited normal growth (Figure 1.4), thus proving that these neurocages are bio-compatible. More importantly, Jon is able to stimulate and record from these networks. Hence, the neurochip can be a useful tool for studying the detailed behaviors of individual neurons, connectivity, and plasticity in a cultured network.

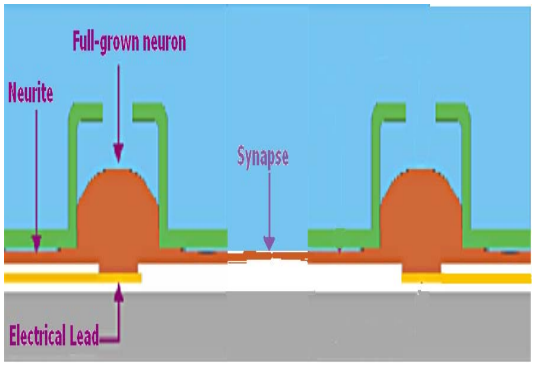

Figure 1.1. Concept of neurocages

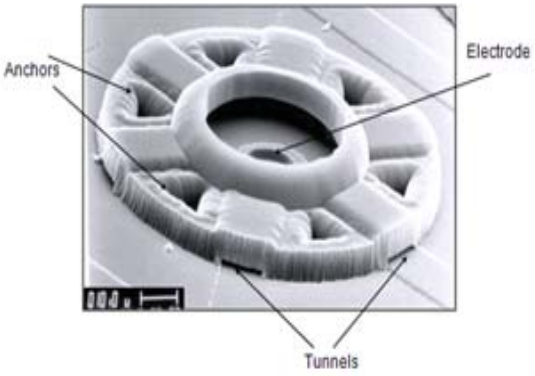

Figure 1.2 Neurocage by SEM

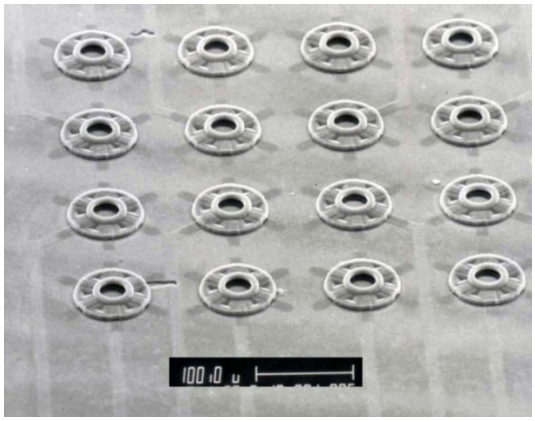

Figure 1.3 4 x 4 array neurocages on silicon substrate

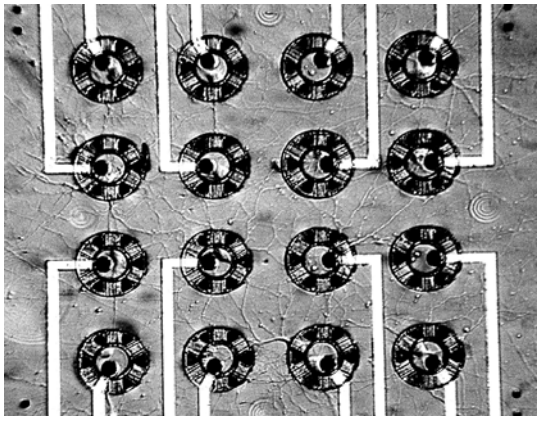

Figure 1.4 10-day-old culture

Loading dissociated neurons into cages with a micropipette is time consuming and labor intensive. The average loading time for each neuron is about three minutes. In addition, larger arrays of neurocages need to be fabricated for the study of larger networks, and with an increased numbers of neurocages loading dissociated neurons manually becomes impractical. To utilize a more effective method of moving live dissociated neurons, we have developed a system of optical tweezers that carry neurons to the parylene cages and drop them in.

This thesis describes the development and characterization of our computer-automated optical tweezers system. Although optical tweezers have been used before to manipulate various cell types, manipulation of live dissociated brain cells has never been done. This research extensively explores the survival of irradiated neurons using different trapping parameters, since laser-induced damage to neurons must be avoided.

The use of laser tweezers requires the neurocages to be anchored on an optically transparent substrate. A trial neurochip with a glass substrate and 60 cages has been designed and fabricated here. Neurons have been successfully moved into these cages with the laser tweezers. Finally, to determine the capability of this neurochip to support the growth of a neural network, the cell survival in these cages was investigated.

1.1 Goals

This work has three main parts: the first part includes the design, construction, and characterization of the laser tweezers system, described in Chapter 3. The second part

reports on studies of photodamage of hippocampal neurons due to laser exposure, described in Chapter 4. Finally, the design, construction, and testing of neurocages on a glass substrate are described in Chapter 5.

The laser tweezers system uses a single, tightly focused IR beam to trap and lift live neurons, and moves them in three dimensions above a culture substrate. Once a neuron is trapped and lifted from a non-adhesive surface, a computer-controlled mechanical stage is moved to locate the neuron above its destination. The system will know the location of the neurocages and will automatically move neurons to their destination. The success of lifting a neuron depends strongly on the substrate surface. Newly dissociated neurons will attach to most substrate surfaces eagerly, and, once attached, lifting a neuron is impossible. After studying a variety of surfaces, it was discovered that a non-adherent surface can be created and maintained for more than an hour by treating the surface with four layers of PolyHEMA.

The major limitation of optical tweezers is the potential photodamage caused by the highly focused laser beam. One can minimize the damage by properly selecting a trapping laser with a wavelength in the near infrared region. Photodamage to CHO cells, C. elegans, and E. coli bacteria after optical trapping has been studied using different laser powers, laser wavelengths, and exposure times (Liang, 1996; Leitz, 2002; Neuman, 1999). These results can be used as a general guide when selecting optical trapping parameters; however, neurons may respond differently. The goal here was to determine the suitable intensity and exposure time for moving neurons quickly and non-destructively at each of two wavelengths (980 nm and 1064 nm). Cell survival dependencies on intensity, exposure time, and wavelength were determined and

compared to published experiments using non-neural cells. These are the first such measurements with neurons.

The laser tweezers system uses an inverted microscope in which the focused IR beam goes up through the bottom of a culture dish for trapping. Therefore, it is necessary for neurocages to be constructed on a glass substrate. The main criteria for the neurocage design were: few or no obstacles on the light pathway, and support of development of neural networks. We collaborated with Angela Tooker of the Yu-Chong Tai lab, who fabricates neurocage structures on glass. We have demonstrated that dissociated neurons can be moved with optical tweezers into the these neurocages, and more importantly, that afterwards neurons grow normally on these neurochips.

1.2 Summary of Results

The laser tweezers system has proven to be user-friendly. A person can search and trap neurons by simply moving the stage with a joystick. The system knows the cage locations and automatically brings trapped neuron to its destination. Both 980 nm and 1064 nm can be used for moving live dissociated neurons non-destructively, however, the survival studies show that 980 nm is a much better candidate than 1064 nm (Chapter 4) because a cell can be moved quickly owing to the larger non-damaging power available with the 980 nm system.

More than 200 neurons were successfully moved into neurocages on glass with the laser tweezers system, and most of them were still alive after three days (Chapter 5).

The survival possibility of moved and control neurons was not statistically different. All surviving cells exhibited normal growth and had at least two or three processes growing outside the cage. The average loading time per cage was about 1.5 minutes and average speed was about 75 um/s.

In summary, the laser tweezers proved to be an excellent tool for loading live dissociated neurons easily, undamaged, and precisely. After loading, many caged neurons were kept alive for more than a week. Thus, planned neurochips with 60 cages on glass can be used to study larger neural networks in long-term experiments.

1.3 Thesis Outline

Chapter 2 provides the background for this study. It begins with a brief history of optical tweezers, and then describes the physics behind the technology. Basic trapping forces and the calculations and measurement of these forces are described in detail. Trapping criteria and a typical setup for an optical tweezers system are described. Finally, biological applications of optical tweezers are briefly reviewed.

Chapter 3 describes the design, construction, and characterizations of both 980 nm and 1064 nm optical tweezers systems. It first provides an overview for both systems and then describes each component in detail. Alignment of the beam for each system is then discussed and, finally, characterization of each system is described in detail, including beam profile measurement, power output measurement, microscope objective

IR transmission measurement, and maximum neuron speed measurement as a function of power level.

Chapter 4 describes the experiments that were performed to investigate cell survival under different trapping conditions and the results. It first describes the experimental methods and apparatus. It then describes the experiments for finding the non-sticky substrate in detail, because it is essential for successful trapping, and concludes by describing intensity, temporal, and wavelength dependence of photo-damage for both stationary and moved cells.

Chapter 5 first describes the design and construction of neuro-cages on glass substrates. It then describes preparations and procedures for moving neurons into the cages and finally, it describes cell survival in neuro-cages and the survival results.

CHAPTER 2
Review of Optical Tweezers

A laser tweezers system uses a highly focused IR beam to trap small particles in three dimensions. The technique is based on the forces of radiation pressure, which are generated from refraction of the beam by a particle with index of refraction greater than the medium in which it is suspended. The main attractions of a laser tweezers are: they are non-invasive, they provide the ability to control microscopic particles precisely, and they are easy to set up with a single microscope that can be used to trap and view a particle simultaneously. In addition, they are versatile and can be scaled from one trap to many by multiplexing the laser to trap many particles simultaneously. With continual technology advances in the laser industry, high power IR lasers are becoming more available and less expensive. Laser tweezers have become a standard tool for manipulating and studying a variety of biological specimens such as viruses, single living cells, and even DNA. This chapter reviews the technique and principles of optical trapping to provide background information for the reader, and describes its history, usage, and significance in biological science.

2.1 History

2.1.1 Birth of Optical Trapping

In 1969, A. Ashkin (Ashkin, 1970) at Bell Labs accidentally discovered that a sample was sticking to the center of a beam and was following it during studies of radiation pressure on a small particle. His continued investigation of this phenomenon revealed that two force components (gradient and scattering) originate from radiation pressure (Figure 2.1). The gradient force generated by the light intensity gradient pulls the sample towards the highest intensity region. The scattering force pushes particle away from the beam center along the direction of the incident light. Using the properties of these two basic force components, Ashkin constructed the first optical trap.

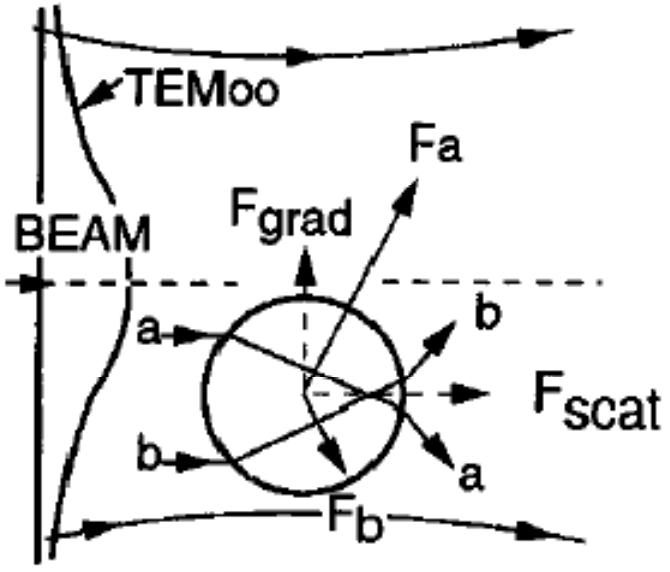

Figure 2.1 Origin of F_{scat} and F_{grad} for high index sphere displaced from TEM00 beam axis (from Askin, 1970)

2.1.2 Early Optical Trap Design

The first stable, three-dimensional optical trap used two counter-propagating Gaussian beams (2-beam trap) to balance forces acting on a particle (Ashkin, 1978). The particle is trapped between two beams at an equilibrium point by the opposing scattering forces of these two beams, and the radial displacement is countered by the gradient force of both beams (Figure 2.2). The particle can be moved forward in the direction of one beam and guided by this beam by reducing the intensity of other beam.

The optical levitation trap in air was designed and demonstrated earlier (Ashkin, 1971). A single beam is used to levitate and trap the particle at a point where the upward scattering force is balanced by gravity (Figure 2.3). The particle is confined radially as well, due to the gradient force. The particle can be moved by simply moving the beam around.

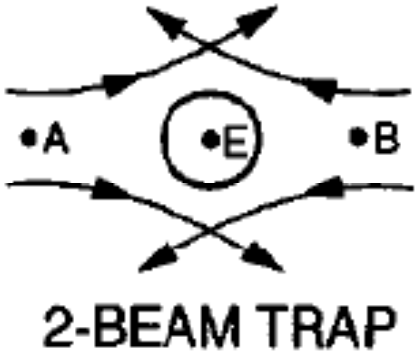

Figure 2.2 Geometry of 2-beam trap (Ashkin, 1997)

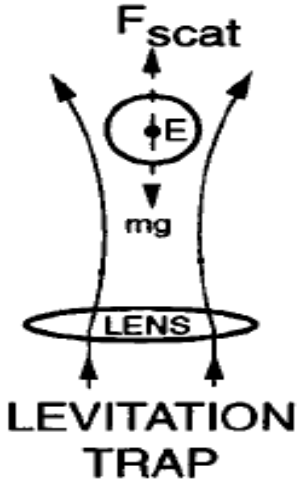

Figure 2.3 Geometry of levitation trap (Ashkin, 1997)

In 1986, the first single-beam trap was demonstrated and reported by Ashkin and Chu (Ashkin, 1986); who showed that a tightly focused single beam can be used to trap particles stably in three-dimensions. The trapping results from the opposite pointing of the longitudinal gradient force component, with respect to the direction of the incident light which is greater than the scattering force. The single-beam trap is used for the research in this paper.

2.1.3 Optical Trapping in Biology

In 1987, Ashkin discovered that an optical trap could be used for moving biological specimens without inflicting any discernable damage to the cells (Ashkin, 1987). He observed that E coli and yeast cells were able to reproduce while trapped, which indicated that the cells were not damaged by the IR beam (1064 nm). In the same study, human blood cells and plant cells showed no apparent damage from trapping. He also successfully manipulated organelles and particles inside a plant cell without damaging the cell membrane. Since then, optical tweezers have been used extensively in many biological applications.

2.2 Theory

2.2.1 The Force Exerted by Light

The optical trap is based on transfer of momentum from the photons of the beam to the particle being trapped. This transfer of momentum is the result of the refraction of light at the boundary separating the object and medium. By conservation of momentum, an equal and opposite force is exerted on the object. For a tightly focused Gaussian beam, the exerted net force pushes the object towards the beam focus where the intensity of light is greatest. The outcome of this interaction strongly depends on the ratio between the refractive index of the object and the surrounding medium, and in general trapping requires that the refractive index of the object to be higher than that of its surrounding medium.

Figure 3.4 shows an idealized spherical neuron placed at the right side of the incident beam axis and below the beam focus. Here one can use simple ray analysis to describe forces exerted on the neuron. Force F_1 is generated by the momentum change of the thicker ray (higher intensity), and force F_2 is generated by momentum change of the thinner ray (lower intensity). By combining F_1 and F_2, a resultant force, $F_{net}=F_1 + F_2$, is formed which pushes the neuron towards the beam focal point.

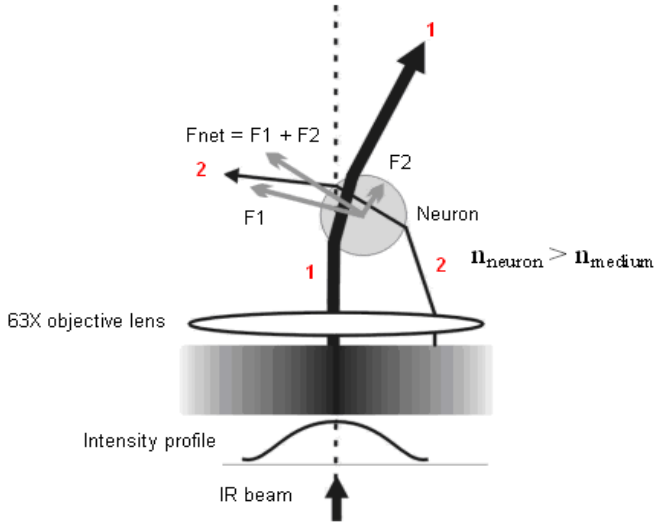

Figure 2.4 The cartoon shows the basic forces that trap a neuron to the beam focus.

For a stable trap, the longitudinal component of the gradient force has to be greater than the scattering force. The scattering force results from the reflection of light by the particle and pushes it along the direction of light propagation. A gradient force generated from the refraction of light pushed the particle along the direction of the light intensity gradient toward the focus. A steep intensity gradient is needed to longitudinally trap effectively. For this reason a high NA objective is used for trapping. Note that the trapping is ineffective if n_{medium} is greater than n_{neuron}, because this would result in a net force that pushes the neuron away from the beam's focal point. This describes the physics behind optical trapping for particles that are much larger than the beam waist (Mie-regime, $r>>\lambda$). The neurons used in this research have an average radius of 5 um which is greater than the laser wavelength. The physics is different for particles that are much smaller than the wavelength (Rayleigh-regime, $r<<\lambda$) and will not described here.

2.2.2 Force Calculation and Measurement

Ashkin computed the optical forces for the Mie regime, assuming that all rays are focused to a point and diffractive effects are negligible (Ashkin, 1992). The total light beam can be decomposed into individual rays, each with appropriate intensity and direction. The forces due to a single ray of power P hitting a dielectric sphere at an angle of incidence θ are given by

$$F_Z = F_s = \frac{n_m P}{c}\left\{1 + R\cos 2\theta - \frac{T^2[\cos(2\theta - 2r) + R\cos 2\theta]}{1 + R^2 + 2R\cos 2r}\right\}$$

$$F_Y = F_g = \frac{n_m P}{c}\left\{R\sin 2\theta - \frac{T^2[\sin(2\theta - 2r) + R\sin 2\theta]}{1 + R^2 + 2R\cos 2r}\right\}$$

where Fs is the scatter force, Fg is the gradient force, n_m is the refractive index of the medium, r is the angle of refraction, and T and R are the Fresnel reflection and transmission coefficient of the surface at θ. The computation includes all the forces due to internal reflection and refraction. The equations can be simplified by setting $Q_g = \left\{1 + R\cos 2\theta - \frac{T^2[\cos(2\theta-2r)+R\cos 2\theta]}{1+R^2+2R\cos 2r}\right\}$ and $Q_s = \left\{R\sin 2\theta - \frac{T^2[\sin(2\theta-2r)+R\sin 2\theta]}{1+R^2+2R\cos 2r}\right\}$. So, the magnitude of total force is $F_{mag} = (F_s^2 + F_g^2)^{1/2}$, and the magnitude of dimensionless factor is $Q_{mag} = (Q_s^2 + Q_g^2)^{1/2}$. The force can be expressed in term of dimensionless factor Q and power P, $F = Q\frac{n_m P}{c}$. The total trapping force on a dielectric sphere can be found by summing the force contributions of each ray.

Although different methods have been published for calculating trapping power at the specimen plane, trapping force on a particle has to be determined empirically due to

the limitation of the computational model (biological objects are not homogeneous and spherical). The lateral trapping force can be calibrated against viscous drag exerted by fluid flow. This determines the force it takes to remove the particle entirely from its trap. Fluid is moved past a stationary trapped particle at an increasing speed until the particle just escapes and velocity of the liquid is measured and recorded. Or, the fluid remains stationary while the optical trap is moved until the particle escapes. Then, the force can be calculated using Stoke's law. Drag forces on a sphere with radius a are defined by $F = 6\pi\eta a v$, where η is the fluid viscosity and v is the velocity of the fluid. Inertial forces can be neglected because the Reynold's number Re is small for micron-size particles; $Re = va\rho/\eta \approx 10^{-5}$ where ρ is the particle density.

Another way to measure the force applied on a particle in a trap is to measure its displacement from the center of the trap. The restoring of the optical trap works like an optical spring for which the displacement from the trap center is proportional to the force applied on the object (Figure 2. 5). K_{trap} can be found if a known force is applied and the position of the particle from the trap center is measured. The common method to apply a known force is to use viscous drag force on a particle just asdescribed in the last paragraph. Determination of the particle position within the trap requires precise measurement within a few nanometers. To achieve this, a sensitive setup with a quadrant photodiode and good electronic amplifiers is needed. The detector must be properly aligned with the optical trap at all times. The detector measures the deflection of the laser beam after it passes through the particle (Block, 1994). We have not used this method.

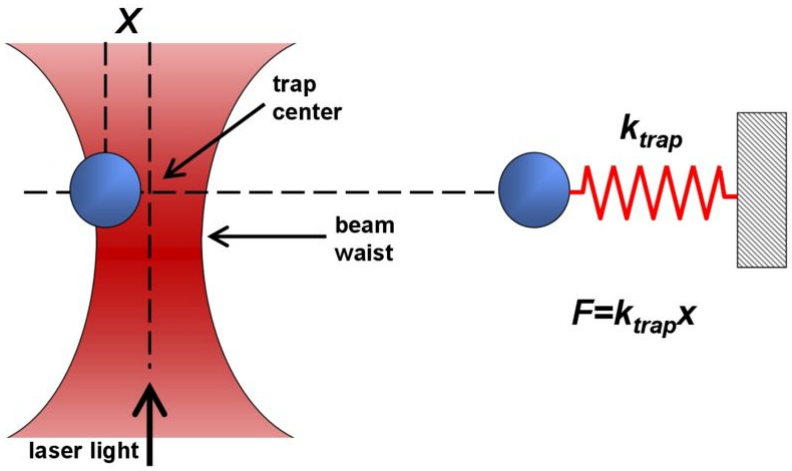

Figure 2.5 The force is linearly proportional to the displacement out of the trap. (Photo Credit: *Wikipedia)*

2.3 Trapping Criteria

For stable three-dimensional trapping, a large longitudinal component of the gradient force is needed to overcome the scattering force. To accomplish this, a steep gradient in light intensity is necessary, which can be produced from light with a high convergence angle. A high numerical aperture (NA) objective is needed to produce light with a high convergence angle. The relation between NA and convergence angle is defined by Snell's law, $NA = \mathrm{n}\sin\theta$, where n is the refractive index of the objective and θ is the maximum incident angle. Oil or water immersion objectives are typically used for trapping due to their large NA. In addition, the objective must be over-filled with the laser beam to achieve the maximum angle of convergence. There are several drawbacks when using a high NA objective lens. First, due to the large convergence angle, the trapping depth is shallow and the working distance is small. The sample has to be positioned very close to the objective. Second, a high NA objective typically has many

optical elements that can greatly reduce the IR transmission. Power loss is even greater when the objective is over-filled by the beam.

2.4 Typical Setup

A typical laser tweezers inverted microscope system is shown in Figure 2.6. The objective is below the sample plane, which allows the sample to be manipulated and accessed easily from above. The beam is expanded to over-fill the back aperture of the objective. Then, the expanded beam is reflected into the objective by a dichroic mirror, which reflects the laser wavelength, while transmitting the illumination wavelength. A CCD video camera is used to see the illumination image and the laser spot.

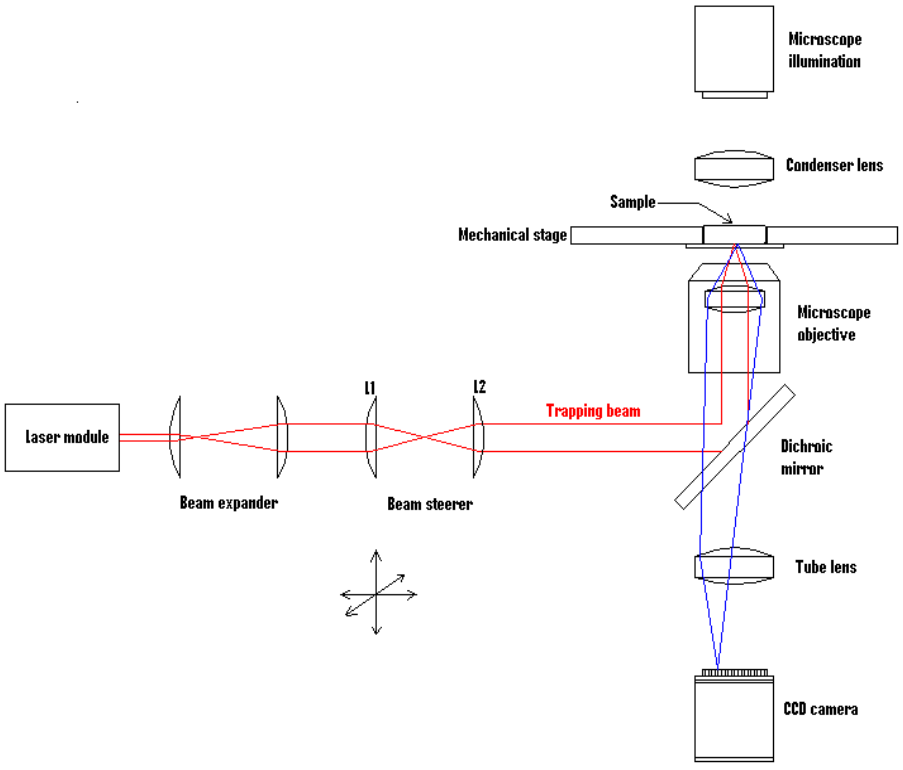

Figure 2.6 A generic setup of laser tweezers

Many steering systems have been devised to steer the beam. The configuration here places two lenses (L1 and L2) with equal focal lengths before the microscope objective. They form a 1:1 telescope which is used for manually moving the position of the optical trap in the specimen plan. Lens L2 images lens L1 onto the back aperture of the objective. Therefore, a motion of lens L1 produces change in angle at the objective and a translation at the specimen with minimal beam perturbation. Beam steering by a moving lens displacement can allow fast movements of the laser tweezers. Manipulation with the laser system can also be accomplished by translating the sample on a motorized stage. This allows large movements using the laser tweezers. These are the two simplest systems. Sophisticated steering systems using fast galvanometer-driven mirrors and acoustic-optical modulators have been designed for applications such as fast scanning and nano-level force/position feedback laser tweezers (Kuo, 1995).

2.5 Applications

2.5.1 Biological Applications of Optical Tweezers

Biological applications of optical tweezers are numerous (Ashkin, 1997; Kuo, 1995; Block, 1992). They have been used to manipulate, sort, and immobilize various cell types and numerous components within a cell (Ashkin, 1987, 1989; Burns, 1992). Cells can be transported from one place to another, and brought together by optical tweezers to study interactions among them (Townes-Anderson, 1998). Many biologists are interested in measuring the force that joins two biological objects together by pulling them apart

with optical tweezers. Attaching spherical handles to molecules provides optical tweezers something to hold onto, so the mechanics of many types of motor molecules can be studied (Block, 1990, 1995; Finer 1994; Svoboda, 1994, 1994; Yim, 1995). Optical tweezers are also useful for studying the viscoelasticity and mechanical properties of various membranes (Editin, 1991; Wang, 1993) and molecules (Perkin, 1994; Smith, 1996) by pulling or bending them with the laser tweezers. In addition, optical tweezers can combine with ultraviolet microbeams (optical scalpels) to cut biological material and fuse it together (Seeger, 1991; Steubing, 1991; Liang, 1993). Optical tweezers have also been used for studying laser-induced damage to various cell types (Konig, 1995; Liang, 1996; Liu, 1996, 1996; Neuman, 1999; Sacconi, 2001; Leitz, 2002). The applications of optical tweezers are wide-ranging.

2.5.2 Future Applications

Optical tweezers have many potential future applications as well. Here are some examples mentioned by McGloin (McGloin, 2006): Integration of optical tweezers systems into lab-on-chip types of micro-fluidic devices is an idea just beginning to be researched. Optical cell sorting with optical tweezers combined with single-particle spectroscopy is a very exciting development. Near field and holographic tweezers offer the possibility of manipulating large numbers of particles simultaneously. Novel force-sensing techniques based on optical tweezers are worth exploring. Angstrom-scale position and femtonewton force measurements are also being explored.

CHAPTER 3

Laser Tweezers Apparatus

Our computer based automated optical tweezers system has been developed for loading live dissociated neurons into cages quickly and precisely. Like any practical engineering design, it must to be simple and easy to operate. The systems we studied use either a 1064 nm or a 980 nm laser source to generate the beam. To see how the IR beam is collimated, directed, aligned, and focused to trap a neuron, the design and construction of the system is discussed in this chapter. It is important to obtain optimal power output to trap and move cells effectively. Selection of components and characterization of the system are described. The system characterization includes measurement of the light intensity profile, power measurement, IR transmission of the lens, and the maximum speed a neuron can be moved as a function of power level.

3.1 Summary of Apparatus

A typical laser tweezers system has four major components: laser source, beam expander, beam steering system and microscope. The system described here has all these essential components. This section first presents an overview of the system and describes each

component in detail. The fundamental differences between 1064nm and 980nm systems are the laser source and the beam steering method.

3.1.1 System Overview and Light Pathway

The system consists of an inverted microscope, a 1064 nm or 980 nm laser module, a beam expander, a motorized mechanical stage, a CCD camera, and steering mirrors. Figure 3.1 provides an overview of the setup. A laser beam is generated by the IR laser module, and the beam is expanded by the beam expander to match the size of the back aperture of the objective. The beam is then steered into an inverted microscope (Olympus IX71) via a fluorescent port and reflected by a dichroic mirror into a 63x oil-immersion objective (Zeiss 440460, 63x, N.A. 1.25) where it is focused to a point (Figure 3.2). The mirror transmits visible light for phase contrast imaging and a very small fraction of the IR back-scattered from the sample. A CCD video camera is used for viewing the laser spot and capturing videos or images. The captured videos and images are stored in the computer. LabVIEW software is used to control the stage. The software is programmed so the system knows the cage locations and guides each cell to its destination.

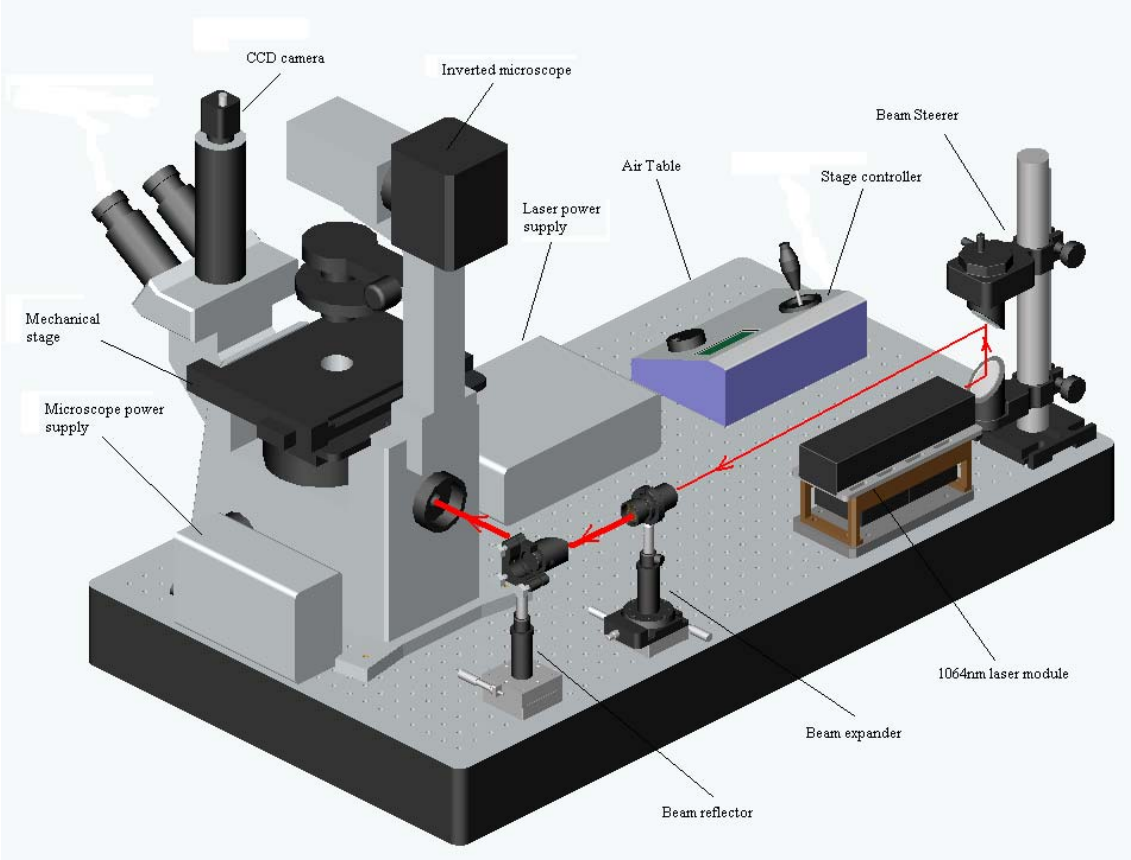

Figure 3.1 A system overview

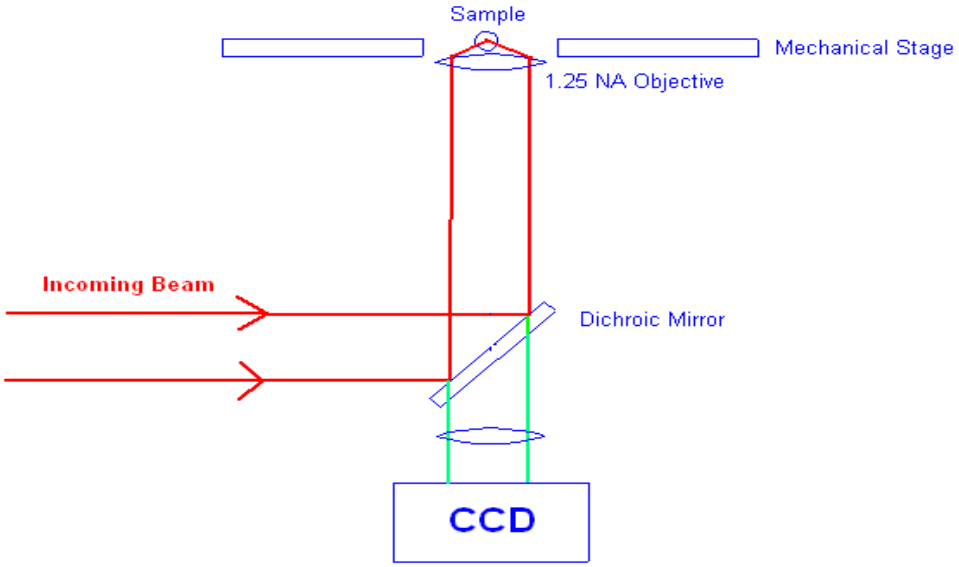

Figure 3.2 The incoming beam is reflected by a dichroic mirror into the microscope objective.

3.1.2 Beam Expander

For successful trapping, it is essential to fill the back aperture of the objective with the incoming beam. This produces a focal spot with maximum angular spread. To expand the beam uniformly to match the size of the back aperture of the lens, a 5x beam expander is used here. The purpose of a beam expander is to take a small diameter collimated input beam and produce a larger diameter collimated output beam. The beam expander also reduces beam divergence. The two basic types of beam expanders are derived from Galilean and Keplerian telescopes (Figure 3.3).

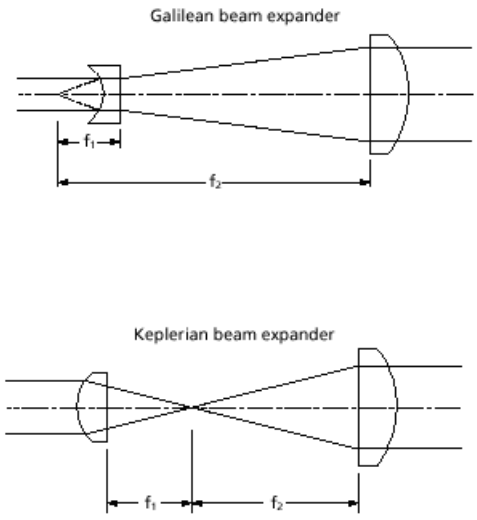

Figure 3.3 Two basic configurations of beam expander

A Galilean beam expander has one negative input lens and one positive output lens. The input beam is first diverged (expanded) by the negative lens, then the beam is restored by the positive lens. The input lens produces a virtual focus f1 at the focal distance of the output lens. A Keplerian beam expander consists of a positive input lens

and a positive output lens. In this case, the input lens produces a real focus at the focal distance of the real focus f2 of the output lens. The expansion factor is determined by the ratio of f2/f1 for both types of expander. The divergence angle of the output beam θ_{out} can be found using the equation $\theta_{out} = \theta_{in}\frac{f_1}{f_2}$ where θ_{in} is the divergence angle of input beam.

A 5x Galilean beam expander (BE5-C) from Thorlabs was used. The expander has a broadband anti-reflecting coating for maximum transmittance. The Galilean beam expander is chosen because it is small, inexpensive, and readily available. The measured transmittance is about 90% for both 1064 nm and 980 nm.

The beam expander must be collimated for each wavelength before usage. This is done by adjusting the distance between the two lenses and observing the beam profile and size at different distances. If the beam expander is well collimated the beam will have a minimal divergence angle and a slightly larger beam waist at a distance 2 m away from the expander.

3.1.3 Laser Source

A laser source that generates the necessary light to trap a neuron is the heart of a trapping system. To minimize potential photodamage to biological materials, a near-infrared laser source between 700 nm and 1300 nm should be used. It can be either a crystal or a diode laser. The laser needs to operate in the TEM_{00} mode to produce a beam with a Gaussian profile. The power output at the trap is typically between 10 mW and 1 W. Two laser

sources were used in this work, a 1064 nm Nd:YAG crystal laser and a 980 nm diode laser. The following section describes the working principle, construction, and specifications of each laser module.

3.1.3.1 1064 nm Laser Module

For the 1064 nm system, a solid-state Nd:YAG laser that emits at a wavelength of 1064 nm was used. The manmade yttrium-aluminum-garnet (YAG) crystal is doped with 2% neodymium (Nd) because neodymium readily absorbs light emitted by a krypton lamp during pumping. As illustrated in Figure 3.4, a krypton arc lamp is used to optically pump atoms in the crystal from the ground state (E1) to a pump band (E4). These atoms decay rapidly from E4 to E3, then from E3 to E2, and finally from E2 to E1. The atoms radiate heat during the transitions in E4→E3 and E2→E1. The laser rod needs to be cooled because the atoms only decay rapidly from E2 to ground level at a low temperature. Therefore, an effective cooling system is essential for a high lasing efficiency. The laser rod is usually made very thin, about 1 to 4 mm in diameter, because it easier to cool a thin rod than a thick rod. A resonant cavity formed by end mirrors allows the light to make many passes through the crystal so that stimulated emission ("lasing") takes place. One mirror is mounted at each end of the laser rod with one being a 100% reflector while the other is a partial reflector which allows a portion (1 to 8%) of the generated beam to pass outside the cavity.

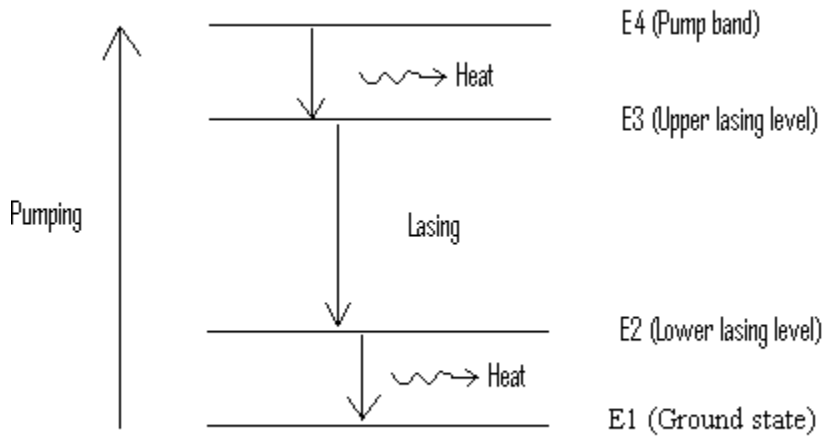

Figure 3.4 Energy levels in a Nd:YAG crystal

The high power continuous wave laser module (Intelite ISF064-1000P) used here consists of a laser head, a heat sink with two fans, and a power supply. It generates a collimated beam with a diameter of 1.5 mm and divergence of 1 mrad. This particular unit had a measured maximum power of 890±3 mW initially. However, this output was significantly reduced after many hours of usage.

3.1.3.2 980 nm Laser Module

The 500 mW fiber Bragg grating stabilized 980 nm laser diode used here (JDSU 29-8052-500) is particularly useful for laser tweezing because it provides a noise-free narrow band spectrum, even under changes in temperature and drive. It uses a polarization maintaining (PM) fiber and a semiconductor Bragg grating to "lock" the emission wavelength. It is integrated with a thermoelectric cooler, a thermistor, and a monitor diode.

The development of semiconductor diode laser technology was motivated by the use of fiber-optics in communication, and the need for compact and inexpensive sources of optical energy in information handling applications. The diode lasers can be made from materials which emit in the near-infrared region.

In a laser diode, the laser medium is the junction between the n-type and p-type semiconductors. Voltage is applied to the p-n junction with the negative terminal connected to the n-region and the positive terminal connected to the p-region. This causes electrons to move to the p-type region while holes to move toward the n-type region simultaneously. A photon is emitted when the system is relaxed back to its electron equilibrium distribution. The band gap between valence and conduction bands determines the energy of the emitted photon (Figure 3.5). A population inversion can be created at the energy level if sufficient energy is applied to the junction. The current density through the junction must exceed some minimum value and therefore provide enough holes and electrons so that the radiation generated by their recombination exceeds the losses. As in other lasers, a laser diode is in an optical cavity where stimulated emission takes place. The optical cavity consists of multilayer Bragg reflectors on either side of the junction. The photons are emitted into a flexible optical fiber which can be as long as a meter.

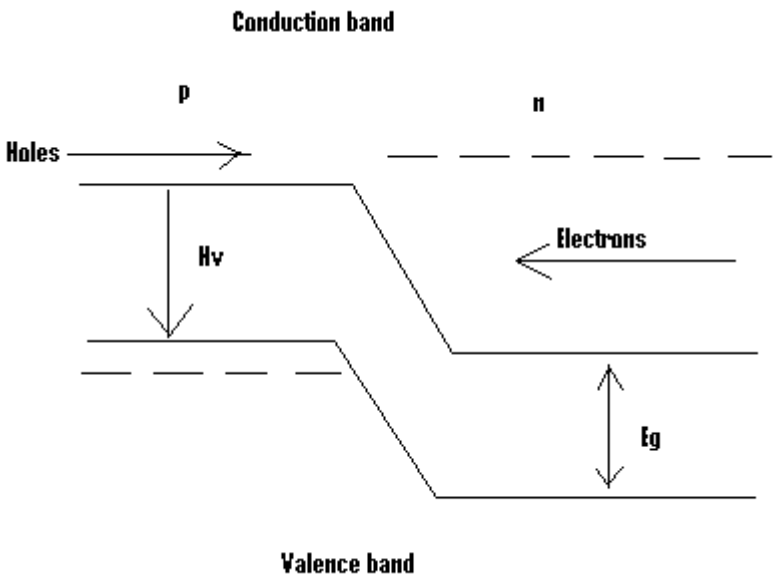

Figure 3.5 Energy levels in a laser diode

The 980 nm system used here consists of a thermo-electrical cooler (TEC) controller, a "butterfly" laser mount, a laser power supply, a laser diode, and a collimator.

The laser mount (Thorlabs LM14S2) provides a zero insertion force socket for mounting a 14-pin "butterfly" laser diode (LD) that has an integrated TEC and Thermistor sensors. The top surface of the mount provides a heat sink and a recessed area to mount the diode. The laser diode outputs through a polarization maintaining (PM) fiber which is flexible and can be placed anywhere on the air table. The PM fiber is connected to a fiber collimator (Microlaser FC5) to generate a Gaussian beam. The fiber collimator used has an aperture of 6 mm and generates a beam 2.1 mm in diameter.

3.1.4 Beam Steering System

The beam is directed from the laser source to the microscope via a beam steering system, which consists of various mechanical stages, mirror mounts, and reflecting mirrors. It reflects and directs the light beam to the objective.

3.1.4.1 1064 nm

The 1064 nm laser module is on a mounting plate which was designed to align the module on an air table, as illustrated previously in Figure 3.1. A precision beam steering assembly is used for adjusting the height of the beam. The assembly is comprised of a top mirror holder, a lower mirror holder, and a damping rod. The top mirror holder has both coarse and fine elevation adjustments so that the height of the beam can be controlled precisely. The lower mirror reflects the horizontal incoming beam up toward the upper mirror, and then the upper mirror returns the beam to its horizontal state.

The beam is directed into the beam expander from the mirrors for expansion. The expander can be adjusted in four directions (xyz and theta). The expander is mounted on an adjustable pole (z-direction), which is mounted on a rotation stage (theta-direction), and, finally, the rotation stage is mounted on a mechanical stage (xy-direction). The xy-stage is made by combining two one-dimensional stages. The expanded beam is then reflected by a mirror into the microscope. This mirror assembly can be adjusted in three directions (xyz). Similar to the beam expander, it is mounted on an adjustable pole and the pole is, in turn, mounted on a mechanical stage for xy movements.

3.1.4.2 980 nm

A steering system is not needed for the 980 nm system because the fiber collimator for the 980 nm laser diode can be placed directly behind the microscope, as shown in Figure 3.6. Like the 1064 nm system, the fiber collimator and beam expander are mounted on xyz stages.

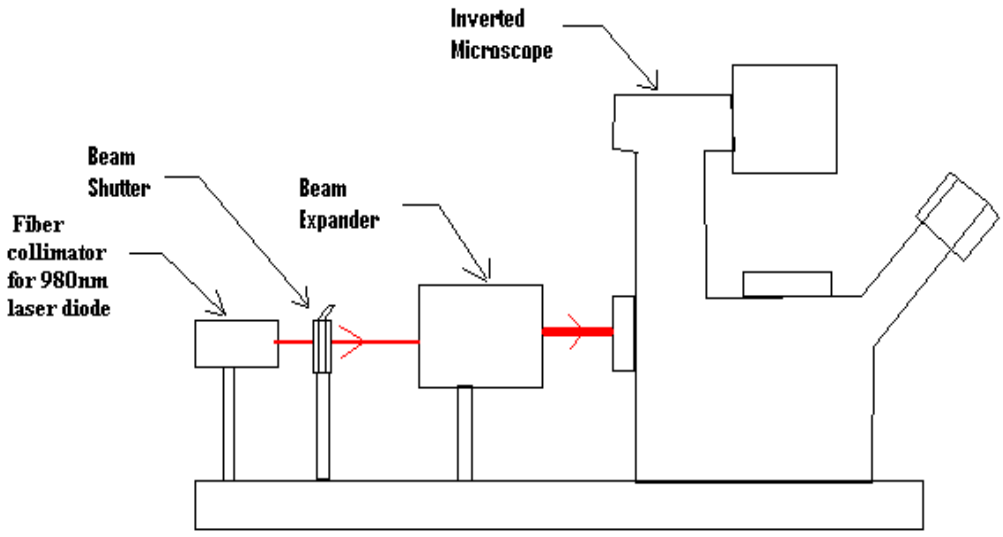

Figure 3.6 980 nm beam path, it is not drawn to scale.

3.1.5 Microscope System

In order to perform experiments, an epi-illumination microscope is needed to produce the focused spot and observe the trapped particles. In the laser tweezers system, the microscope is equipped with a dichroic mirror that reflects 98% of the laser beam towards the specimen plane, a high numerical aperture objective for trapping and

imaging, and a CCD camera for viewing the laser spot. An Olympus IX71 inverted microscope is used here. The inverted microscope is superior for micromanipulation because it provides enough room for neurons in suspension to be easily accessed from the top. Samples are illuminated in the IX71 by a 100 watt source through a condenser.

The IX71 has three objectives; 10x, 20x, and 63x. The low magnification lenses are used to locate the neuro-cages and neurons. The 63x oil-immersion lens is used to trap the neuron and is modified to protect it from laser damage. The entrance pupil of the objective is surrounded by a plastic ring, and the expanded beam overfills the entrance pupil and would cause it to warp. A stainless steel protection ring was designed and attached at the entrance pupil.

The IX71 is a multi-port (eight ports) design which includes four ports that can access the primary image simultaneously without any relay lenses, as illustrated in Figure 3.7. A CCD camera is attached to the trinocular port via a tube lens. The IR beam enters the microscope through the fluorescent port. A fluorescent light source can be easily attached to another port for viewing stained neurons, if required.

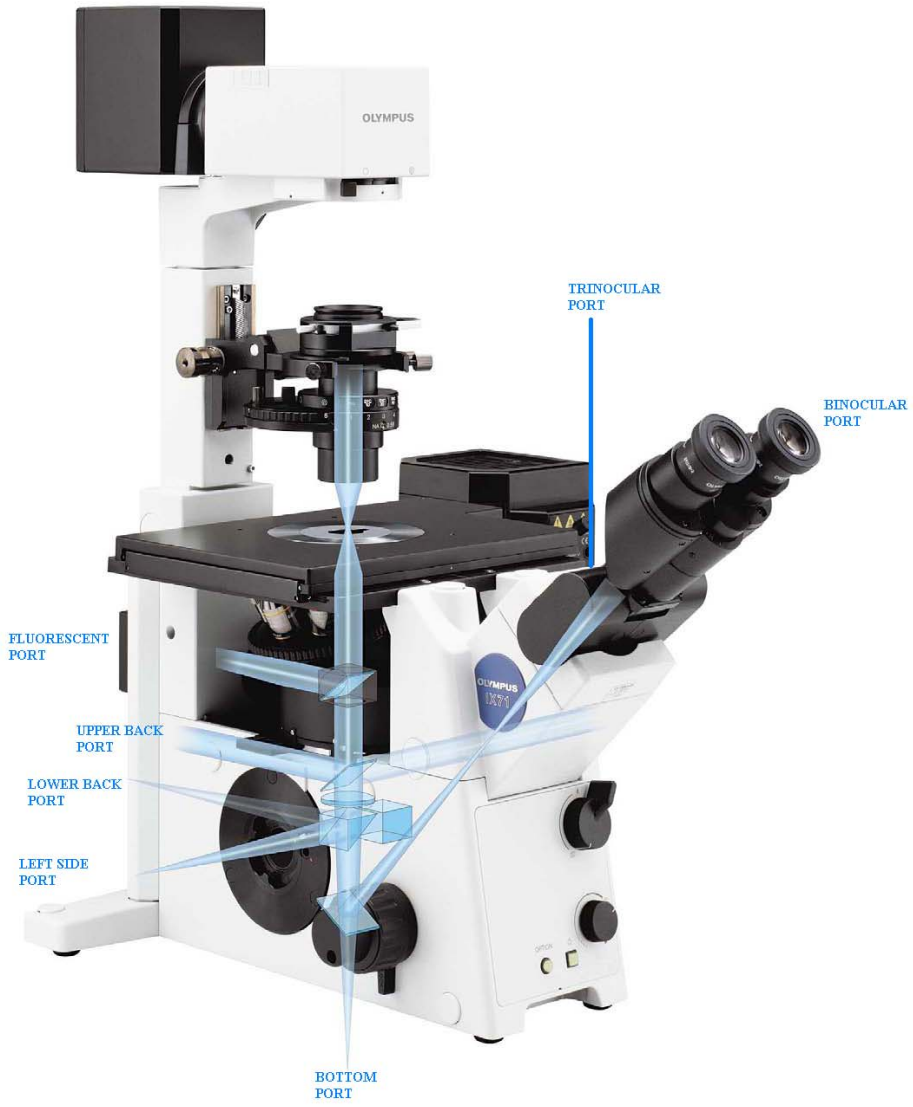

Figure 3.7 Port configuration for Olympus IX71 inverted microscope

A charge-coupled device (CCD) video camera is used to image the neurons and laser spot. Most CCD cameras are sensitive to IR illumination because the semi-conductor material (e.g., silicon) used in CCD cameras is sensitive to IR. The CCD camera used in this study is very sensitive to the 980 nm IR light, so the laser spot

appears so bright that nothing else can be viewed. A filter (KG1 from Thorlabs) was cut and inserted into the camera to reduce the transmission of the 980 nm IR light by 98%.

3.1.6 Moving Cells at the Specimen Plane

For a small movement within the viewing field, the trap could be steered in the specimen plane by translating a lens or a mirror in the beam pathway. But for this application, it is desired to move cells over a few millimeters distance. Therefore, instead of moving the trap, a computer controlled motorized mechanical stage is used to move the culture dish. An MS-2000 mechanical stage from Applied Imaging System was used. The xy stage was attached to the frame of the Olympus IX71 microscope on top of the objective. The z stage is simply a motor that is attached to the fine-adjustment knob of the microscope. The system uses servo feedback motors that can control movement with 0.3 um precision, which is sufficient for positioning the neurons. The system comes with a controller that can be controlled either by a joystick or a computer interface.

3.1.7 Software

A LabVIEW program was used to control the mechanical stage. It first resets the stage and computes the location of each cage after two reference points are manually input into the program. Then, it sets the speed of the stage according to the user. Then, the user selects a target cage by inputting a number that corresponds to that cage. Finally, the program instructs the mechanical stage to bring the neuron to the pre-selected cage after

the neuron is trapped by the laser tweezers. Programming details and procedure are described in Appendix B.

3.2 Beam Alignment

Alignment of the optical system can be difficult because IR radiation is invisible to the human eye. However, the system can be easily aligned with the help of an IR viewing card and a power meter. The alignment procedure for both the 980 nm and 1064 nm systems is described in Appendix C.

3.3 System Characterization

3.3.1 Light Profile Measurement

The laser mode used here is TEM_{00}. It is important for producing a Gaussian beam profile for effective trapping. The beam profile for the 1064 nm system was measured after the 10x beam expander by moving a detector across the beam. The opening of the detector was restricted to a 2.5 mm diameter hole by attaching a predrilled metal plate to the detector. The detector was moved horizontally across the beam in 1 mm steps by a mechanical stage. The intensity at each step was measured and recorded, and the distance traveled was 18 mm. This only measures the beam profile in one direction (0°). The detector was then moved across the beam spot diagonally (45°) and vertically (90°).

The data are plotted and results shown in Figure 3.8. The beam shape is approximately Gaussian in all the directions that were measured.

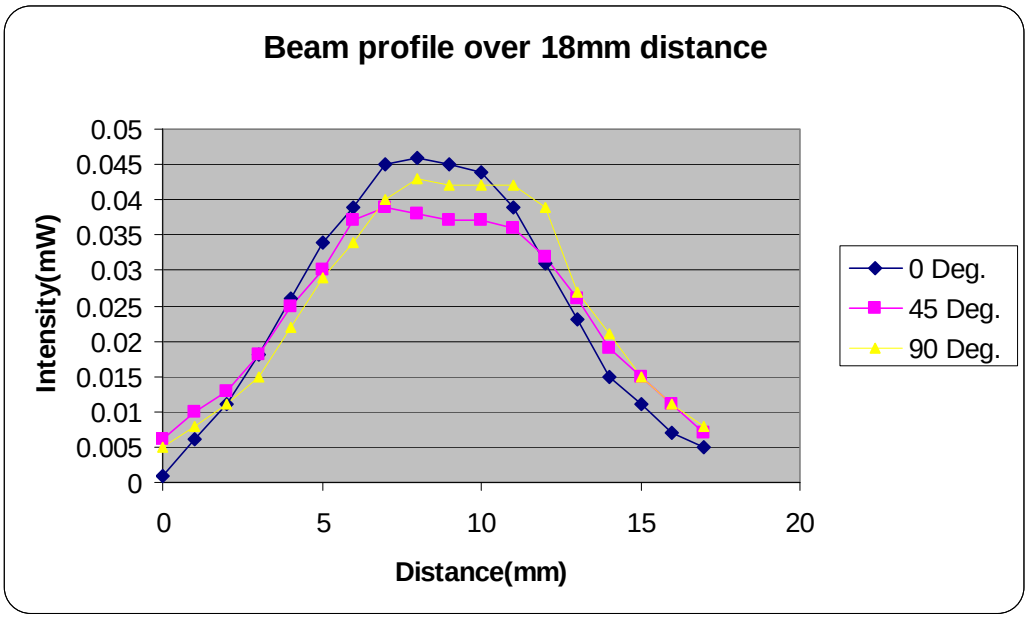

Figure 3.8 The laser profile after the beam expander was measured in the directions of 0°, 45°, and 90° with respect to horizontal.

3.3.2 Power Output Measurement

A method was devised to measure IR transmission of a high NA objective without using the dual-objective technique [Misawa, 1991] in which two identical objectives are used to focus and then re-collimate the beam. The transmission for a single objective is the square root of the transmission of the objective pair. The dual-objective was used because it was believed that the steep focusing angles produced by a high NA objective can cause the rays from the outer part of the beam to reflect from the surface of the detector at the focus. So, the transmission measurement would be underestimated. However, for us this was not the case. The transmission was measured by simply passing

an IR beam through the objective and measuring its power by using an IR power detector (Coherent PM10-19B) at the focus. The detector has a broadband coating and can be used to measure laser output with wavelength between 0.11 and 11 um. It has a BNC connector that can be connected to a volt meter for readout. The power loss due to reflection when measuring the transmission did not have to be accounted for, because the absorbability of the power detector was found experimentally to vary little with incident angles (0–75°) of an incoming beam. This is shown in Figure 3.9.

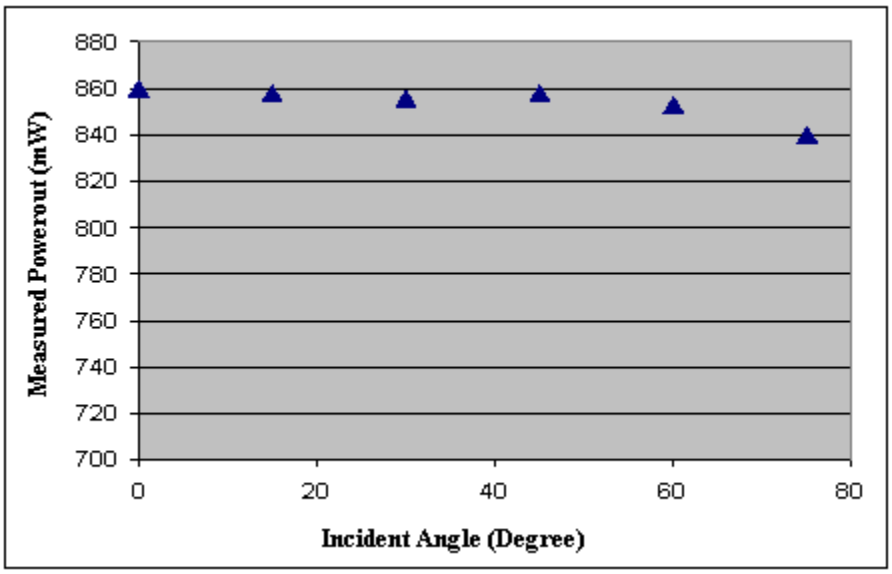

Figure 3.9 At maximum power, the detected output was measured when the incident angle of an incoming beam was at 0, 15, 30, 45, 60, and 75 degrees. For power detector PM10-19B, the power reflected is negligible for incident angles between 0 to 75 degrees.

3.3.3 Lens IR Transmission

An optical tweezers uses a highly focused IR laser beam to trap and manipulate small particles. The oil immersion objective lens is normally used due to its high numerical

aperture. But oil immersion objectives generally do not transmit IR well. As a result, most of the power loss in the system comes from the objective lens. The trapping force of optical tweezers is proportional to the laser power, and one needs a good trapping force for optimal tweezers design. The objective lens selection is thus critical, and the actual transmission was measured before the designed was finalized. The transmission for Zeiss and Olympus lenses was measured and compared.

The laser beam was expanded, and the diameter of this beam was then reduced with a restrictor aperture to a size that was slightly smaller than the diameter of the back aperture of the objective lens. The intensity of this laser beam was measured before and after the beam passed through the objective lens. The transmission in percent was computed using following formula:

$\text{TransmissionRate}=100\% \times \frac{Input}{Output}$.

For these transmission measurements, a 10x beam expander was used to expand the beam. A customized objective mounting fixture was used between the beam expander and the power meter. A fixture was designed to mount the size restrictor and the objective. For the input measurement, only the beam restrictor was attached to the mounting fixture, as shown in Figure 3.10. The intensity of the restricted beam was recorded. For the output measurement, both beam size restrictor and objective were attached, as shown in Figure 3.11. The intensity of the beam that passed through the objective was then measured. Since the back aperture of the Olympus lens was different from the Zeiss lens, a beam size restrictor matching the back aperture of each lens was made.

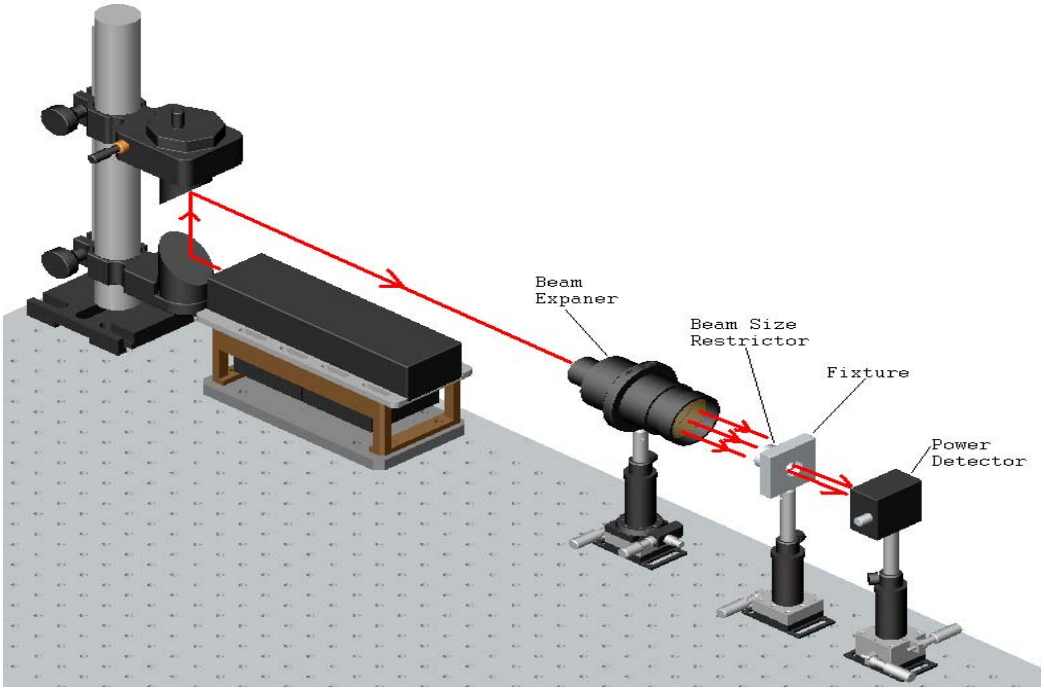

Figure 3.10 The beam is expanded by the beam expander, and it is then partially blocked by the beam size restrictor to simulate the input beam. The restricted beam is measured by a power meter.

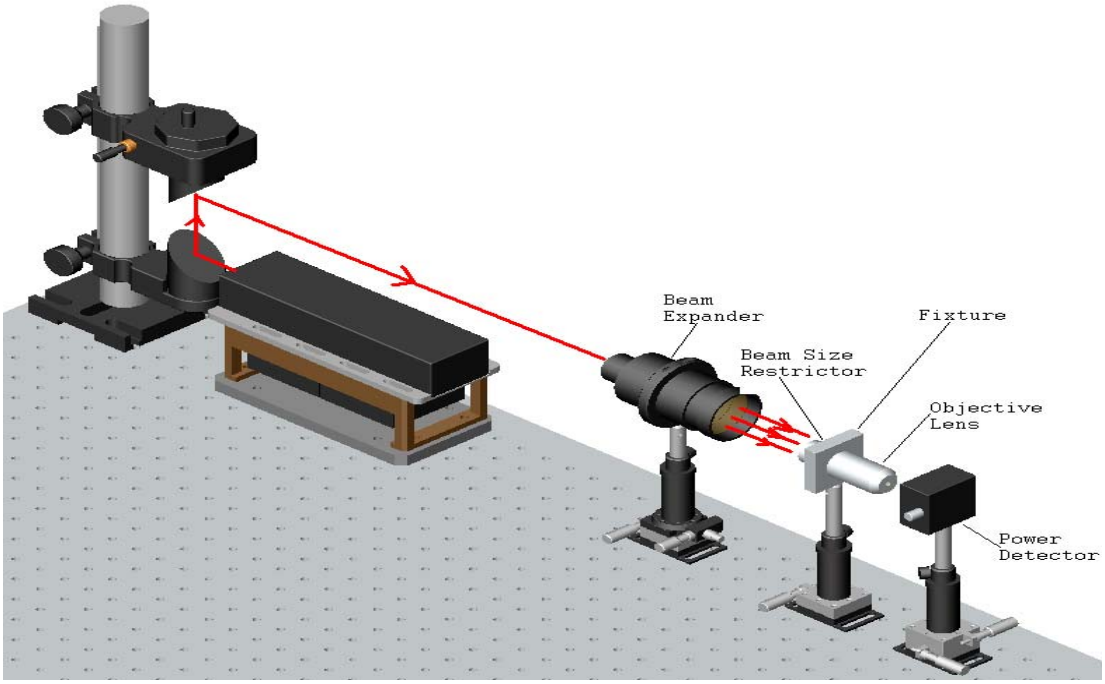

Figure 3.11 The objective lens is attached to the fixture, and the beam goes through the objective lens; its output is measured by a power detector.

By using the equation $NA=nSin\theta$, where n is the refractive index of the oil and NA is the numerical aperture of the objective, the angular aperture θ of the Zeiss and Olympus objectives were found to be 55.4° and 72.8º, respectively. In the previous section, it was shown that the detector sensitivity is virtually unchanged up to 75°. Therefore, transmission for these objectives can accurately be measured by simply placing the detector at their focus.

The transmission for the Olympus 60x, 1.4 N.A., oil immersion objective (PLAPO60XO) was determined to be 17.9 %, which is much lower than the 40% specified by the manufacturer. The transmission rate of a 63x, 1.25 N.A., oil immersion Zeiss objective (440460) was also obtained by using the same measuring technique. The transmission was found to be 62.2% which is essentially the same as the 60% specified by the manufacturer. Consequently, the Zeiss lens is more suitable for maximizing the IR laser output for optical tweezing and was chosen.

3.3.4 Speed Vs. Laser Output

We have determined the maximum speed a trapped cell can be moved without escaping as a function of laser intensity. The cell was held stationary by the laser tweezers while the stage was moving. For a given laser intensity, the speed of the stage was increased in increments of 5 μm/s until the cell just escaped. The maximum speeds vs. laser power for both 1064 nm and 980 nm are plotted on the same graph in Figure 3.12. The maximum speed seems to be linearly dependent on laser power and the slope for 980 nm is slightly higher than for 1604 nm.

The linear relationship between maximum speed and laser power is what we expected. Forces due to a single ray are proportional to power output at the specimen plane, and the total trapping force on a dielectric sphere is the summation of the forces contributed by each ray, described previously in Chapter 2. According to previous studies, for a rigid dielectric particle, the trapping forces are proportional with laser powers. Trapping forces can be calibrated against drag exerted by liquid flow. Inertial forces can be ignored since the Reynold number is small ($Re = \frac{vap}{\eta} \approx 10^{-4}$; where υ is fluid velocity, a is the cell radius, ρ is the fluid density, and η is the fluid viscosity). Drag forces on a stationary sphere in liquid flow are proportional to fluid velocity, $F = 6\pi\eta av$. Therefore, the maximum speed varies linearly with laser power.

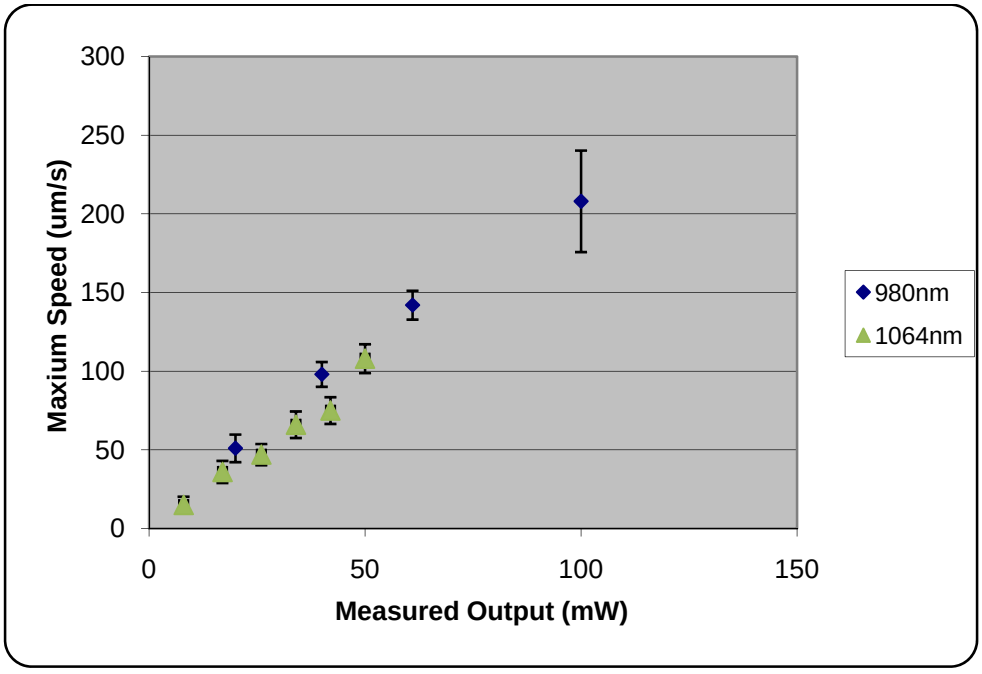

Figure 3.12 The maximum speed is linearly dependent on measured laser power output at the specimen plane.

3.4 Summary

Both the 1064 nm and the 980 nm systems are relatively simple to build and to align. However, the 980 nm system is clearly a better choice than the 1064 nm system because the use of a laser diode for trapping provides a low-cost alternative to the expensive crystal laser. It is also compact, so that the mechanical support is smaller and lighter, making it easier to set up and align in an optical system. The beam steering system was unnecessary for the 980 nm system because the collimator and the beam expander can be placed directly behind the back-port of the microscope.

The beam after the beam expander was found to have a Gaussian profile which is necessary for trapping small objects (Chapter 2). The experiment has shown that the laser power at the specimen plan can be easily measured by a power meter which eliminates the complicated procedure devised by Misawa. The maximum speed varies linearly with laser power at the specimen. It is about 250 um/s at 100 mW for 980 nm and is about 125 um/s at 50 mW for 1064 nm. These are satisfactory for moving neurons to their cages in less than a half minute.

CHAPTER 4
Photodamage Studies

The main drawback of optical trapping has been the possibility of damage induced by the highly focused beam. Risks of optical and thermal damage may increase with increasing laser power. These risks can be reduced by choosing appropriate laser wavelengths. According to previous studies on non-neural cells, 830 and 970 nm are the best choices for moving live cells and 870 and 930 nm are the worst (Liang, 1996; Liu, 1996; Neuman, 1999). Studies have also shown that different cell types respond to light differently. For example, a few minutes of 50 mW trapping with 1064 nm reduces the rotation speed of an E. coli cell (Neuman, 1999), while the human sperm cell experiences a loss of viability at a much higher power of 300 mW (Liu, 1996). Fortunately, many manipulations require only a few milliwatts, and thus can be performed safely. However, high-irradiance manipulations require careful planning and thorough investigation of light-induced damage to the specimen. We have investigated photo-toxicity on stationary and moved neurons. Survival experiments were done using different trapping parameters such as trapping power, irradiation time, and wavelength, and are presented in this chapter. The first part of this chapter outlines culturing and experimental methods. Survival results are then presented and discussed.

4.1 Cell Culture

4.1.1 Glass Substrate

The use of laser tweezers requires very thin glass slides, about 100 um thick (Carolina Biological, special order). The high power objective used for focusing the beam has a very shallow working distance. A thick glass slide would not leave enough room for lifting. The glass slides have to be culture-ready since neurons will not grow on untreated glass surfaces. By treating them with nitric acid and hydrogen peroxide followed by vigorous cleaning, glass slides were made culture-ready. They were used to make gold-grided glass slides and neurochips.

4.1.2 Gold Patterned Dishes

To quickly and easily identify individual neurons, gold-patterned glass-bottom dishes were constructed. Gold was patterned onto a 1" x 1" number zero cover-slip by Angela Tooker in Tai's lab. It is a square pattern shown in Figure 4.1a that contains 36 large square boxes. Each box is numbered and then further divided into 36 small square boxes. The gold lines are 10 um wide, 3000 angstrom thick, and spaced 100 um apart. The gold was attached to the glass surface by a 700-angstrom-thick platinum layer, since gold does not adhere to glass. A 0.75" clearance hole was drilled at the bottom (center) of a 35 mm tissue-culture Falcon Petri dish. The cover-slip was glued to the bottom side of the dish and across the clearance hole using Sylgard 184, as shown in Figure 4.1b. There are four square patterns at each corner of the cover-slip, which was glued in a way that

enough space is provided for lifting neurons to one or two patterns that can be accessed. Figure 4.1b shows that two square patterns on the right side of the dish can be used for identification.

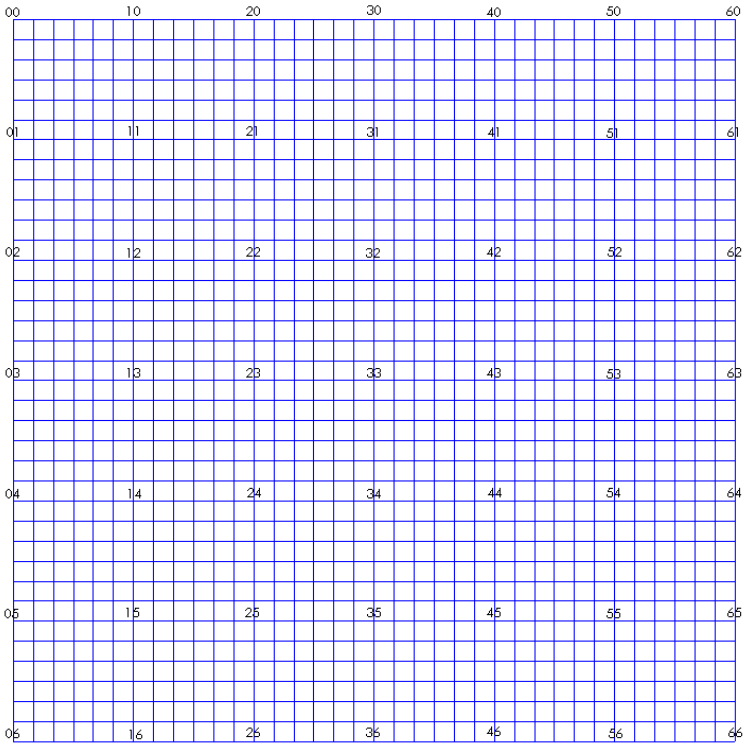

Figure 4.1a Gold pattern

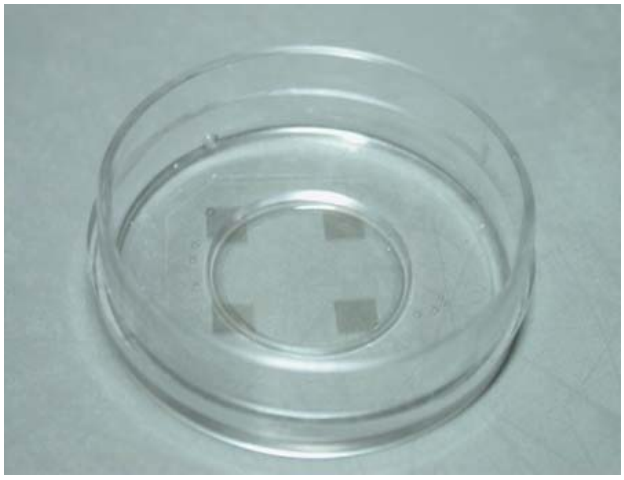

Figure 4.1b Gold patterned glass-bottom petri dish

4.1.3 Dish Preparation

Each dish was treated with 0.05% Poly-ethyleneimine (PEI) (Sigma P3143) in borate buffer solution and incubated at 37º C overnight to promote cell adhesion to the substrate. PEI was discarded from the dish and the dish was rinsed six times using double distilled water. Each dish was then treated with 2 ul laminin (Sigma L2020) per 1 ml of Hanks balanced salt solution (HBSS) (Gibco 24020-117) for 2 hrs in an incubator to promote outgrowth of neurons. The dish was then rinsed with double di-water three times. Next, about 40 ul of a solution of 20 mg Poly-2-hydroxyethyl methacrylate (polyHEMA) (Sigma P3932) per 1 ml of 95% EtOH was applied to half of the dish to make the surface non-sticky. The polyHEMA was allowed to evaporate slowly in a container to leave a smooth surface. A total of six layers of polyHEMA were applied to the culture surface. Finally, the dishes were sterilized by UV for 20 minutes.

4.1.3.1 Non-Sticky Substrate

Hippocampal neurons adhere to almost any substrate at a level which makes it impossible to lift them off with optical tweezers. This presented the biggest challenge in neuron manipulation. Finding a way to prevent neurons from sticking to the surface was challenging and time consuming. Fortunately, after extensive research, a method was found to successfully repel neurons from the substrate. The methods attempted, both unsuccessful and successful ones, are described in this section. The two basic approaches used were modifying the substrate and modifying the cell surface.

4.1.3.1.1 Modification of Cell Surface

The first attempt was to modify the cell surface with the enzyme trypsin. Trypsin is a pancreatic enzyme that catalyzes the hydrolysis of proteins to form smaller polypeptide units. In a cell culture lab, it is commonly used to dissociate neural tissue or to re-suspend cells adhering to a culture dish. Hence, it was believed that trypsin might cleave off the surface proteins that are responsible for cell adhesion.

Dissociated neurons were suspended in plating medium containing 0.25% trypsin (Sigma T4549). These neurons could be lifted with optical tweezers easily with a power of 17 mw for at least 30 minutes. Trypsin worked well, but the cells would not adhere to the PEI coated plating substrate after being moved. To address this issue, soybean trypsin inhibitor (Sigma T6414) from Glycine max 1x solution or 30% horse serum was added to the medium without washing the cells to stop the enzyme reaction. The cells stuck to the plating substrate half an hour after adding the trypsin inhibitor, but the cell survival was terrible after three days. The experiment was repeated using plating medium containing 0.125% trypsin. Two thirds of the cells were lifted in a 30 minutes period but the survival result was similar to that of 0.25% trypsin.

To improve cell survival, an alternative preparation was used. Instead of suspending the neurons directly in a trypsin solution and adding the inhibitor later, they were treated with 0.25% trypsin solution first for 30 minutes, spun out, and washed with inhibitor solution. The neurons could be lifted with 17 mw for more than 30 minutes. Although survival was improved slightly, it was still not satisfactory. This indicated that prolonged treatment with trypsin might have damaged the neurons. An alternative

trypsin-like enzyme was used to try to reduce damage. TrypLE (Gibco, 12604-013) is a recombinant enzyme derived from microbial fermentation. The enzyme is stable at room temperature and gentle on the cells. Neurons were treated with trypLE for 30 minutes, spun out, and rinsed with 30% horse serum solution. However with TrypLE treatment, neurons could not be lifted, even at a higher power of 34 mW.

The use of papain (Sigma 76216) was then explored. Papain is a cysteine protease present in papaya. It is another enzyme commonly used to dissociate cells. Papain breaks down the extracellular matrix molecules that hold the cells together. Pieces of hippocampus were treated with 10% papain solution in a 37° C water bath for 30 minutes. The solution was triturated using a pipette to dissociate cells. Then, the dissociated neurons remained in the papain solution for a set of amount time (2.5, 3, 5, and 10 minutes). Finally, the cells were spun out and re-suspended in the plating medium with 5% horse serum. The experiment resulted in two findings: that only about 40% of the neurons could be lifted within the first 30 minutes at 17 mw, and that neurons usually die off after 7 days.

In summary, inhibiting cell attachment to the substrate by modifying cell surface properties using an enzyme was unreliable. Also, possible damage to neurons due to the enzyme treatment makes it undesirable. Therefore, surface modification of the substrate could be a better alternative.

4.1.3.1.2 Modification of Substrate Surface

Teflon (Polytetrafluoroethylene) has a very low friction coefficient and is commonly used as a non-stick coating for cookware. For this reason, the use of a Teflon surface was investigated. A Teflon surface was made by attaching a piece of Teflon film onto the bottom of a petri dish. The neurons were well stuck to the Teflon surface within a few minutes after plating, and could not be lifted even at a maximum laser power of 100 mW. Corning's ultra low attachment culture dish (3261) was investigated because Corning claims that it features a covalently bonded hydrogel layer that effectively inhibits cellular attachment. Five minutes after plating, the dish was tapped and neurons were stuck to the surface. The substrate surface was lubricated with various silicon based fluids such as Dow corning 200, 300, 360, and Sylgard 184. These surfaces repelled more than 50% of the cells for the first 10 minutes, but neurons stuck to them after 10 minutes.

Surface-bound, poly-ethylene glycol (PEG) is commonly used to retard adsorption of non-specific proteins and other biological molecules. PEG chains can be covalently attached to the surface either directly by a one-step coupling procedure, or a multiple-step procedure that involves first coupling a precursor to the surface, followed by coupling PEG. Four PEG derivatives were used here: 1) PEG-Silane from Gelest (SIM492.7-25GM) was first investigated because it requires only one step for coupling. The PEG-Silane solution was made by mixing 200 ul of PEG-Silane with 25 ul of acetate, and 10 ml of 95% EtOH for 20 minutes. The dish was treated for 5 minutes and dried overnight in a 50° C oven. Neurons remained non-stuck for only about 5 minutes. 2) PEG-Silane (1 mg/ml and 2 mg/ml) was linked to the surface for use with N-[γ-maleimidobuyryloxy] sulfoscuccinimide ester (sGMBS) by Bruce Wheeler's student,

Betty Ujhelyi (Branch, 2000). The surface treated with 1 mg/ml PEG-Silane did not repel any neurons, while the surface treated with a higher concentration (2 mg/ml) repelled 50% of the neurons for the first 10 minutes. 3) With the help of Raman Shah in Pat Collier's lab at Caltech, PEG-maleimide was linked to the surface with 3-mercaptopropyltrimethoxysilane (MPTMS) (thiol-functionalized glass) (Emoto, 1996; Halliwell, 2001). MPTMS was evaporated onto a pre-cleaned cover-slip (with piranha solution for 60 minutes ataround 80 °C) in a closed jar for 16 hrs at 100 °C. Then, the cover-slip was soaked with 2 ml of 1mM PEG-malimide solution for 10 minutes and thermally cured for 16 hrs at 100°C. Neurons got stuck immediately. 4) PEG-DOPA was then used to treat the surface. 3,4-dihyroxyphenylalaine (DOPA) is an important component of mussel adhesive protein which anchors PEG onto a surface (Dalsin, 2003). The PEG-DOPA solution was prepared by mixing 100 mg of PEG-DOPA powder with 0.1 M 3-(N-morpholino) propanesulfonic acid (MOPS) containing 0.6 M K_2SO_4. Each dish containing 2.5 ml solution inside a closed container was put into a 50° C oven overnight for absorption. Neurons could be lifted for more than 20 minutes. Although the method worked well for repelling neurons, the chemical is not commercially available and the preparation is tedious. All the methods described above use PEG chains as a backbone; however, the effectiveness of inhibiting cellular adhesion varies with the anchoring method used. It seems that effectiveness is related to the surface density of PEG chains (how much PEG can be uniformly packed onto the surfaces). Uncoated regions would expose the underlying material that can provide sites for promoting cell adhesion.

Bovine serum albumin (BSA) was used to treat the surface because it is used to prevent adhesion of enzymes to surfaces, and it is otherwise inert in many biological reactions. The BSA surface was prepared by putting enough 25% BSA in a phosphate buffered saline (PBS) solution to cover half of the surface and allowing the solution to evaporate. The surface successfully repelled most neurons for more than 30 minutes. However, this solution is very viscous and leaves a thick, rough surface which greatly reduced the cell visibility.

PolyHEMA on glass was then investigated. PolyHEMA is normally used to inhibit cell adhesion to surfaces in culture vessels. PolyHEMA solution was prepared by dissolving 40 mg of polyHEMA in 2 ml of 95% EtOH. A few drops of solution were enough to cover the working surface. The solution was allowed to evaporate slowly in a closed jar to prevent rough surface formation. A total of six layers were plated onto the dish. The treated surface works very well, repelling most neurons for more than an hour, and it is optically smooth. This is the method used here for making the surface non-sticky.

4.1.3.1.3 Summary

All of the methods described are summarized in the following comparative table. The table provides the neuron repelling times, as well as benefits and limitations.

Method	Repelling time	Comments
Trypsin	Most neurons ~ 30 min	Terrible cell survival
TrypLE	None	
Papain	40% of neurons ~30 min	Terrible cell survival
Teflon	None	
Corning ultra low attachment dish	None	
Silicone lubricant (Dow corning 200, 300, 360, Slygard 184	50% < 10 min	Hard to spread the drops on the glass surface
PEG-Silane (Gilest)	Most neurons < 5 min	Easy to prepare
PEG-Silane with sGMBS linker	50% ~ 10 min	Hard to prepare
PEG-maleimide with MTPMS linker	None	
PEG-DOPA	Most neurons ~ 20 min	Non-commercial chemical, hard to prepare
BSA	Most neurons ~ 30 min	Easy to prepare, rough surface, inexpensive chemical
PolyHEMA	Most neurons > 1 hr	Easy to prepare, effective, inexpensive chemical

Table 4.1 A summary of all the methods used for preparing “non-sticky” surface.

4.1.4 Culture Media

The plating medium was made by mixing 47 ml of Neuralbasal medium (Gibco 21103-049) with 1 ml of 50X B27 (Gibco 17504-044), 0.125 ml of 200 mM (100X) GlutaMAX (Gibco 35050-079), and 2.5 ml of horse serum (HyClone SH.30074.03). This culture medium can be stored at 4° C for a month.

4.1.5 Live Neurons

Live dissociated E18 primary rat hippocampal cells were prepared by Sheri McKinney. Hippocampi from rat embryos (17 to 18 day gestation) were dissected. For the enzyme treatment, the hippocampal tissues were immersed in 0.25% trypsin in HBSS at 35.5 C° for 15 minutes. Then, the tissues were rinsed with normal plating medium with 5% serum to neutralize the enzyme. The solution was gently triturated to separate the cells. 5% BSA was added to the bottom of the test tube before the spinning to help remove debris from the neurons. The solution was spun for 6 minutes to separate debris from neurons. Finally, the cells were gently re-suspended in the HBSS and stored in the refrigerator at 4 °C.

4.1.6 Cell Plating

The neuron suspension was diluted in Neurobasal to 20 k/100 ul and plated within 12 hours of the dissociation. 20 k neurons were plated onto the PEI treated surface in a grid. The plated neurons were allowed to settle and adhere to the substrate in an incubator for one hour before adding additional culture medium. Half an hour after adding the medium, the dish was moved to the microscope stage for experiments. After each experiment, each culture dish containing 2 ml of culture medium was placed into an incubator. Cultures were maintained in a 5% CO_2 sterile environment at 37 °C. Cultures were fed every 7 days by removing 0.5 ml of old medium and adding 1 ml of fresh medium.

4.2 Irradiating the Neurons

4.2.1 Stationary Cells

Forty cells were selected from a two-hour-old culture plated in a grid, as shown in Figure 4.2; the location of each cell was recorded, and numbered. Cells were selected on the criteria that they were already flattened out on the plating substrate and possessed at least one or two short processes. Individually chosen cells were at least 30 um away from adjacent cells to allow easy identification later on. Ten test cells were then randomly selected from these forty cells. This was done by drawing 10 cards from a 1–40 deck and selecting the cells with corresponding numbers. The remaining cells were a control population. To irradiate a neuron, it was first positioned on the stage at the location of the center of the laser beam. The beam was then brought to a focus to irradiate the

neuron. The beam focus was about 3.7 um above the gold grid, similar to its location when lifting a cell. Test cells were exposed to different laser powers, duration times, and wavelengths.

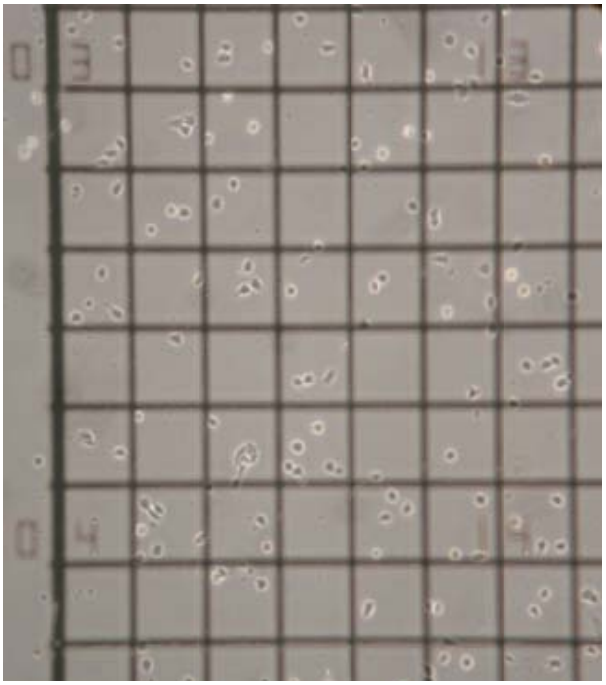

Figure 4.2 Two-hour-old cell culture on a gold grided petri dish

4.2.2 Moved Cells

Thirty control cells were first selected from a two-hour-old culture and the location of each cell was recorded. A low density of cells was then deposited onto the polyHEMA treated surface. The stage was moved to locate a free neuron and bring it to a known location near the control cells. It was assumed that the beam was focused at the center of the cell when it was lifted. Each moved cell was allowed to adhere to the substrate before moving the stage again. Ten test cells were carried from the polyHEMA side to the PEI

side in a dish. Similar to stationary cells, test cells were exposed to a fixed laser power for a set amount of time.

4.2.3 Analysis

Ten to 20 test cells and 30 to 60 background cells were used for each power level and exposure time. Both test cells and background cells were selected from the same culture. The number of dead cells was counted the day after plating for both test and control cells. Cells that had either disappeared or became glial cells were rejected from the pool. For example, if a dead cell body was observed and one cell had disappeared after one day, then the survival would be 8/9 (10 cells to start with). The cell that disappeared was eliminated from the original pool because the status (dead or alive) of this particular cell was unknown. Cell survival at day 1, day 2, and day 3 was observed for both test and control cells.

4.2.3.1 Error Analysis

A cell can either be dead or alive after laser irradiation. The probability (ρ) that a cell will stay alive can be found precisely if a large number of (thousands) test cells was used. However, only a limited number of cells can be used during an experiment. A binomial distribution was assumed and used for error analysis because it provides a good approximation, even with a small sample size. The standard deviation for survival was

calculated using $\frac{\sqrt{n\rho(1-\rho)}}{n}$; ρ is the cell survival (ratio of survived cells over original cells) and n is number of original cells. To minimize variation among dishes, survival was compared between test cells and control cells for each individual culture. The survival ratio of test cells to control cells vs. power intensities and exposure times was measured for both 1064 nm and 980 nm. The error (δq) for the survival ratio was calculated using a standard error propagation method; $\frac{\delta q}{|q|} = \sqrt{(\frac{\delta x}{x})^2 + (\frac{\delta y}{y})^2}$ where δx is the survival error from test cells and δy is the survival error from control cells. There were concerns that the ratio between the two binomial distributions is no longer binomial, and, thus the results may not be accurate. However, methods described by Gart (Gart, 1998) for calculating the ratio between two binomial distributions and standard errors were used for many cases and generated similar results within 5%. Therefore, our method was good enough for accurate calculation of the ratio and standard error.

4.2.3.2 Results

The survival graphs are shown below. Each survival graph has three sets of data corresponding to 1, 2, and 3 days old. The error bar on each data point represents a 67% confidence interval for a binomial distribution. The survival ratio rarely varied for these three days because if a cell was alive after the first day, then most likely it remained alive for the next few days. Cell death was typically seen to occur before day 1 (second day in culture). However, the error bar can sometimes increase after day 1 due to loss of total number of samples.

4.3 Cell Survival Studies

4.3.1 1064 nm Stationary Cells

Cells can be suspended in a medium with a laser power of 9 mW, and can be moved slowly (< 30 um/s) with 17 mw. For this reason, the survival at 17 mw for different exposure times was first investigated. The irradiation time was varied and increased up to 4 minutes while the laser power at the focus was held constant. The survival ratio was close to 100% for all data points (Figure 4.3). This indicates that at a low power level, the cell survival was not affected by increasing exposure time.

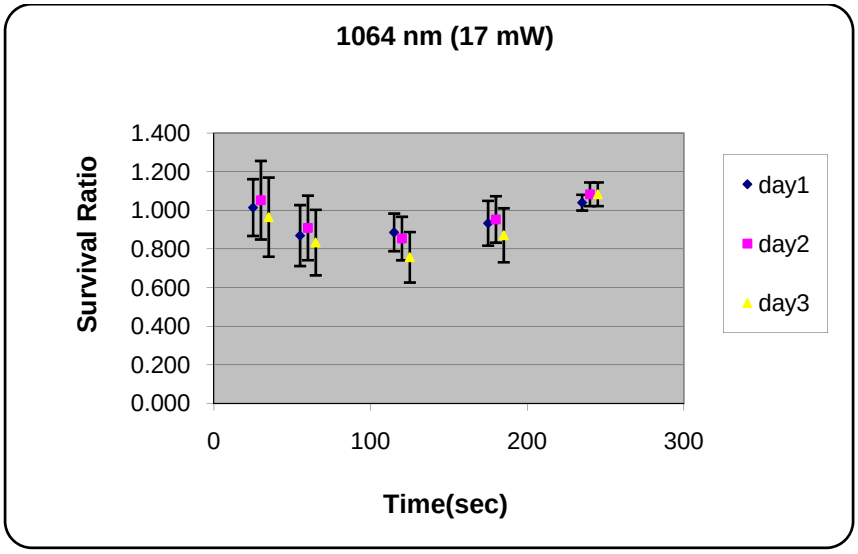

Figure 4.3 Survival ratio vs. exposure time at a fixed laser power of 17 mW

In order to load a neuron quickly, a higher trapping power is needed for the stage to travel over a 3 mm distance (maximum distance between neurons and cages) in 60 seconds or less. Survival at different laser powers (17 mW to 102 mW in increments of 17 mW) was then investigated. For irradiation lasting one minute, neuron survival was

unaffected until laser power at the focus exceeded 51 mw. For power greater than 51 mw, the survival decreased dramatically, as shown in Figure 4.4.

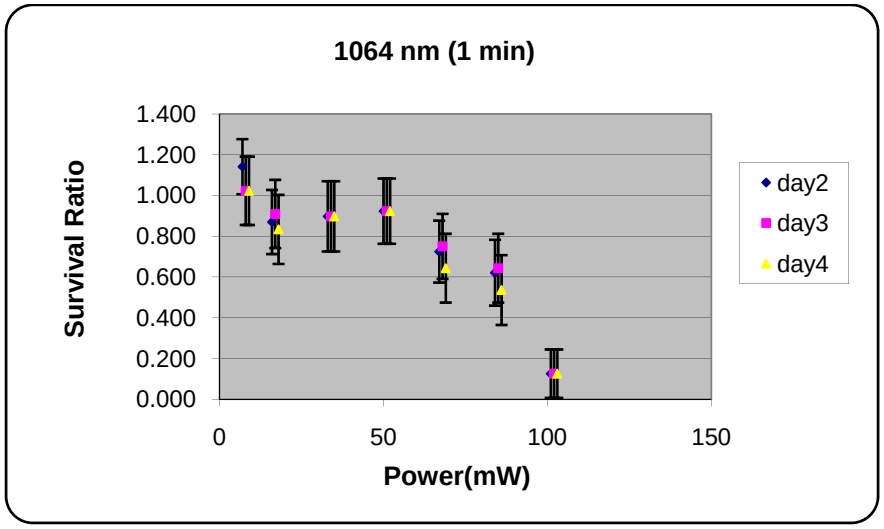

Figure 4.4 Survival ratio vs. laser power for a fixed exposure time of one minute

After finding the threshold for damage, the next step was to study the time that a cell could be irradiated safely at 51 mW. The survival ratio was around 92% for one minute of exposure and 98% for two minutes. However, the survival ratio was poor for four minutes of exposure; about 21% (Figure 4.5).

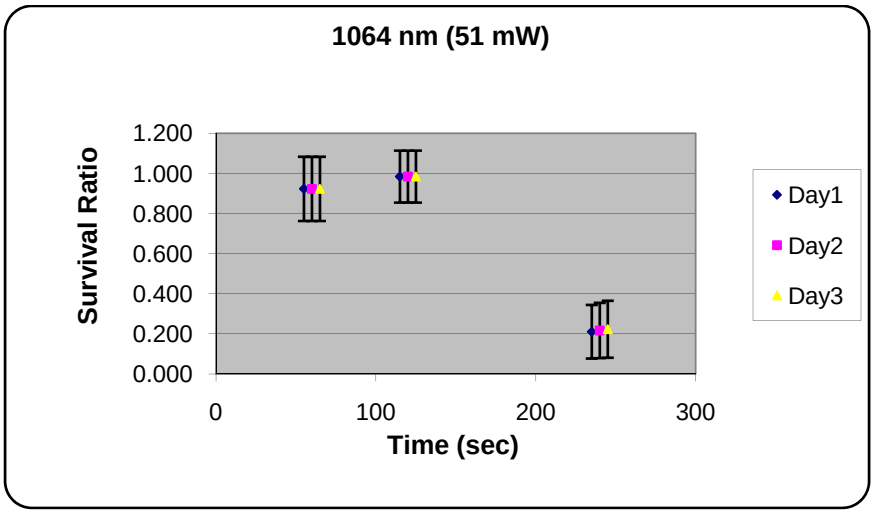

Figure 4.5 Survival ratio vs. exposure time at a fixed laser power of 51 mW

4.3.2 1064 nm Moved Cells

Survival may differ between moved and stationary cells due to different geometries of the cell and the beam. Similar survival studies for moved cells were conducted. First, survival at different laser powers (28 mW, 40 mW, and 51 mW) was studied for a one minute exposure. Both data sets (moved and stationary) are presented for comparison on the graph of Figure 4.6. The dotted purple line was created by connecting the data points from the stationary cells. These powers were approximately the same as the threshold power obtained from experiments for stationary cells. The results were consistent with threshold studies that showed that the cells were not harmed up to a laser power of 51 mW. However, survival for laser powers greater than 51 mW is unknown because the laser module was no longer capable of producing power greater than 51 mW after many hours of usage.

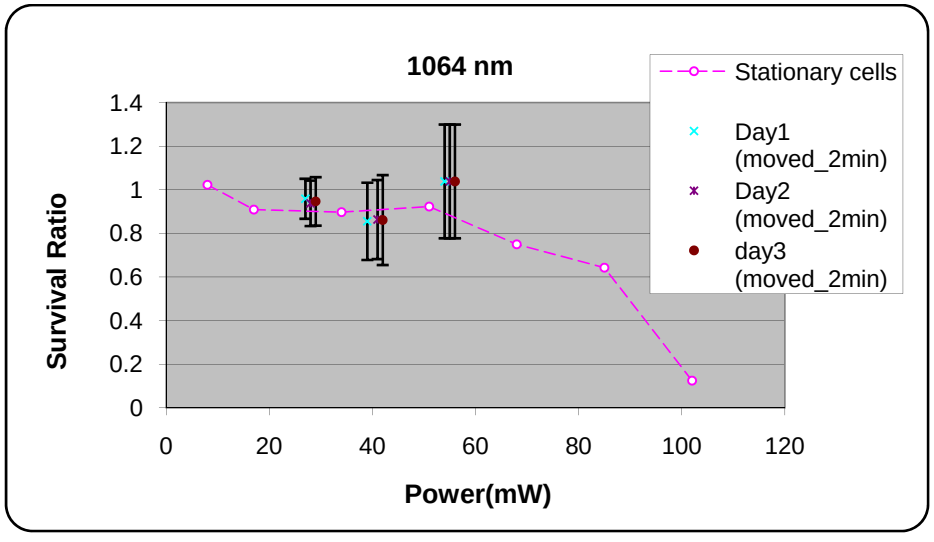

Figure 4.6 Survival ratio vs. power for a fixed exposure time of one minute

For a fixed power of 51 mW, survival at different exposure times (2 minutes, 3 minutes, and 4 minutes) was studied. Once again, two sets of data are plotted on the same graph for comparison (Figure 4.7). The survival ratio was 100% for 2 minutes, 37% for 3 minutes, and 0% for 4 minutes. These results were similar to those of stationary cells. Based on these results, at 1064 nm, 50 mW laser power can be used safely to move neurons at 100 µm/s for two minutes.

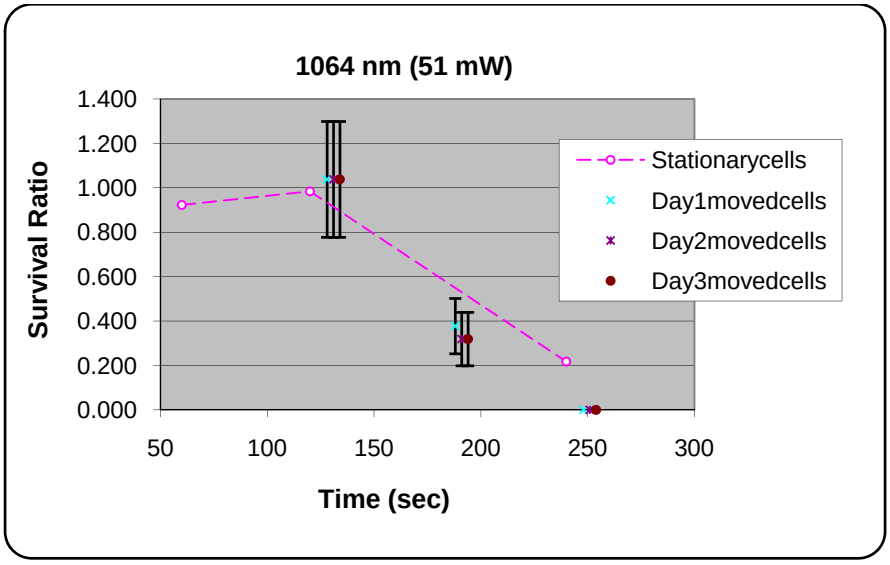

Figure 4.7 Survival ratio vs. exposure time at a fixed laser power of 51 mW

4.3.3 980 nm Stationary Cells

Larger non-damaging trapping power was needed to move neurons faster than 50 um/s for swift loading. Previous work on non-neural cells showed that the 980 nm is less damaging than the 1064 nm. Consequently, similar sets of cell survival experiments were conducted using 980 nm. Survival at different laser powers (51 mW, 68 mW, 99 mW, 130 mW) for one minute was first investigated. It was logical to start the

experiment at 51 mW; the damaging threshold power for 1064 nm. The survival ratio was between to 90 to 100% for all data points (Figure 4.8). The results showed that the survival was not decreased even at a maximum power of 130 mW. However, a damage threshold power was not discovered since the maximum trapping power available at the focus was 130 mW.

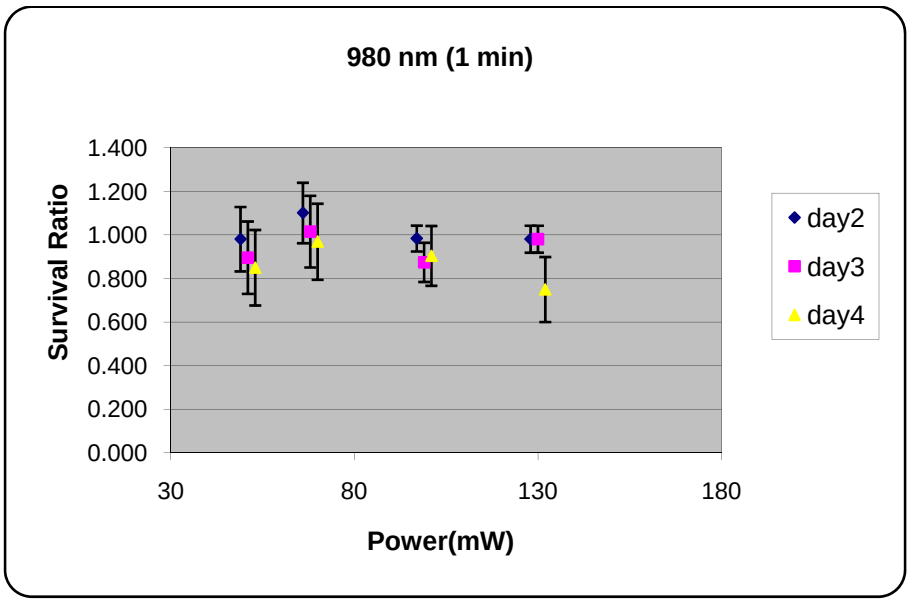

Figure 4.8 Survival ratio vs. laser power for a fixed exposure time of one minute

Survival at different exposure times (2 minutes, 3 minutes, 4 minutes) was then investigated at maximum laser power. The survival ratio was essentially 100% for 2 minutes, 3 minutes, and 4 minutes (Figure 4.9). Therefore, a cell can be irradiated safely at 130 mW for 4 minutes or longer.

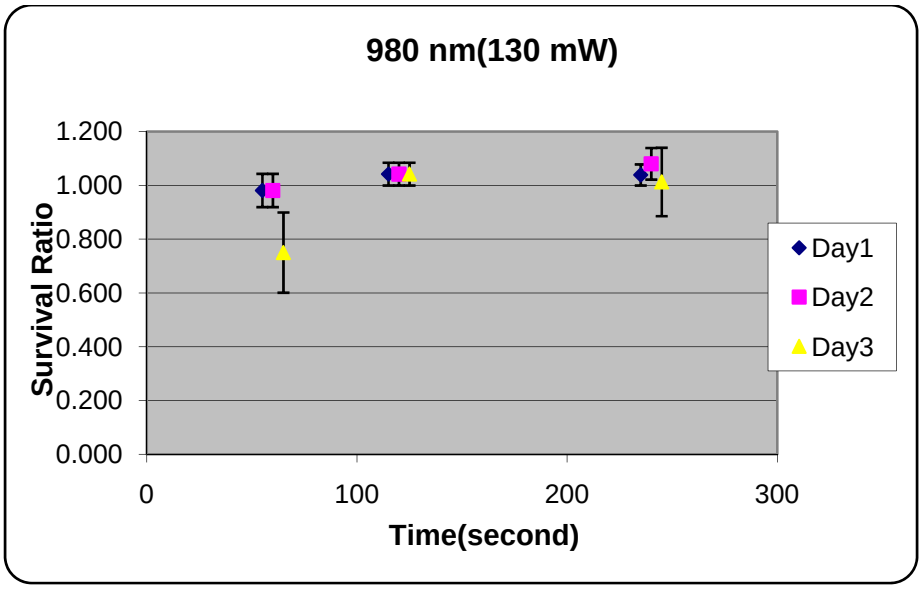

Figure 4.9 Survival ratio vs. exposure time at a fixed laser power of 130 mW

4.3.4 980 nm Moved Cells.

The survival at 980 nm for moved cells was then investigated to confirm the receding results. It was determined previously that a cell was unharmed after 4 minutes exposure at a laser power of 130 mW. A group of neurons was moved using under the same conditions. Once again, two sets of data (moved and stationary cells) were plotted on the same graph for comparison (Figure 4.10). The survival ratio was close to 100%, which is similar to that of stationary cells. From these results, a trapping power of 130 mW can be used to manipulate a neuron safely for 4 minutes.

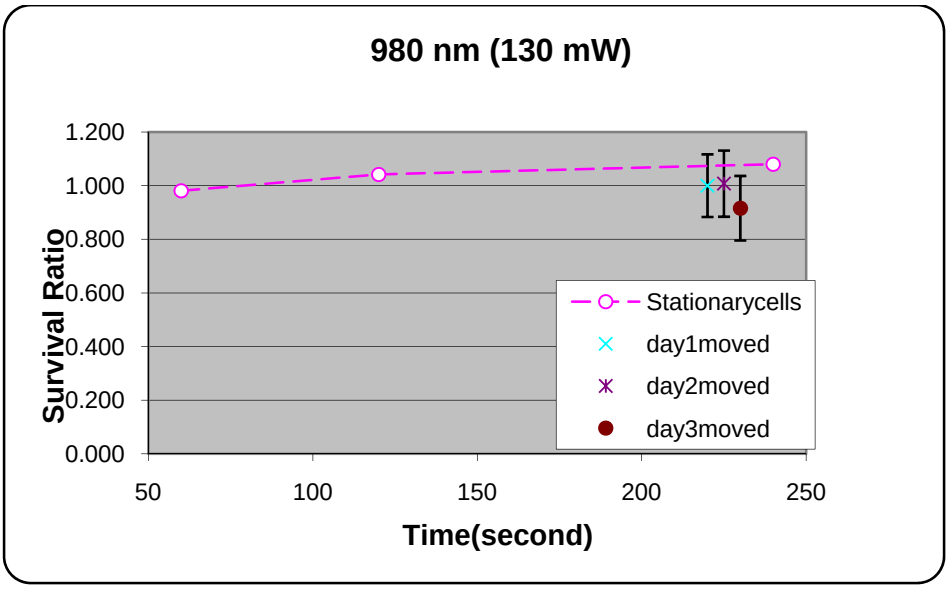

Figure 4.10 Survival ratio vs. exposure time at a fixed power of 130 mW

4.3.5 Summary

4.3.5.1 1064 nm Stationary and Moved Cells

For both stationary and moved cells, cell survival after irradiation was studied as a function of laser power (8 mW to 102 mW) and exposure time (30 to 240 s at a fixed power of 50 mW). For a fixed exposure time of 1 minute, the survival decreased significantly after laser power at the specimen plane exceeded 50 mw. At a fixed power of 17 mw, the survival was not affected by increasing exposure time (up to 240 s). However, at a fixed threshold power of 50 mw, survival was poor at longer exposure times.

4.3.5.2 980 nm Stationary and Moved Cells

For both stationary and moved cells, cell survival after irradiation is independent of laser power up to 130 mW and exposure time up to 4 minutes at a fixed power of130 mW. For a fixed exposure time of 1 minute, the survival varied little with laser power. The survival was not altered even for cells exposed to a maximum power of 130 mW for 4 minutes.

4.4 Localized Heating in Cells

4.4.1 Introduction

For wavelengths between 700 and 1100 nm, biological material and water are very transparent. Only a minute amount of light is absorbed by a neuron and the rest passes through. Thermal effects on cell physiology should still be considered, although the absorption coefficient is small at the trapping wavelength. Some biological specimens are sensitive to temperature changes of even a few degrees. For example, a few degrees temperature change in a sperm cell can affect its motility and thus its fertility. Localized heating at the focus of an optical trap can cause cell temperature to increase several degrees centigrade. The final temperature change is linearly proportional to applied laser power and absorption coefficient. The temperature is raised rapidly about 10 ms after the laser exposure and steady state is reached within several hundred milliseconds. In this section, the temperature rise in hippocampal neurons for 1064 nm and 980 nm system was estimated.

4.4.2 1064 nm

Temperature rise data have been reported previously using temperature sensitive dye (Liu, 1995). An average temperature rise during the first several hundred milliseconds was measured to be 1.15±0.25 °C per 100 mW for Chinese hamster ovary (CHO) cell and 1.45±0.15 °C per 100 mw for multilamellar vesicles. The temperature rise for a neuron is expected to have a similar value to that of a CHO cell because both experiments were performed under comparable conditions; both cell types have similar sizes (8–15um in diameter) and were irradiated by a 1064 nm beam which was brought to a focus by an oil immersion objective with numerical aperture (NA) of 1.25. Temperature rise at 10 s can be extrapolated from Figure 8 in Liu's paper. For a 10 s irradiation, the temperature rise would be 1.65 °C per 100 mW. Although the maximum irradiation time here was 4 minutes, ΔT should not exceed 1.65° C/100 mW (10 s irradiation) because Liu has shown that a thermal equilibrium will be attained in the laser focal volume within the first 10 s.

4.4.3 980nm

The temperature rise in water in the focus of a 985 nm laser was determined by another group (Cellier, 2000). They used an optical technique that detects small changes in the refractive index due to thermal expansion of the heated liquid volume. The objective used in that experiment was also an oil immersion lens with a numerical aperture of 1.25. For a 250 ms irradiation, the temperature rise was extrapolated from the experimental results (Table 2, Cellier, 2000) and determined to be 6.9±0.1 °C/mW which was about

four times higher than the temperature rise using a 1064 nm laser. The temperature rise for a 10 s irradiation was not determined empirically but proposed to be 8.7 °C/100 mW in the same study.

4.4.4 Summary

The temperature rises for hippocampal neurons can be estimated from the existing data and may be different from the actual measured temperature rises, because hippocampal neurons have a different absorption coefficient than CHO cells and culture medium is different than water. Also, the heating effect increases as the sample is trapped further away from the cover-slip (Peterman, 2003). Liu and others did not record the trapping distance from the cover-slip when measuring heating in cells. Finally, although the temperature rises for 1064 nm and 980 nm were determined by different groups using different techniques, the results are still comparable. 980 nm has a four times higher temperature rise because its absorption coefficient in water is four-times-larger than that of 1064 nm (Palmer, 1974). Obtaining the temperature rise experimentally is beyond the scope of this research, however, these values suggest possibly significant rises for the short time of the laser exposure.

4.5 Discussion

The results presented in this chapter show that neural survival depends strongly on laser wavelength, for reasons that remains unknown, and paradoxically appearing to favor the laser with the higher heating. A 980 nm laser is more suitable than a 1064 nm laser for trapping hippocampal neurons. Neurons were unharmed when using the 980 nm laser with trapping power up to 130 mw and exposure time up to 4 minutes. In contrast, survival was poor at 100 mW when a 1064 nm laser was used. For 100 mw and 1 minute exposure, survival ratio was 13% for 1064 nm while survival ratio was 90% for 980 nm after 3 days (shown in Figure 4.11). For 4 minutes laser exposure, survival ratio was 22% (51 mW) for 1064 nm while survival ratio was 100% (130 mW) for 980 nm after 3 days, shown in Figure 4.12. These results are in agreement with studies of other cells that suggest 980 nm is less damaging than 1064 nm (Liang, 1996; Liu, 1996; Neuman, 1999).

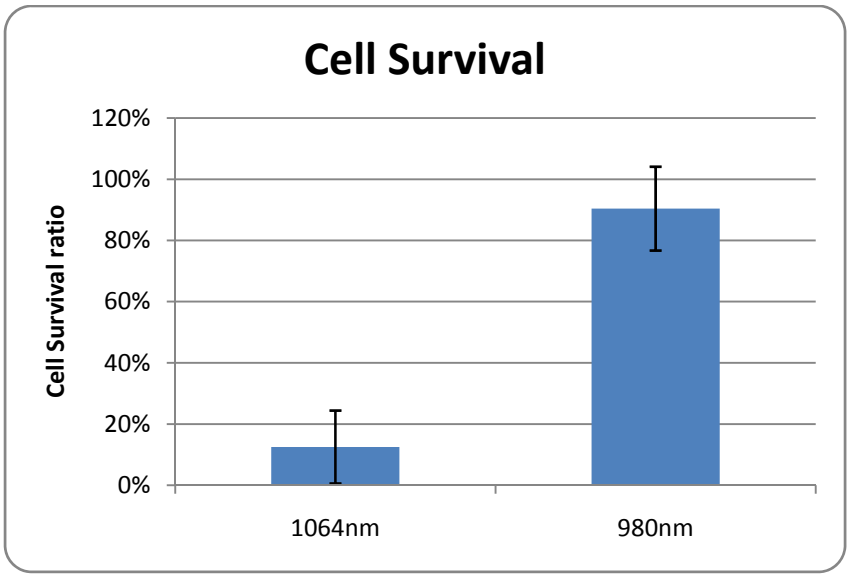

Figure 4.11 Survival ratio comparison between 1064 nm and 980 nm at a laser power of 100 mW for one minute

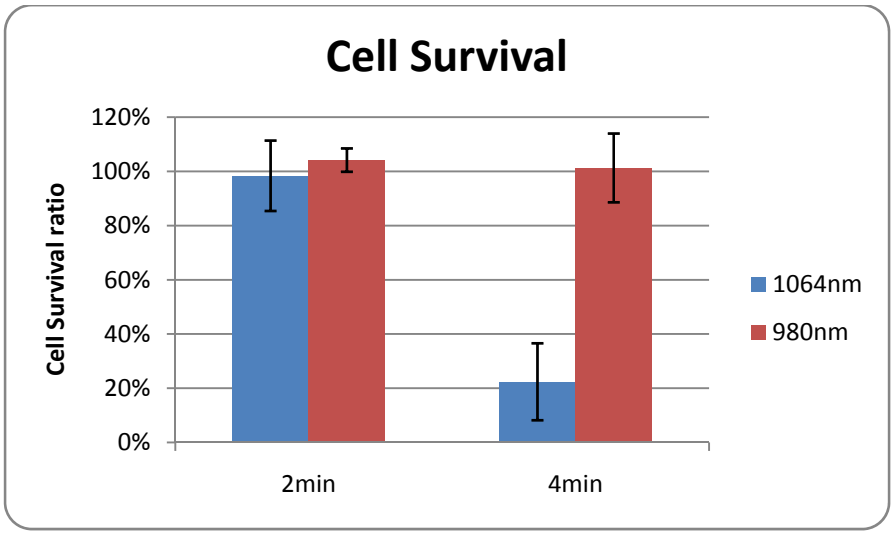

Figure 4.12 Survival ratio comparison between 1064 nm (51 mW) and 980 nm (130 mW) for different exposure times

For 1064 nm, both intensity of laser and duration of exposure affect survival of neurons. It might have been expected that survival is proportional to power flux (time x laser power), but, this was not the case. For example, survival ratio was 13% at 100 mW for one minute (power flux = 6 W-min) and survival ratio was 98% at 51 mW for two minutes (power flux = 6 W-min). Both cases have the same power flux but survival was significantly different. In addition, survival declined only when the laser power was increased above a damage threshold. Even at the threshold, cell death did not occur until the duration of exposure exceeded 2 minutes. This damage threshold seems to be real because irrespective of exposure time, the cell was unaffected by a laser power below the threshold. For 980 nm, the damage threshold was not found and neural survival is independent of laser powers for power under 130 mW.

4.5.1 Possible Cause of Laser-Induced Damage

Laser induced damage cannot be thermal because 980 nm has a higher temperature rise than 1064 nm, and yet it has much better neural survival. Therefore, laser-induced damage to neurons has to be photochemical. Some disastrous events apparently occur in a neuron that cause it to die over a short time (less than 24 hrs) when trapping power exceeds a damage threshold. One study has suggested laser-induced damage is caused by a single-photon absorption process, such as single molecular oxygen (Neuman, 1999), while others believed that damage is due to a two-photo absorption process (Liu, 1996). Either way, absorption of photon(s) is likely to cause some toxic species to build up inside the neuron and accumulate to a level (damage threshold) that is high enough to produce irreversible damage to a neuron. The strong laser wavelength dependency is hard to understand.

An irradiated neuron's surface properties were not altered by the laser because the irradiated neuron did not lose its ability to attach to substrate. Neurons that later died attached to the culture substrate a few minutes after movement indicating that cell death is not instantaneous but rather gradual. Another possibility for cell death is that toxic species might inhibit neural growth rather than causing direct damage to the neuron. An irradiated neuron that is not able to develop normally and grow process would lead to a premature death. This might explain why irradiated neurons die within a 24-hour period. The exact mechanism of cell death cannot be pinpointed here.

4.6 Summary

The 980 nm laser is a better candidate for moving neurons because it is less damaging than the 1064 nm laser. The wavelength dependency of neural survival is not understood. Even though results show that a neuron can be manipulated safely at low power and short exposure time using a 1064 nm laser, the 980 nm laser is still preferred over the 1064 nm laser because 980 nm produces larger, non-damaging trapping power and thus more trapping force. Three reasons for using large trapping powers are that a neuron can be moved at a higher speed, more easily moved over objects that partially block the beam, and cannot escape easily when colliding with debris in medium.

CHAPTER 5

Survival Studies of Loaded Neurons in Neurocages on Glass

This chapter describes the design, construction, and testing of neuro-cages on a 100-um-thick glass cover-slip. The configuration is especially designed for the use of optical tweezers to load the cages. The chapter emphasizes the loading techniques and procedures, and cell survival, growth, and network formation are investigated. The investigations include two versions of a glass-substrate neurochip: with tunnels and without tunnels. The chapter describes the experiments in detail and the survival results are analyzed and discussed.

5.1 Neurocages on Glass

5.1.1 Design

Neurocages on glass similar to those on silicon were fabricated by Angela Tooker from the Tai group at Caltech. Each neurochip consists of 60 cages, spaced at 110 um (center to center) (shown in Figure 5.1). A scanning electron micrograph of a neurocage is shown in Figure 5.2. It consists of a chimney, five anchors, and six tunnels. The

chimney is 40 um in diameter, and 4 um tall. The tunnels are 10 um wide, 1.5 um tall, and either 4 or 25 um long. The cage is fixed onto the glass substrate by five inverted mushroom shaped anchors. The insulation layer is comprised of 4 um of Parylene-C (Tooker, et al, 2004).

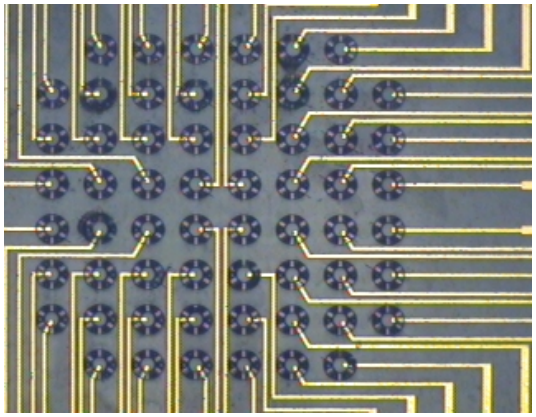

Figure 5.1 60 cages on glass substrate

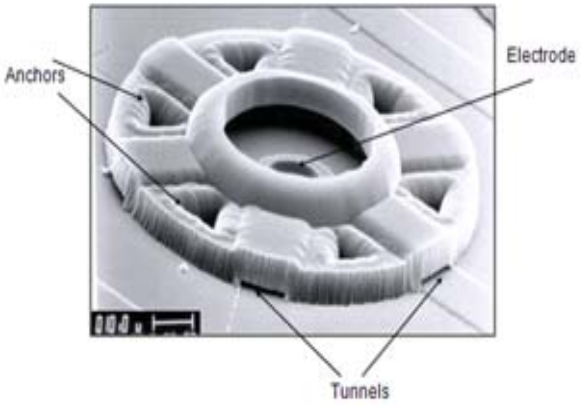

Figure 5.2 Neurocage by SEM

5.1.1.1 Electrode Design

The size of the electrode and electrode lead is limited by the laser tweezers. The laser power is attenuated as the laser focus passes over an electrode or a lead. A neuron would escape from the trap if the power is attenuated too much. It was found that the maximum electrode lead width that the laser tweezers can successfully carry a neuron across is 15 um. The electrode inside the cage is 8 um in diameter and the center of the electrode is offset from the center of the cage by 10 um. This configuration provides a large area where neurons can be placed without the electrode interfering with the laser tweezers. The electrode lead that extends out of the cage is 8 um wide. The lead increases to 20 um

wide where it is 100–200um away from the cage, at which point it can no longer interfere with the laser tweezers.

The layout of electrodes and bonding pads for 60 cages is shown in Figure 5.3. The total area of the chip layout is 1 cm by 2 cm. The design is not symmetrical because two separate regions are needed for loading neurons. The open space on the right is the non-sticky region where the dissociated neurons can be placed and picked up. The space on the left is the plating region where the background and caged neurons can attach and grow.

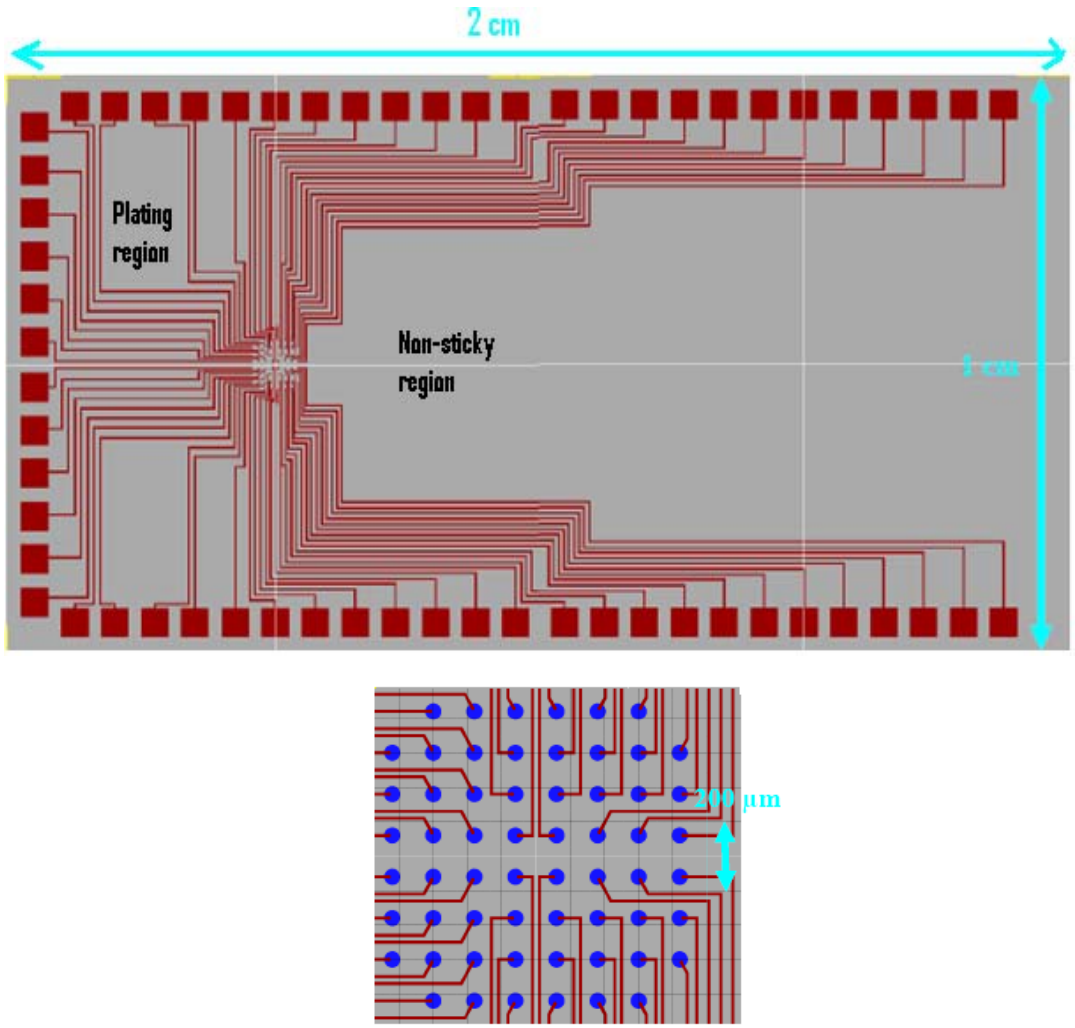

Figure 5.3 The layout of electrodes and detailed view of the 60-electrode system.

5.1.1.1.1 Electrode Design Improvement

In order for the optical trap to lower neurons into the cages more easily without neurons escaping, the electrode was moved away from the center of the cage. This change also solved the following problems: When the electrode was originally located at the center of the cage, caged neurons were hard to visualize. More importantly, neurons avoided the platinum part and ended up elongating and pinning themselves up against the wall of the cage. With the electrode located off the center of the cage, neurons were able to flatten themselves and grow nicely.

5.1.1.1.2 Electrode Resistance and Capacitance

For a neurochip on glass, both electrode and electrode lead were made smaller than in the previous version. The new electrode resistance and capacitance were computed to ensure that the electrode design was suitable for stimulating and recording. A bipolar current source is used to stimulate neurons. The voltage drop across the capacity bilayer of the medium next to the electrode should be kept below 1.2 V to prevent cell damage during stimulation (Maher, 1999). To supply 10 uA for 400 ms without exceeding 1.2 V, the electrode capacitance must be at least 3200 pF. The capacitance after platinization for a 10 um electrode is about 5000 pF (Erickson, 2005). Base on this, the capacitance for an 8 um electrode was calculated to be 3200 pF, which is satisfactory.

To avoid significant signal loss during recording, the electrode capacitance must be much greater than the parasitic capacitances from cables, chip wires, pre-amplifier, shunt, and cross talk. The shunt and cross talk capacitances were calculated to be very

small, and thus, can be ignored. The combined capacitance for cables, chip wires, and pre-amplifier is estimated to be 150 pF (Erickson, 2005). There is only a 4% loss in signal strength for an electrode capacitance value of 3200 pF. Therefore, the electrode and electrode leads are good enough at these sizes.

5.2 Loading Neurons with Laser Tweezers

5.2.1 Culture Dish

A custom rectangular window (8 mm x 17 mm) was cut on the bottom of a 35 mm culture dish (Falcon 1008), as shown in Figure 5.4. The neurochip is slightly larger than the cut, so, it can be bonded underneath the dish where it can cover up the opening. This creates a rectangular well in the culture dish. Sylgard 184 is used to glue the neuro-chip and the dish together. For these experiments, the chip was not connected to external electronics. The focus was on loading, growth, and survival.

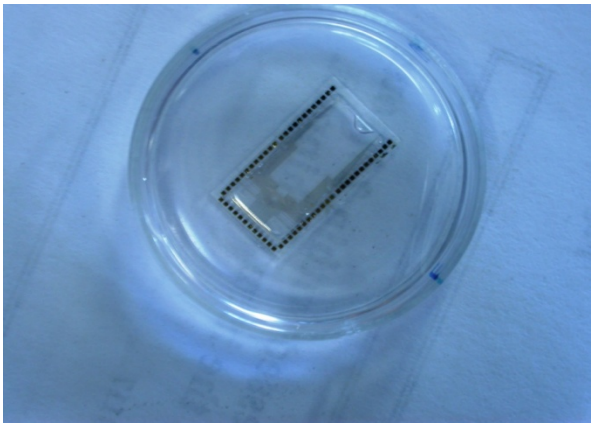

Figure 5.4 Neurocages in a culture dish

5.2.2 Surface Preparation

Proper surface preparation is needed for successful loading and growing neurons. The culture was prepared such that that half of the surface containing neurocages was treated with 0.05 % PEI and other half was treated with polyHEMA. The process is the same to the one described in Chapter 4 except that the PolyHEMA surface was prepared very close to the cages, about 1 to 2 mm away. This shortens the loading time because neurons only need to travel a short distance to get to their destinations.

5.2.3 Loading Procedure

First, a group of background neurons, 20 k in 100 ul of culture medium, were plated in a drop on the PEI side near the cages. They conditioned the culture medium. The background neurons were allowed to settle and stick to the substrate surface for five minutes before moving the dish into the incubator. After a half hour incubation, a drop (about 100ul) of medium was used to wet the cages and the dish was put back into the incubator for about 30 minutes. This allowed bubbles to move out from the cages. Free neurons, 2 k in 100 ul of culture medium, were then placed on the PolyHEMA-treated surface a few millimeters away from the cages. Figure 5.5 shows the overall picture schematically. The neurons were allowed to settle for five minutes before the dish was placed onto the stage for experiment.

The cage location for each chip was calibrated before loading neurons. This was done by finding two specific cages and inputting their stage coordinates manually into the

computer. Based on these two points the location of the rest of the cages was computed in LabVIEW. The mechanical stage was used to manually search and bring a neuron over the beam focus. Once the neuron was trapped and lifted by the tweezers, the stage was moved to position it above a cage by the computer. Finally, the neuron was lowered into the bottom of the cage by the optical trap.

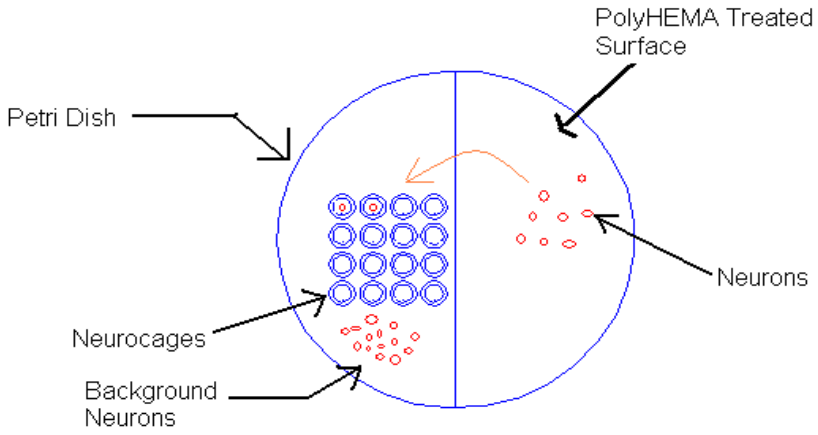

Figure 5.5 The cartoon shows the steps that are involved for loading neurons (not drawn to scale).

5.2.4 Discussion

Thirty to forty neurons were loaded into cages per hour using tweezers at 980 nm. The speed for moving neurons was 60 um to 80 um per second. Finding free single neurons on the PolyHEMA side took some time because neurons tend to stick together after a few minutes of deposition. Neurons were lifted about 50 um above the substrate and brought to the top of a cage quickly (< 30 sec) by the computer automated stage once they were found. A neuron was then lowered into the cage by the trap and was allowed

to settle and stick to the substrate for 10 seconds before the stage was moved to locate another cell. It was important that the medium is free from debris because debris can block the top of a cage or knock the neuron out of the trap.

5.3 Cell Survival in Neurocages on Glass Substrate

5.3.1 Neurocages with Tunnels

Neurons were first loaded into the cages with tunnels, as shown in Figure 5.2. Their growth was observed after 1, 2, and 3 days *in vitro*. The neurons were flattened on the substrate and growing inside the cage. They looked healthy but the processes were not growing out the tunnels. It was very puzzling because the neurons grow well on silicon chips (with the same configuration of the neurocages). The caged neurons on silicon substrates had a 70% survival rate after one week *in vitro*. It was believed the tunnels on glass were not opened due to an imperfection in the fabrication process. After knocking out the tunnels with a pipet, neurons were able to grow on the area where the tunnels used to be. To eliminate this problem, cages without tunnels were then fabricated and tried.

5.3.2 Neurocages without Tunnels

Neurons were loaded into the cages without tunnels, and exhibited normal growth. Their processes grew out of the tunnels and formed networks with neighboring

neurons, and they did not escape from the cages. Even just after 1 day *in vitro*, the processes had already began to grow out of the tunnels. Figure 5.6 shows a three-day-old culture with seven live neurons trapped inside the neurocages. The black arrows label the neurons inside the neurocages and the white arrows label a few of the background neurons. Figure 5.7 shows an enlarged picture of two neurons in cages with processes growing out the tunnels. The black arrows label the cell bodies and yellow arrows label some processes. Initially, it was thought that neurons might escape if cages had no tunnels. However, this was not the case. Only a few out of several hundred neurons escaped from these cages.

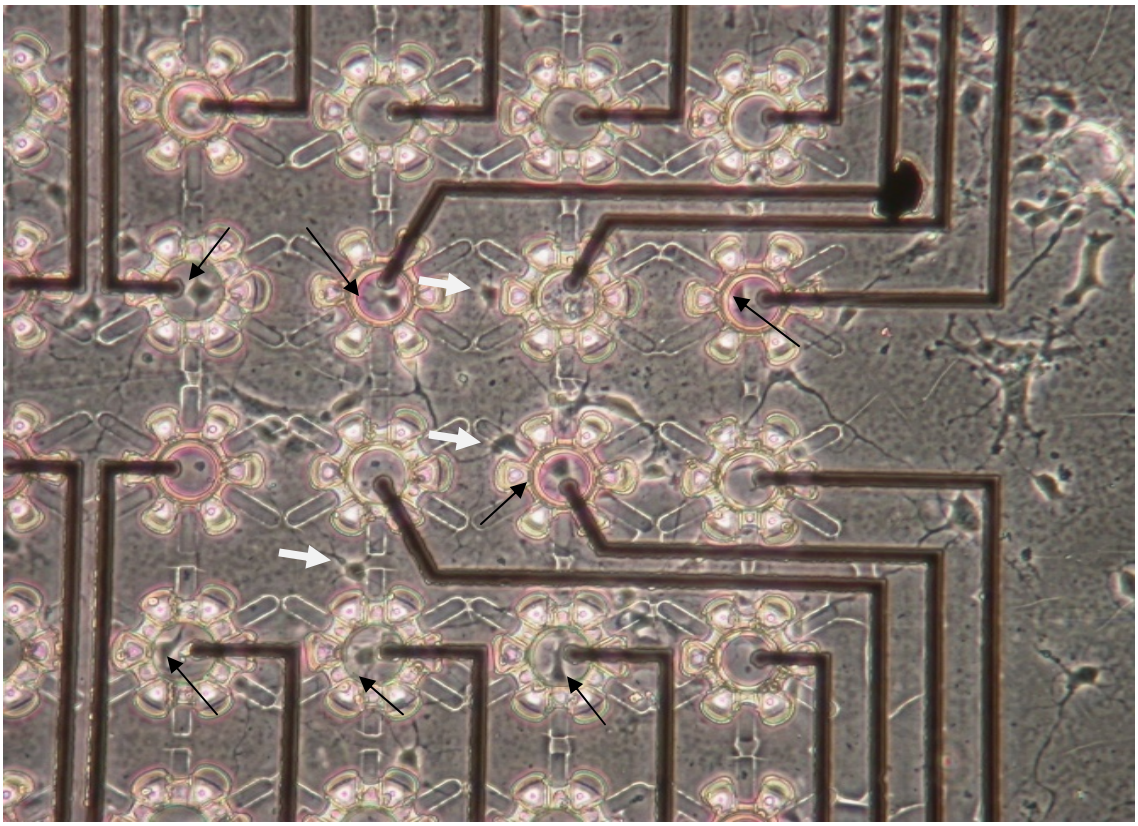

Figure 5.6 Neurons in the cages (three-day-old culture)

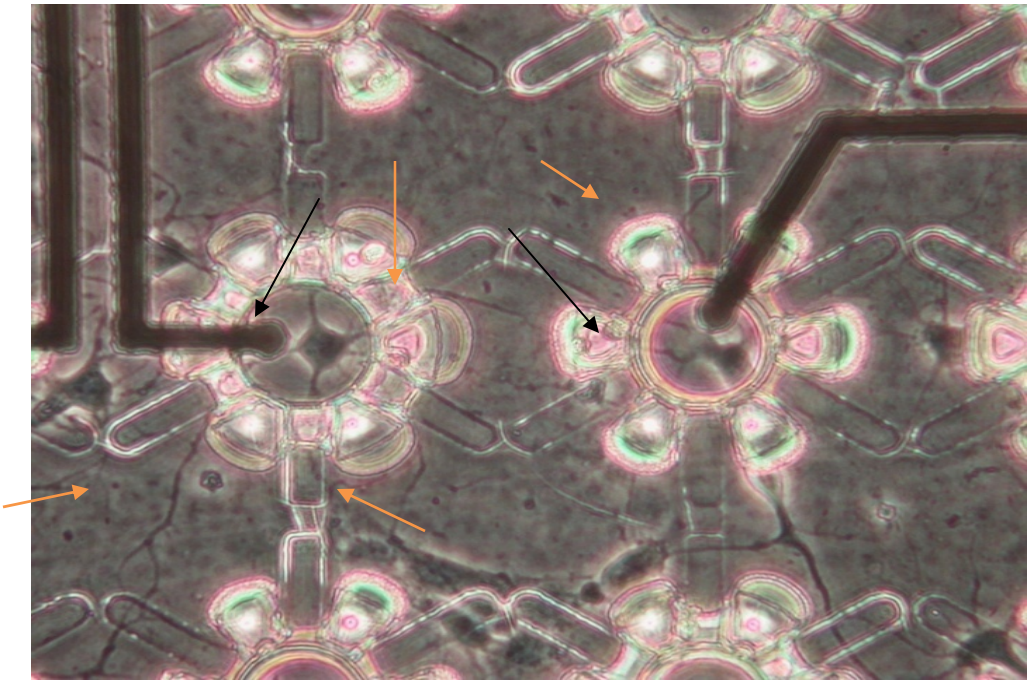

Figure 5.7 Enlarged view of two neurons in two cages

5.3.3 Cell Selection

The test cells (average 10 cells per dish) were selected from the non-adhesive side and loaded into cages with laser tweezers. It was very hard to distinguish the glial cells and the dead cells from the live cells. Small, dark, and shriveled-up neurons were not selected because they might be dead or unhealthy. The cells that were significantly larger than other cells were not selected. The neurons with average size, and a light and semi-smooth surface were normally selected as test cells. When carrying the culture dish to the microscope, some of the neurons migrate from the non-adhesive side to the PEI side and settle down near the cages. The neurons near the cages were randomly selected as control neurons (average 15 cells per dish) because they came from the same group as the test neurons.

5.3.4 Trapping Parameters

From Chapter 4, it was learned that neurons can be safely moved at 130 mw for 4 minutes using the 980 nm laser and 50 mW for 2 minutes using the 1064 nm laser. To avoid laser-induced damage during cell survival studies in cages, non-damaging power was used for each wavelength. The loading time for each cell was less than 2 minutes for both wavelengths. A laser power of 130 mW (max power at the specimen plane) was normally used to move neurons for the 980 nm laser and a power of 34 mW or less was used for the 1064 nm laser.

5.3.5 Error Analysis and Graph Interpretation

The binomial distribution previously described in Chapter 4 was used for the error analysis. Survival probability vs. time was first studied, and the results are plotted in Figure 5.8. This is similar to that for background neurons and shows that the neurochips are bio-compatible, but does not provide anything about effect of cage confinement on neurons. To investigate the effect of cage confinement on neurons, the survival ratio between caged and background neurons versus time was then determined, and the results are plotted in Figure 5.9. Once again, the error bar on each data point represents a 67% confidence interval for a binomial distribution. The error bar on day 10 in each graph is bigger than error bar of other days because fewer background and test neurons were available. Most dishes were dyed for imaging after 5 days and discarded afterward. In

addition to that, the background neurons were hard to track for long times in the remaining dishes.

5.3.6 Results

For 980 nm, cell survival after day 3 was about 70% and survival after day 10 was about 50% (Figure 5.8), and was linearly dependent with time for the first 10 days. However, after the results were normalized by the control cell survival, the survival ratio was close to 90 to 100% for all the days (Figure 5.9), and was independent of time. This indicates that these cages on a glass substrate are appropriate for growing neurons.

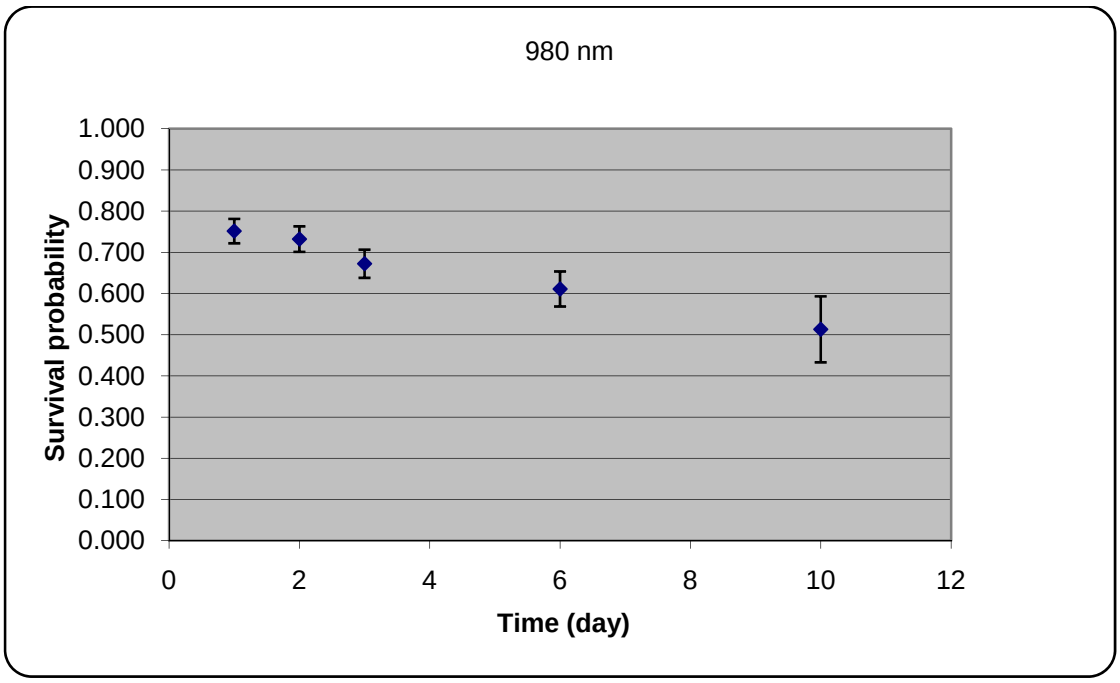

Figure 5.8 Survival vs. time

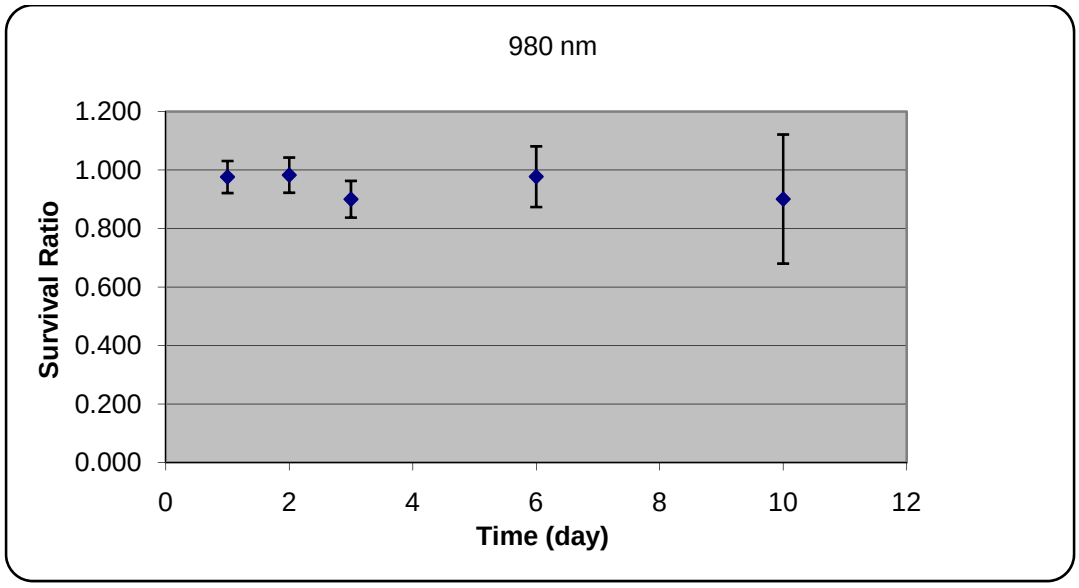

Figure 5.9 Survival ratio vs. time

Cell survival in cages for 1064 nm at a suitable laser power (<51 mW) was then investigated. Two sets of data (1064 nm and 980 nm) were plotted on the same graph for comparison (Figure 5.10 & 11). These results were in agreement with 980 nm survival studies. Again, this shows that 1064 nm can be used to move neurons when it is used properly.

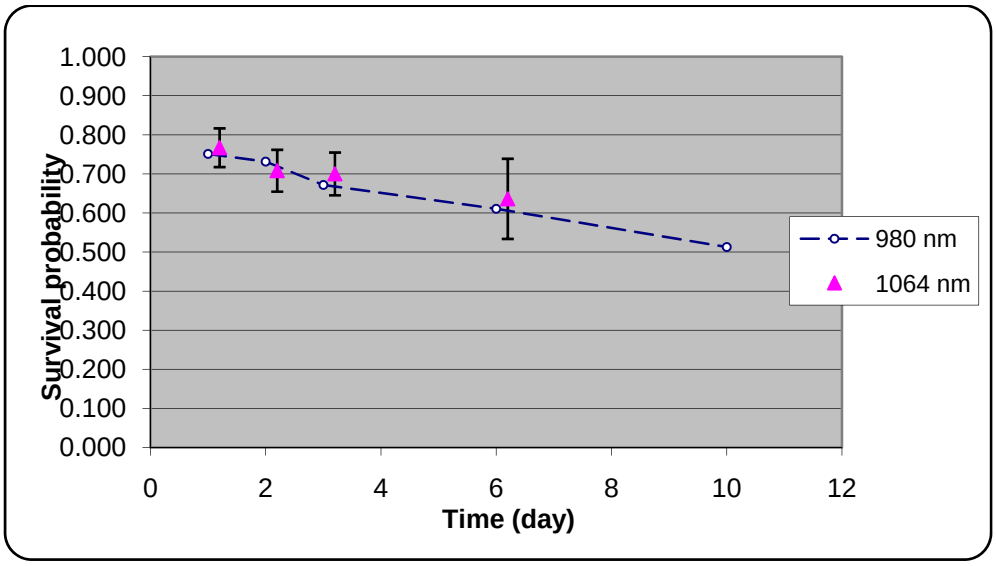

Figure 5.10 Survival vs. time

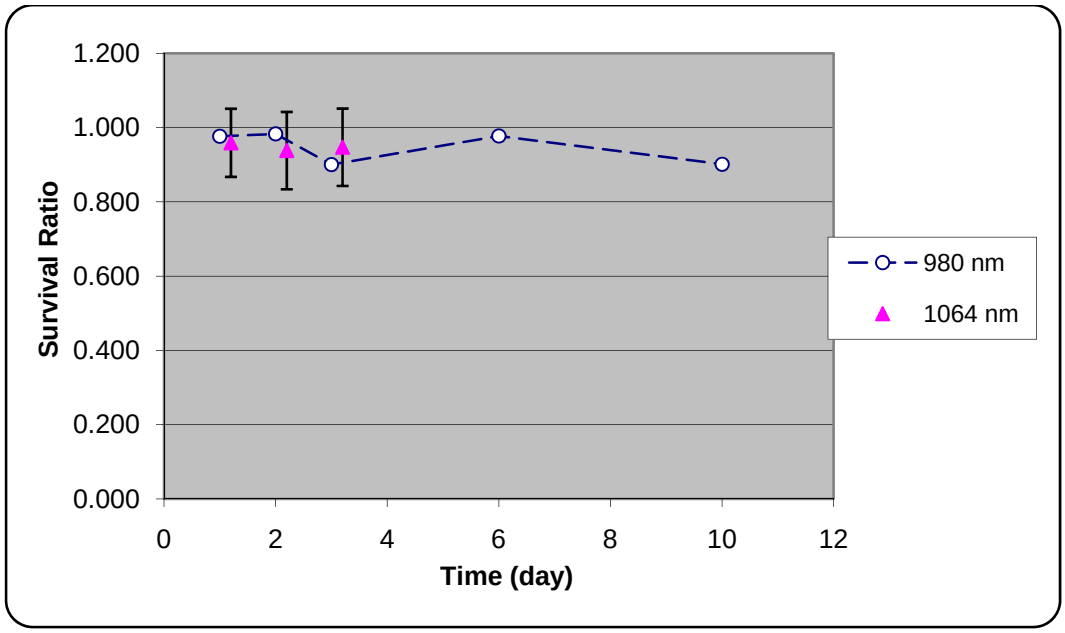

Figure 5.11 Survival ratio vs. time

Finally, the survival ratio between irradiated neurons and caged neurons was compared for both 1064 nm and 980 nm (Figure 5.12 & 5.13). No survival differences were found between irradiated and caged neurons in both cases. Therefore, cage confinement has no significant effects on cell survival and growth.

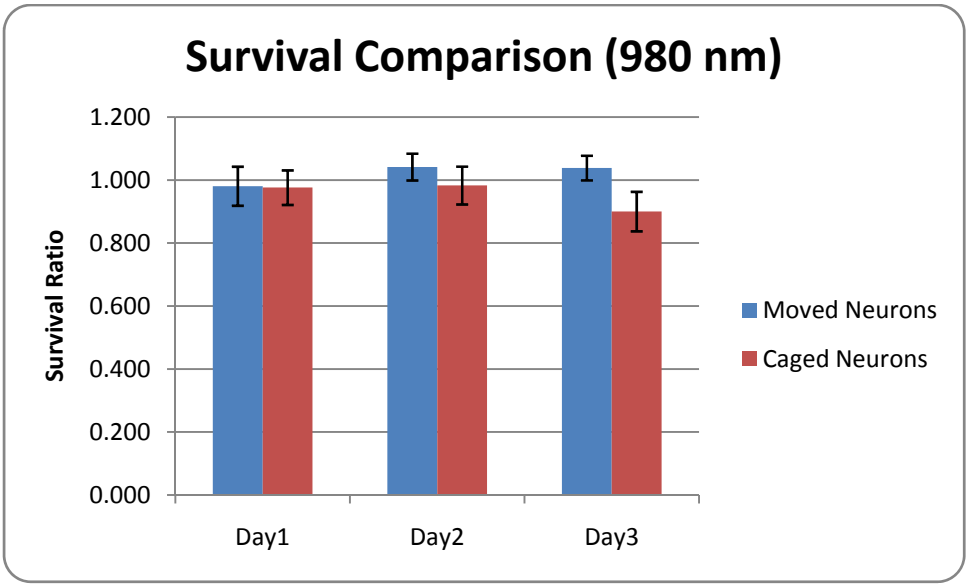

Figure 5.12 Survival ratio comparison between irradiated neurons and caged neurons

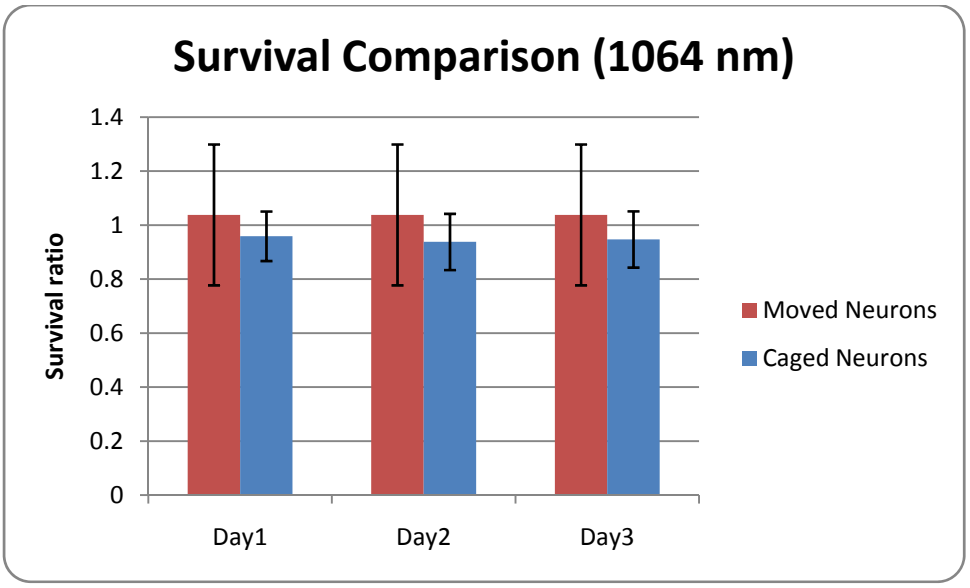

Figure 5.13 Survival ratio comparison between irradiated neurons and caged neurons

5.4 Summary

The neurocages without tunnels have been proved to be useful for studying neural work. A colleague in the Pine lab (Jon Erickson) used similar cages on silicon to trap neurons and he was able to stimulate them and record their responses. The design for cages on glass is almost identical to cages on silicon except for the size of the electrode. The estimates in the previous section showed that this difference is not substantial enough to create problem in stimulating and recording. Therefore, we expect that networks formed on glass substrates can be probed, tested, and investigated in the same manner as those on silicon. They are also mechanically robust and can be repeatedly rinsed with water and bleach, and reused.

References

Ashkin, A., *Acceleration and Trapping of Particles by Radiation Pressure*. Physical Review Letters 1970; 24:156–159.

Ashkin, A., Dziedzic, J. M., *Optical Levitation by Radiation Pressure*. Applied Physics Letters 1971;19:283–285.

Ashkin, A., *Trapping of atoms by resonance radiation pressure.* Physical Review Letters 1978;40:729–732.

Ashkin, A., Dziedzic, J. M., Chu, S., Bjorkholm, J.E., *Observation of a Single-Beam Gradient Force Optical Trap for Dielectric Particles*. Optics Letters 1986;11:288–290.

Ashkin, A., Dziedzic, J. M., *Optical trapping and manipulation of single cells using infrared laser beams.* Nature 1987;330:769–771.

Ashkin, A., Dziedzic, J. M., Yamane, T, *Optical trapping and manipulation of viruses and bacteria.* Science 1987;235:1517–1520.

Ashkin, A., Dziedzic, J. M., *Internal cell manipulation using infrared laser traps.* Proceedings of the National Academy of Sciences USA 1989;86:7914–7918.

Ashkin, A., *Forces of a Single-Beam Gradient Laser Trap on a Dielectric Sphere in the Ray Optics Regime.* Biophysical Journal 1992;61:569–582.

Ashkin A., *Optical trapping and manipulation of neutral particles using lasers.* Proceedings of the National Academy of Sciences USA 1997;94:4853–4860.

Bern, M. W., Aist, J. R., Wright, W. H., Liang, H., *Optical trapping in animal and fungal cells using a tunable, near-infrared titanium-sapphire laser.* Experimental Cell Research 1992;198:375–378.

Block, S. M, Goldstein, L. S. B., Schnapp, B.J., *Bead movement by single kinesin molecules studied with optical tweezer.* Nature 1990;348:348–352.

Block, S. M., *Making light work with optical tweezers.* Nature 1992;360:493–495.

Block, S. M., Svodoba, K., *Biological applications of optical forces.* Annual Review of Biophysics and Biomolecular Structure 1994;23:247–285.

Block, S. M., *Nanometers and Piconewtons: The Macromolecular Mechanics of Kinesin.* Trends in Cell Biology 1995;5:169–175.

Block, S. M., *Constructing optical tweezers.* Cell Biology: A Laboratory Manual, 1998.

Branch, D. W., Wheeler, B. C., Brewer, G. J., Leckband, D. E**.,** *Long-term maintenance of patterns of hippocampal pyramidal cells on substrates of polyethylene glycol and microstamped polylysine.* IEEE Transaction on Biomedical Engineering 2000;47:3:290–300.

Cellier, P. M., Conia, J., *Measurement of Localized Heating in the Focus of an Optical Trap.* Applied Optics 2002;39**:**3396–3407.

Dalsin, J. L*.,* Hu, B-H., Bruce, P. L., and Messersmith, P. B**.,** *Mussel Adhesive Protein Mimetic Polymers for the Preparation of Nonfouling Surfaces.* Journal of the American Chemical Society 2003;125:4253–4258.

Edidin, M., Kuo, S.C., Sheetz, M. P., *Lateral Movements of Membrane Glycoproteins Restricted by Dynamic Cytoplasmic Barriers*. Science 1991;254:1379–1382

Emoto, K., Harris, J. M., and Alstine, J. M. V., *Grafting Poly(ethylene glycol) Epoxide to Amino-Derivatized Quartz: Effect of Temperature and pH on Grafting Density*. Analytical Chemistry 1996;68:3751–3757.

Finer, J. T., Simmons, R. M., Spudich, J. A., *Single myosin molecule mechanics: piconewton forces and nanometer steps*. Nature 1994;368:113–119.

Gart, J.J., Nam, J., *Approximate Interval Estimation of the Ratio of Binomial Parameters: A Review and Correction for Skewness.* Biometrics 1998*;*44:No.2:323–338.

Gross. G.W., E. Rieske, G.W. Kreutzberg, and A. Meyer, *A New Fixed-Array Multi-Microelectrode System Designed for Long-Term Monitoring of Extracellular Single Unit Neuronal Activity* in vitro. Neuroscience Letters 1997;6:101–105.

Gross, S. P., *Application of optical traps in Vivo*. Methods in Enzymology 2003;361:162–174.

Halliwell, C. M., Cass, E. A. G., *A Factorial Analysis of Silanization Conditions for the Immobilization of Oligonucleotides on Glass Surfaces*. Analytical Chemistry 2001;73:2476–2483.

He, Q., E. Meng, Y.C. Tai, C.M. Rutherglen, J. Erickson, and J. Pine, *Parylene neuro-cages for live neural networks study*. Transducers 2003;995–998.

Jimbo Y., T. Tateno, and H.P.C. Robinson, *Simultaneous Induction of Pathways-Specific Potentiation and Depression in Networks of Cortical Neurons*. Biophysical Journal 1996;76:670–678.

Konig, K, Liang, H., Berns, M. W., Tromberg, B. J., *Cell damage by near-IR microbeams.* Nature 1995;377:20–21.

Konig, K., Liang H., Berns, M.W., Tromberg, B. J., *Cell damage in near-infrared multimode optical traps as a result of multiphoton absorption.* Optics Letters 1996;21:14.

Kuo, S. C., *Optical tweezers: A practical guide.* Journal of Microscopy Society of America 1995;1:65–74.

Leitz, G., Fallman, E., Tuck, S., Axner, O**.,** *Stress Response in Caenorhabditis elegans Caused by Optical Tweezers: Wavelength, Power, and Time Dependence.* Biophysical Journal 2002;82:2224–2231.

Liang, H., Wright, W. H., Cheng, S., He, W., Berns, M.W., *Micromanipulation of chromosomes in PTK-2 cells using laser microsurgery (optical scalpel) in combination with laser-induced optical force (optical tweezers).* Experimental Cell Research 1993;204:110–120.

Liang, H., Vu, K. T., Krishman, P, Trang, T.C., Shin, D., Kimel, S., Berns, M.W., *Wavelength dependence of cell cloning efficiency after optical trapping*. Biophysical Journal 1996;70;1529–1533.

Liu, Y., Cheng, D. K., Sonek, G. J., Berns, M. W., Chapman, C. F., *Evidence for localized cell heating induced by infrared optical tweezers.* Biophysical Journal 1995;68:2137–2144.

Liu, Y., Sonek, G. J., Bern, M. W., Tromberg, B. J., *Physiological monitoring of optically trapped cells: assessing the effects of confinement by 1064-nm laser tweezers using microfluorometry.* Biophysical Journal 1996;71:2158–2167.

Maher M. P., Pine J., Wright J., Tai Y-C., *The neurochip: a new multi-electrode device for stimulating and recording from cultured neurons*. Journal of Neuroscience Methods 1999;87:45–56.

McGloin, D., *Optical Tweezers: 20 years on*. Philosophical Transaction of Royal Society A 2006;64:3521–3537.

Meister M., J. Pine, and D. Baylor, *Multi-Neuronal Signals from the Retina: Acquisition and Analysis*. Journal of Neuroscience Methods 1994;51:95–106.

Meng, E., Y.C. Tai, J. Erickson, and J. Pine, *Parylene technology for mechanically robust neuro-cages*. MicroTAS 2003:1109–1112.

Misawa, H., M. Koshioka, K. Sasaki, N. Kitamura and H. Masuhara, *Three-dimensional optical trapping and laser ablation of a single polymer latex particle in water*. Journal of Applied Physics 1991;70:3829–3835.

Morefield S., E. Keefer, K.D. Chapman, and G.W. Gross, *Drug Evaluations Using Neuronal Networks Cultured on Microelectrode Arrays*. Biosensors and Bioelectronics 2000;15:383–396.

Neuman, K. C., Chadd, E. H., Liou, G. F., Bergman, K., Block, S. M., *Characterization of photodamage to Escherichia coli in optical traps*. Biophysical Journal 1999;77:2856–2863.

Palmer, K. F., William, D., *Optical properties of water in the near infrared.* Journal of Optical Society of America 1974;64:1107–1110.

Perkin, T. T., Quake, S. R., Smith, D. E., Chu, S., *Relaxation of a single DNA molecule observed by optical microscopy.* Science 1994;264:822–826.

Peterman, E. J. G., Gittes, F. and Schmidt, C. F., *Laser-Induced Heating in Optical Traps***.** Biophysical Journal 2003;84:1308–1316.

Pine J., *Recording Action Potentials from Cultured Neurons with Extracellular Microcircuit Electrodes*. Journal of Neuroscience Methods 1980;2:19–31.

Sacconi, L., Stringari, C., Antolini, R., Pavone, F. S., *Optical micromanipulations inside yeast cells.* Applied Optics 2001;44:11:2001–2007.

Seeger, S, Monajembashi, S., Hutter, K. J., Futterman, G., Wolfrum, J., Greulich, K. O., *Application of laser optical tweezers in immunology and molecular genetics*. Cytometry 1991;12:497–504.

Steubing, R. W., Cheng, S., Wright, W. H., Numajiri, Y., Berns, M. W., *Laser induced cell fusion in combination with optical tweezers: the laser cell fusion trap*. Cytometry 1991;12:505–510.

Svoboda, K., Block, S. M., *Force and velocity measured for single kinesin molecules.* Cell 1994;77:773–784.

Thomas C.A., Springer, P.A., Loeb, G.E., Berwald-Netter, Y., and Okun, L.M., *A miniature microelectrode array to monitor the bioelectric activity of cultured cells*. Experimental Cell Research 1972;74:61–66.

Towne-Anderson, E, St. Jules, R. S., Sherry, D. M., Lichtenberger, J., Hassanain, M., *Micromanipulation of Retinal Neurons by Optical Tweezers.* Molecular Vision 1998;4:12.

Wang, X. F., Lemasters, J. J., Herman, B., Kuo, S. C., *Multiple microscopic techniques for the measurements of plasma membrane lipid structure during hypoxia*. Optical Engineering 1993;32:284–290.

Appendix A

Laser Systems

A. 1064 nm Laser System

The 1064 nm laser tweezers system consists of a laser module, a microscope assembly, a beam expander assembly, a beam steerer accessory, and a beam reflector assembly. Each assembly, shown in Figure A.1, is labeled, and the parts that belong to the same assembly have the same first number but different letter. (For example, 1a and 1b belong to the same assembly.)

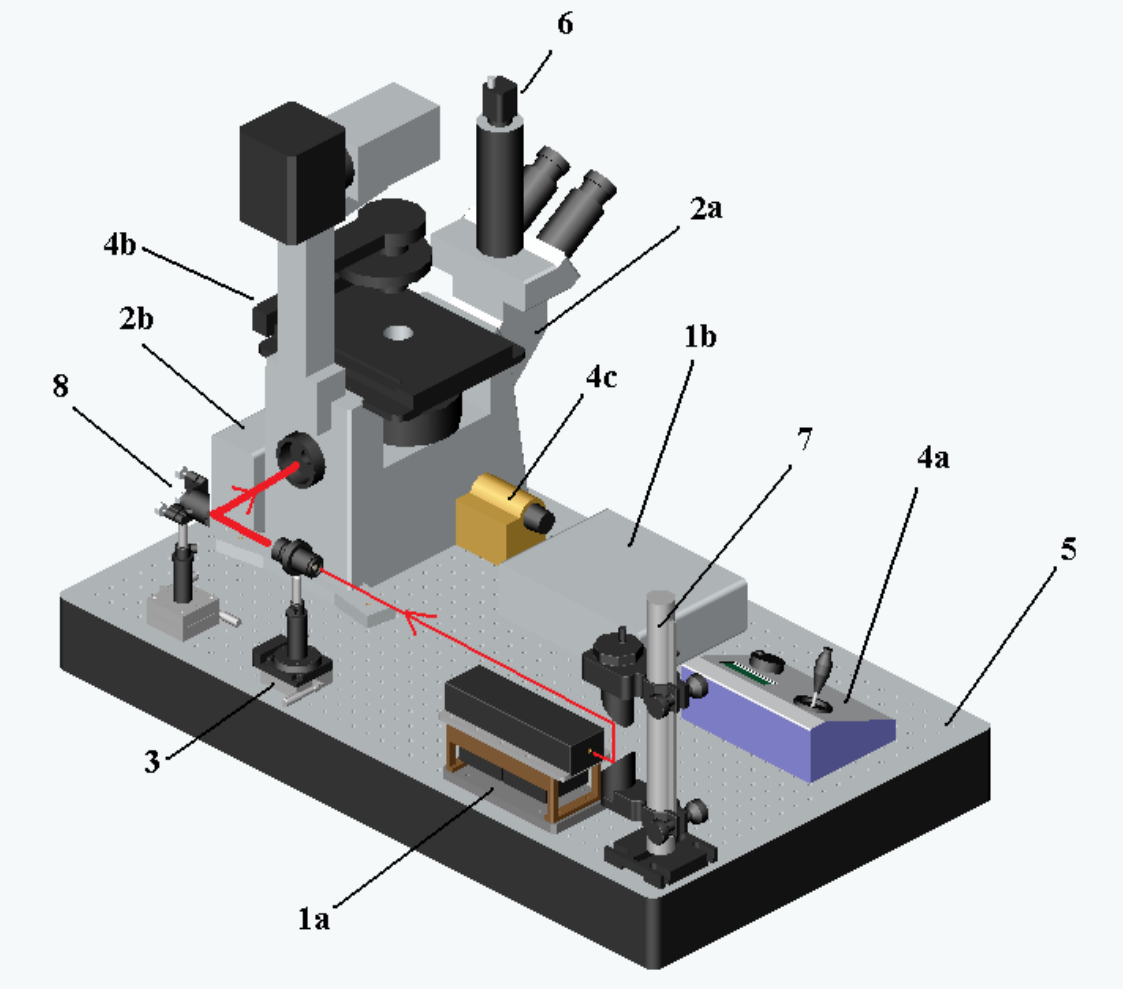

Figure A.1 Each assembly in the 1064 nm laser tweezers system is labeled with a number.

1a—1064 nm continuous-wave IR laser system

The 1064 nm laser module, shown in Figure A.2, includes a laser head, a laser base, two fans, and a beam center locator. The laser head is in close contact with the heat sink which is cooled by the two fans. The beam center locator is used to position the laser module with respect to the air table.

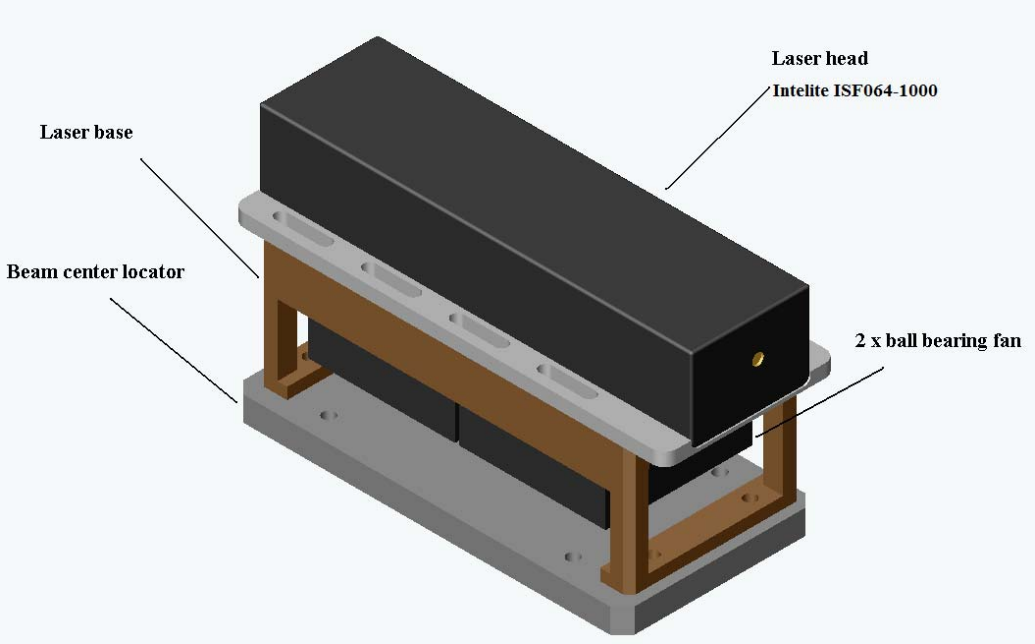

Figure A.2 1064 nm continuous-wave IR system

1b—1064nm laser power supply

The 1064 nm comes with a power supply. The output power can be adjusted via digital controller with 1 mW resolution. It has a LED front panel that displays power level in milliWatts.

2a—Inverted microscope assembly

The microscope, shown in Figure A.3, is modified for the use of laser tweezers. It consists of an inverted microscope, a high numerical aperture oil-immersion objective, an XY mechanical stage, a Z motor attachment, and a CCD video camera. The XY stage positions the petri dish with 0.3 um precision, and Z is attached to the fine adjustment knob of the microscope for focusing the beam. The objective is used for focusing the

beam and viewing the sample at the specimen plan. 10x and 20x phase contrast objectives are used for viewing and positioning the cells. Finally, CCD video camera is used to see and record the laser spot.

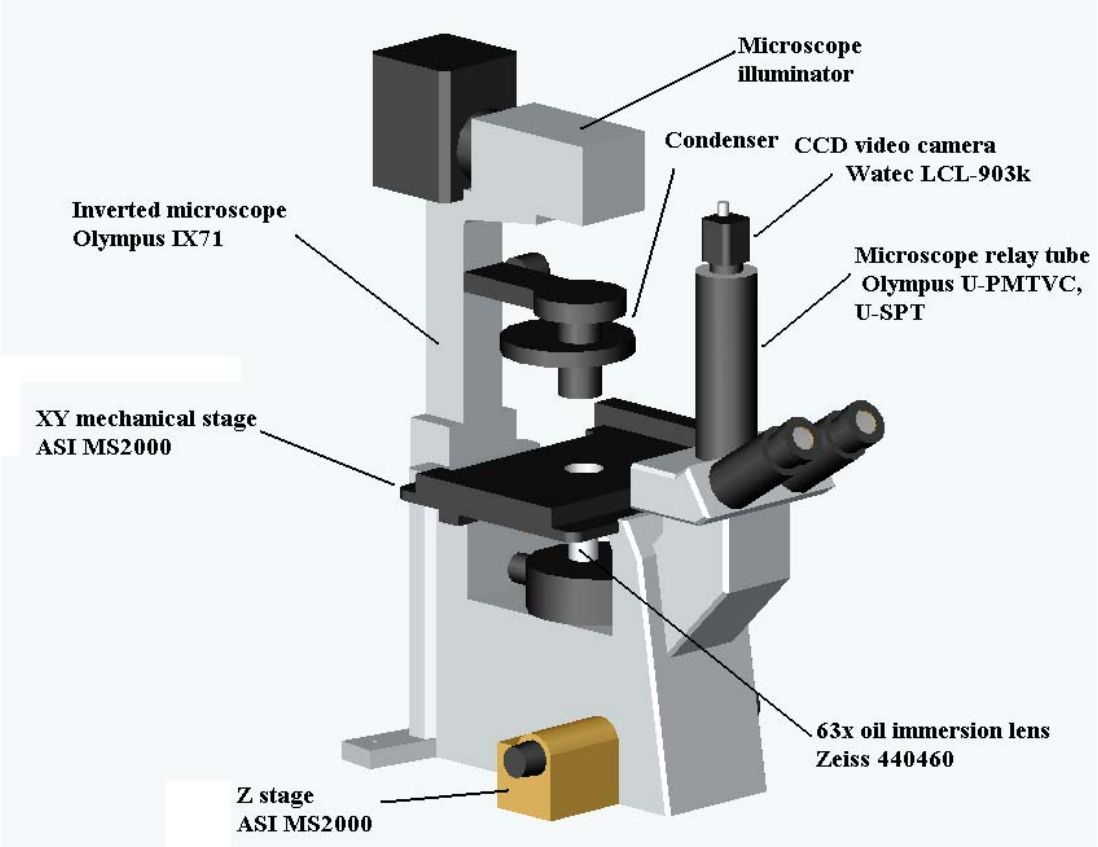

Figure A.3 Inverted microscope assembly

2b—External microscope power supply (Olympus TH4-100/200)

It is used to supply power to the illuminator to illuminate the samples through a condenser.

3—Beam expander assembly

The beam expander assembly, shown in Figure A.4, is used to mount and position the expander. It consists of a 5x beam expander, a slip ring, a post, a post holder, a rotation stage, and a linear mechanical stage. The beam expander is used to expand the beam to match the size of the back aperture of the lens. The expander is held in place by a slip ring which is attached to a post. The post is placed into a post holder and the height of the post can be adjusted. The rotation stage is used to rotate the beam expander, and the linear stage is used to position the beam expander on the air table.

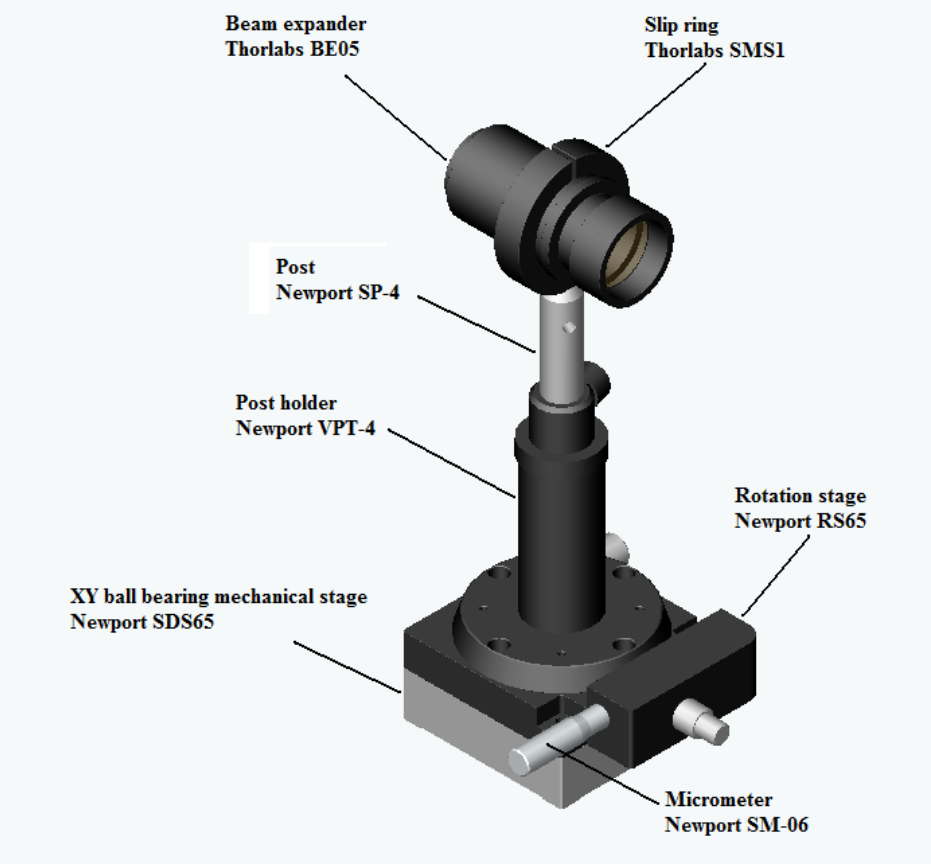

Figure A.4 Beam expander assembly

4a—Mechanical stage controller (ASI MS2000)

It is used to control the XY and the Z stage. It can be controlled manually by a joystick or automatically by a computer interface via a serial port.

4b—XY mechanical stage (ASI MS2000)

The stage is designed for the use of Olympus IX 71 microscope. It is mounted directly to the microscope without any modification or adaptor. It uses servo motors and has a feedback system for fine movement. It is controlled by the controller. The maximum axis speed is 7 mm/s and the axis resolution is 0.088 um.

4c—Z stage (ASI MS2000)

This is an optional motor that comes with the ASI MS2000 stage system. It is attached to the fine adjustment knob of the microscope and is controlled by the controller. The knob is turned by rotating the motor, and, therefore, the objective is moved in the Z-direction. The maximum axis speed is 0.6 mm/s and the axis resolution is 0.05 um.

5—Air table (TMC 78-30885-01)

The air table has threads and screw holes at 1" apart for attaching the optical and mechanical components. Another main function of the air table is keep everything leveled and to provide vibration isolation when it is floating.

6—CCD video camera (Watec LCL-903k)

This is a monochrome camera which has a resolution of 768 x 494 pixels. It has a BNC output connector which can be linked either to a capture card or a monitor. It is mounted to the trinocular port of the camera via a microscope relay tube.

7—Beam steering accessory

The beam steering accessory, shown in Figure A.5, consists of a XY adjustable rod base, a damped rod, a bottom beam steering accessory, a top beam steering accessory, and two broadband coated mirrors. The bottom accessory uses the elliptical mirror to direct the beam up toward the top accessory. Then, the beam is reflected horizontally toward the beam expander by the mirror mounted on the top accessory. The height of the laser beam can be adjusted by moving the top accessory along the damped rod, and direction of the beam can be adjusted by rotating the fine adjustment knob on the top accessory.

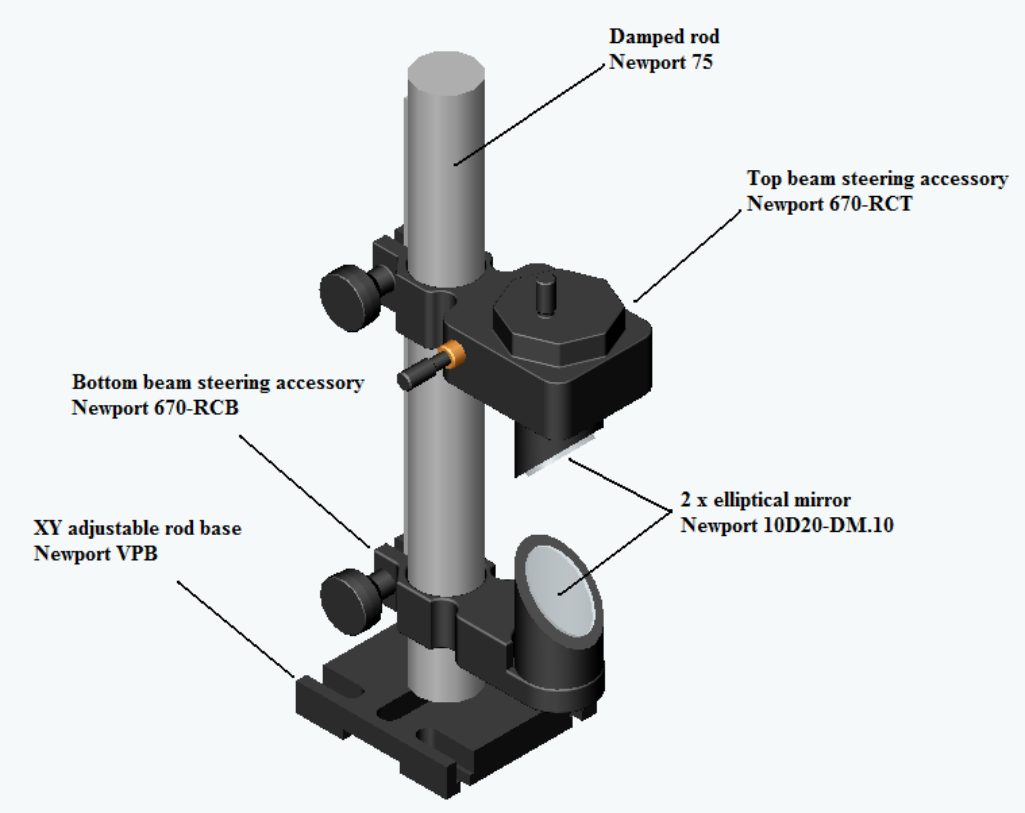

Figure A.5 Beam steering accessory

8—Beam reflector assembly

The beam reflector assembly, shown in Figure A.6, is used to reflect the expanded beam into the fluorescent port of the microscope. It includes a mirror holder, a laser line dielectric mirror, a kinematic optical mount, a post, a post holder, and two linear mechanical stages. The mirror that is used to reflect the beam is attached to a mirror holder which is mounted into an optical mount. The optical mount is screwed onto a post, and the height of the mount can be adjusted by sliding the post inside a post holder. The post holder is mounted to the XY stage (two one-directional stages) which is used for aligning the beam reflector.

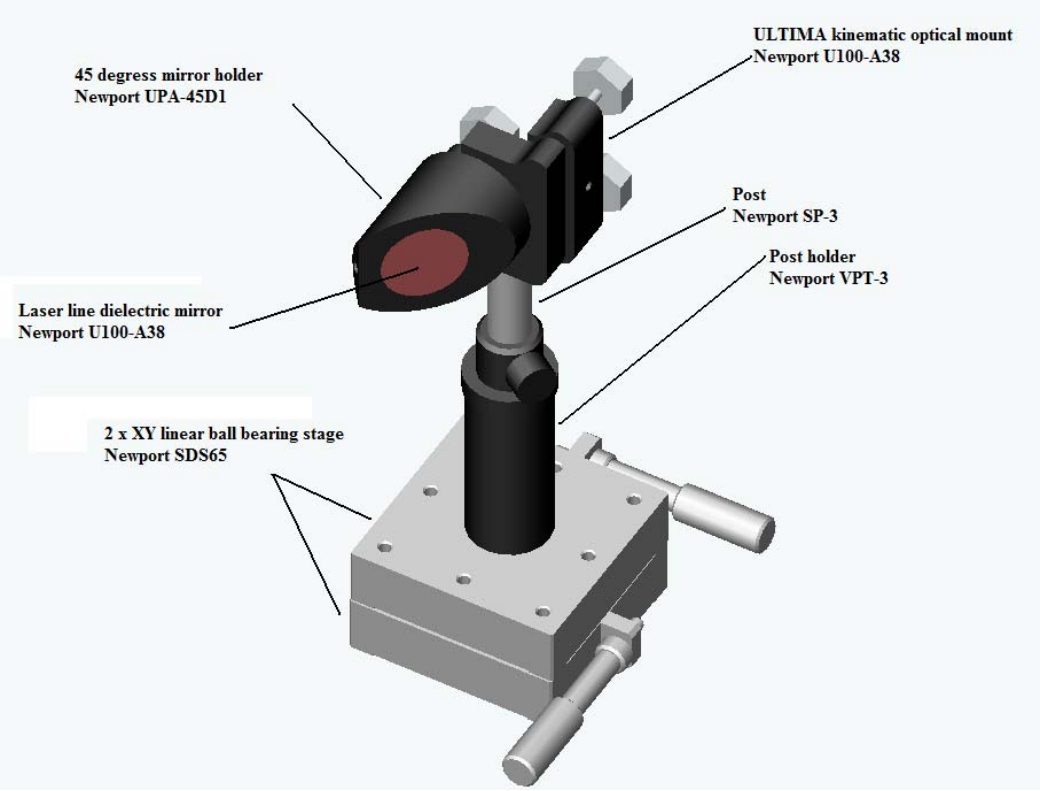

Figure A.6 Beam reflector assembly

B. 980 nm Laser System

This system includes a laser module, a microscope assembly, a beam expander assembly and a collimator assembly. The beam reflector assembly and steerer assembly are no longer needed because the laser fiber collimator can be placed directly behind the microscope, as shown in Figure A.7.

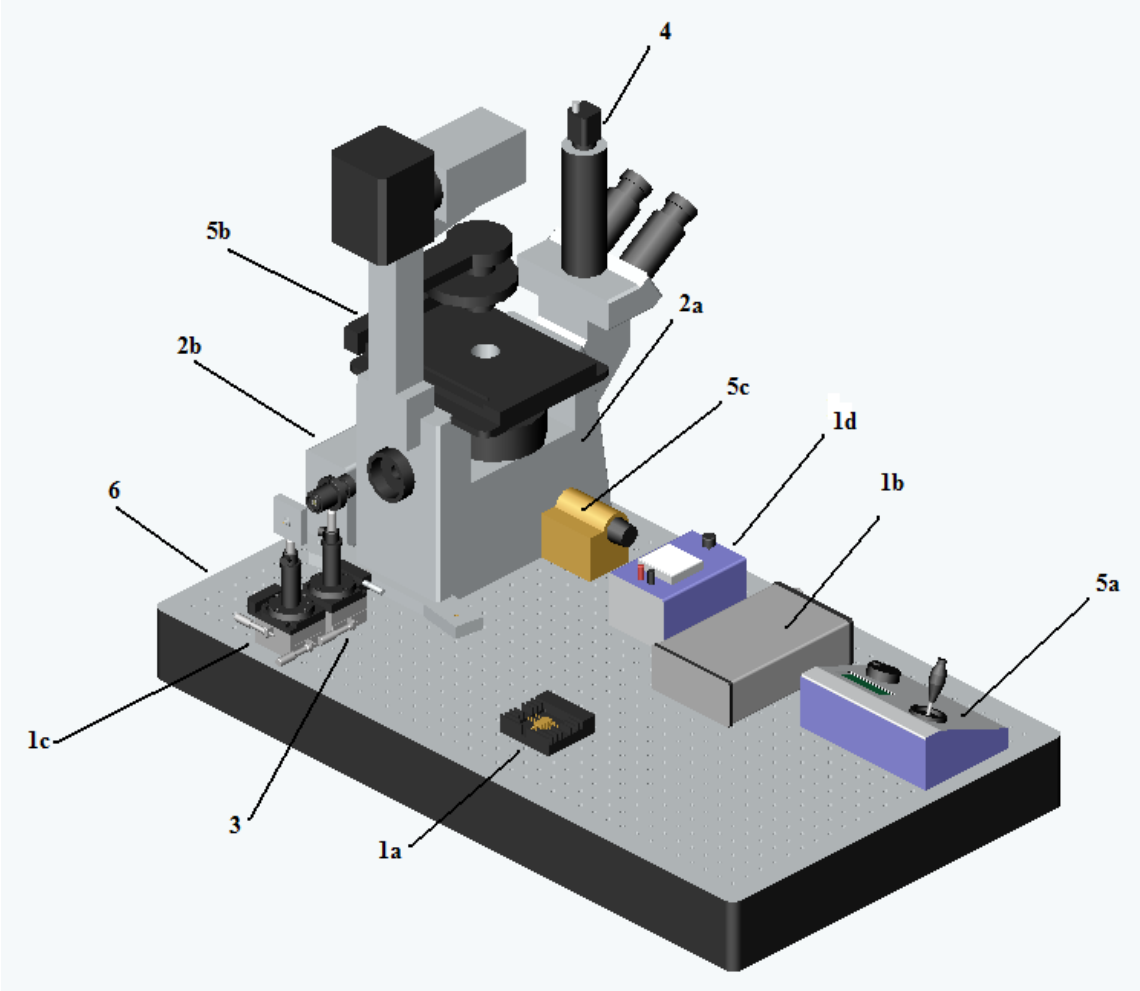

A.7 Each assembly in the 980 nm laser system is labeled with a number.

1a—980nm laser module

The 980 nm laser module, shown in Figure A.8, consists of a butterfly packaged laser diode (JDSU 29-8052-500) (LD) and a mount (Thorlabs LM14S2). The laser diode is integrated with a thermoelectric cooler (TEC), a thermistor, and a monitor diode. The laser mount holds the laser firmly in place and provides connections between the laser diode and both the TEC controller and the LD power supply. The laser output is connected with a fiber-optic cable to the collimator.

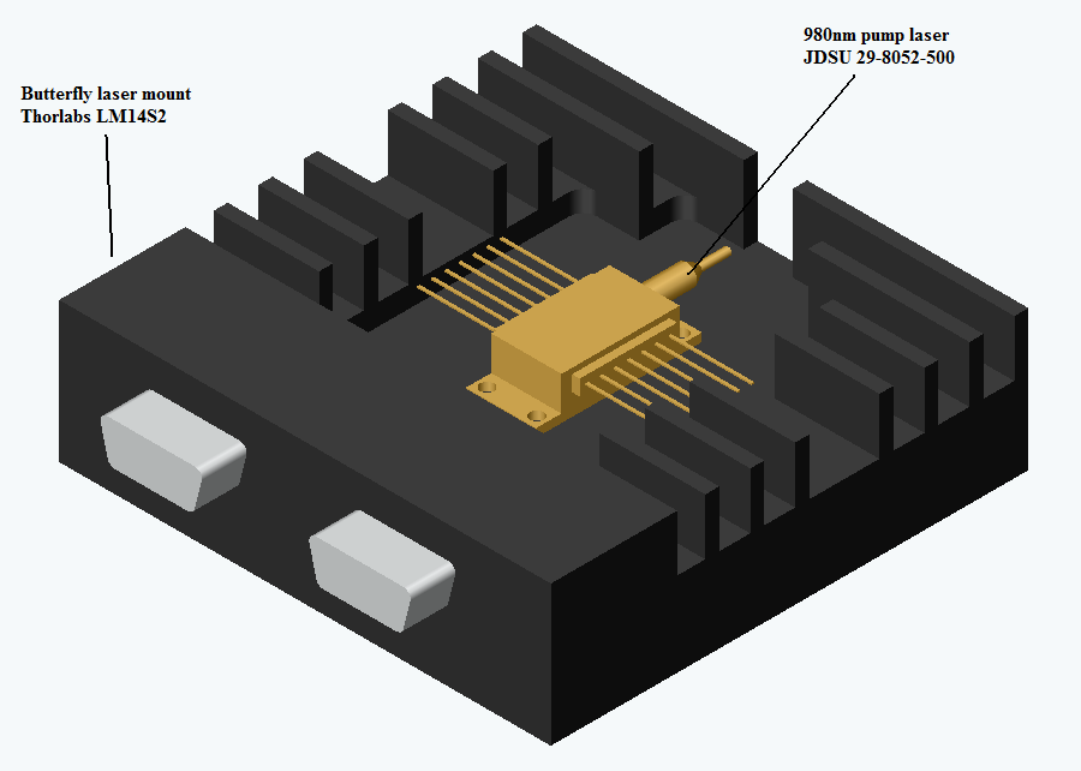

Figure A.8 980 nm laser module

1b—980 nm laser collimator assembly

The collimator assembly, shown in Figure A.9, is used to mount and position the collimator. It consists of a beam collimator, a collimator holder, a post, a post holder, a rotation stage, and two linear stages. The collimator is used to generate a Gaussian parallel beam. The collimator is hold in place by a holder which is mounted onto a post. The height of the collimator can be adjusted by sliding the post inside the post holder. The collimator can be rotated using the rotation stage and moved in XY directions using two linear stages.

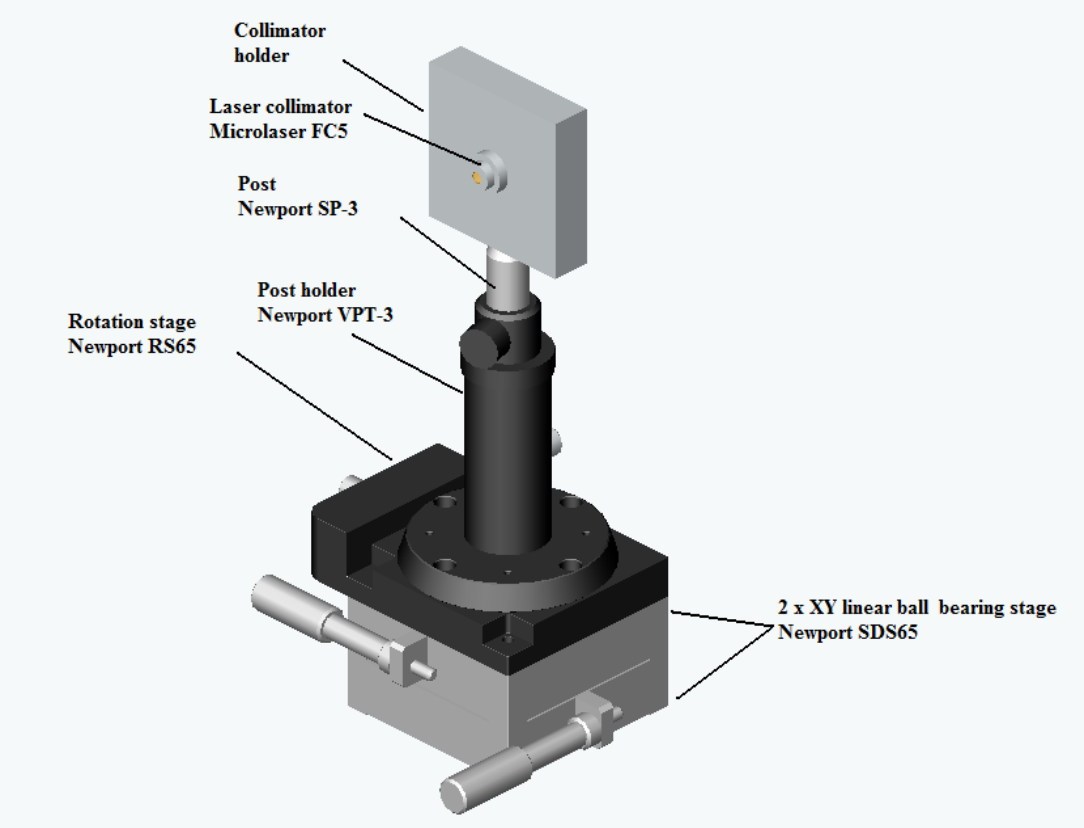

Figure A.9 980 nm laser collimator assembly

1c—980 nm laser custom power supply

The laser diode driver was designed by Mike Walsh. It is built so that the maximum current supplied to the diode is less than 1100 mA and maximum voltage is less than 2.5 V. It is a simple power supply using an adjustable 3-terminal positive voltage regulator (LM117) and a potentiometer to regulate the current supplied, as shown in Figure A.10. It is used as a negative current source because the laser diode has its anode common to the butterfly mount.

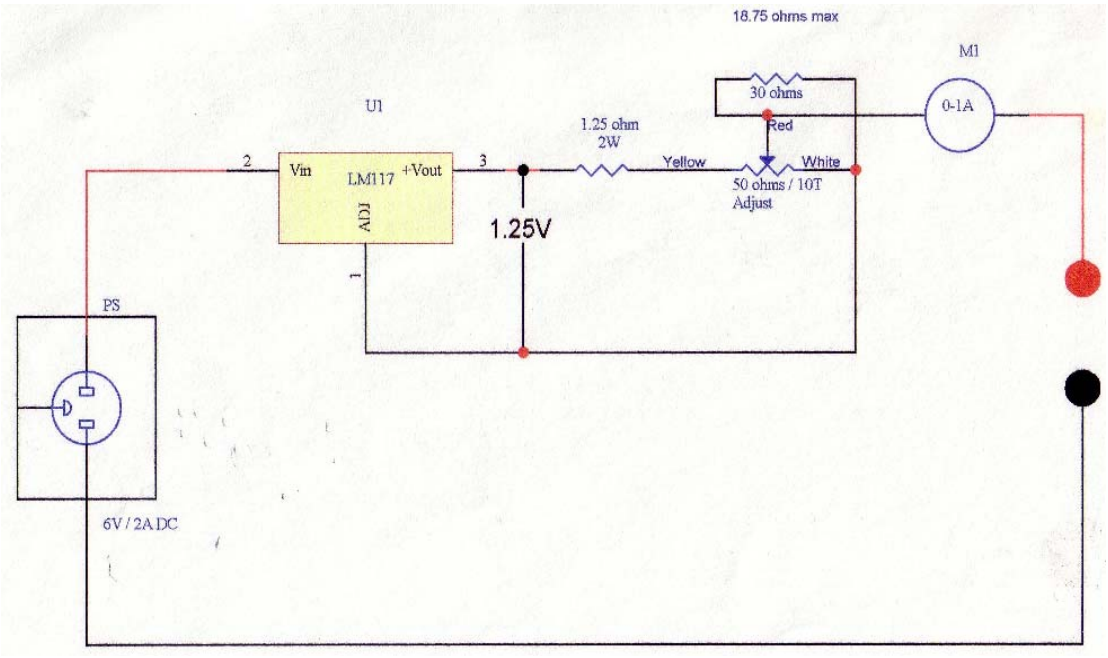

Figure A.10 Laser diode power supply circuit design

1d—TEC controller

The TEC controller is used to control the temperature of the laser diode. It has a temperature stability of 0.01 °C and limits the amount of current supplied to the laser diode. For this research, the limit was set to 1A although according the manufacturing specification the laser diode can handle a max TEC current up to 2A.

Schematic of connections

The TEC controller and the LD are connected the laser mount by a customized cable. The polarization maintaining fiber is connected to the collimator. Figure A.11 shows the schematic of connections for the 980 nm laser module, and Figure A.12 shows the cable configurations.

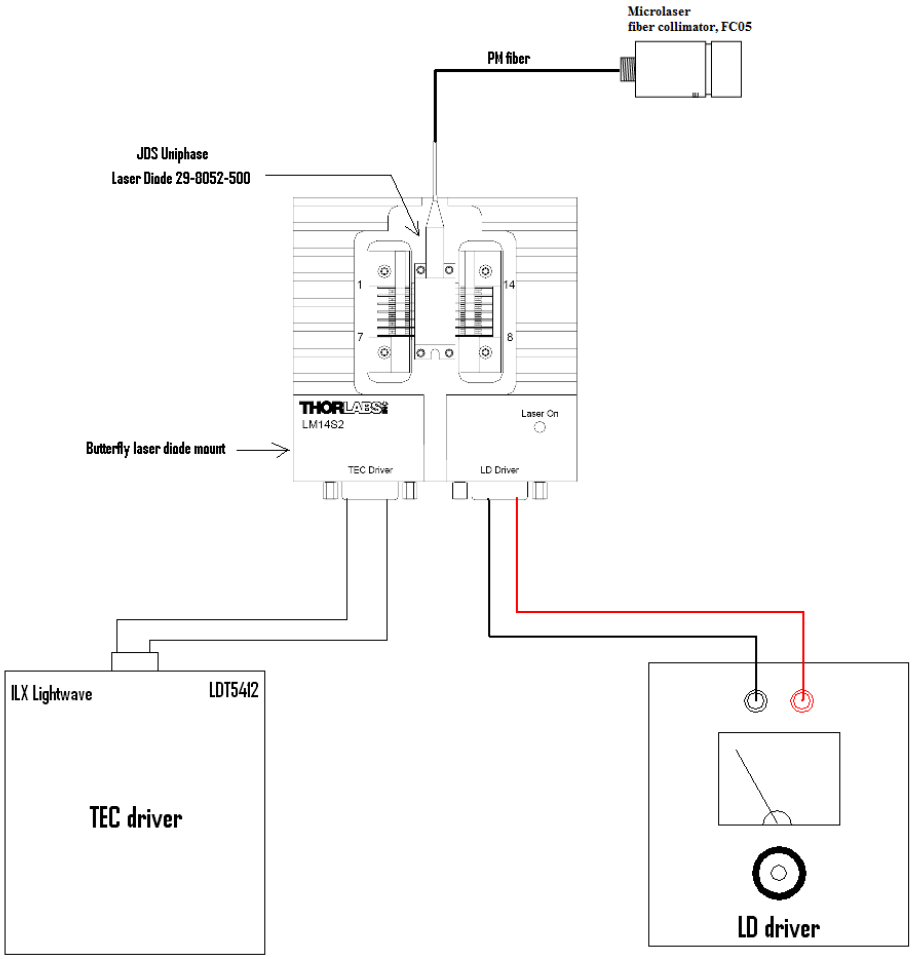

Figure A.11 Connections for 980 nm laser module

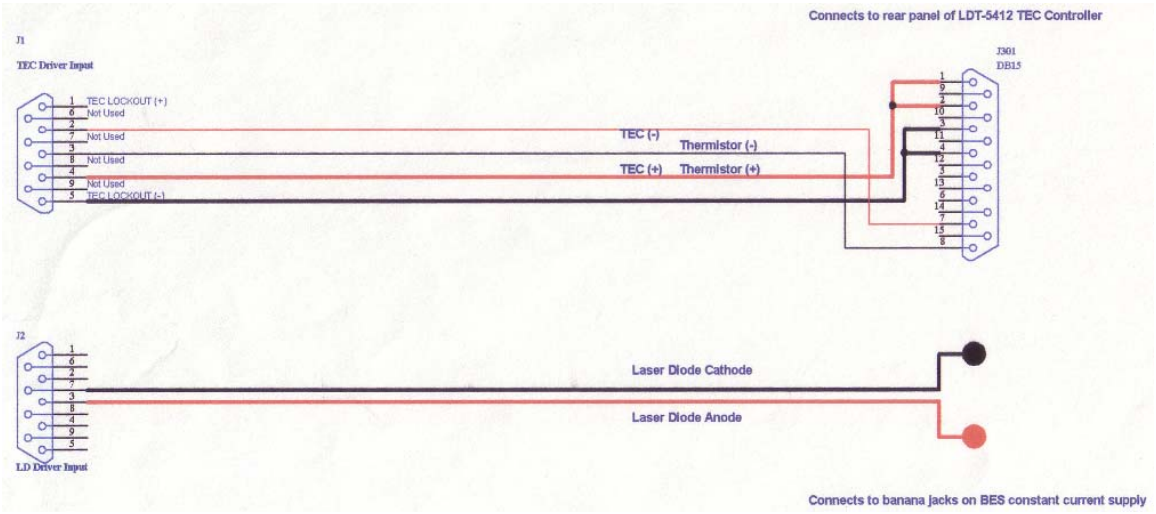

Figure A.12 Cable configurations

2a—Inverted microscope assembly

See the description in the 1064 nm laser tweezers system.

2b—External microscope power supply (Olympus TH4-100/200)

See the description in the 1064 nm laser tweezers system.

3—Beam expander assembly

The beam expander assembly, shown in Figure A.13, for the 980 nm system has the same setup as the 1064 nm except it has an extra longitudinal linear stage.

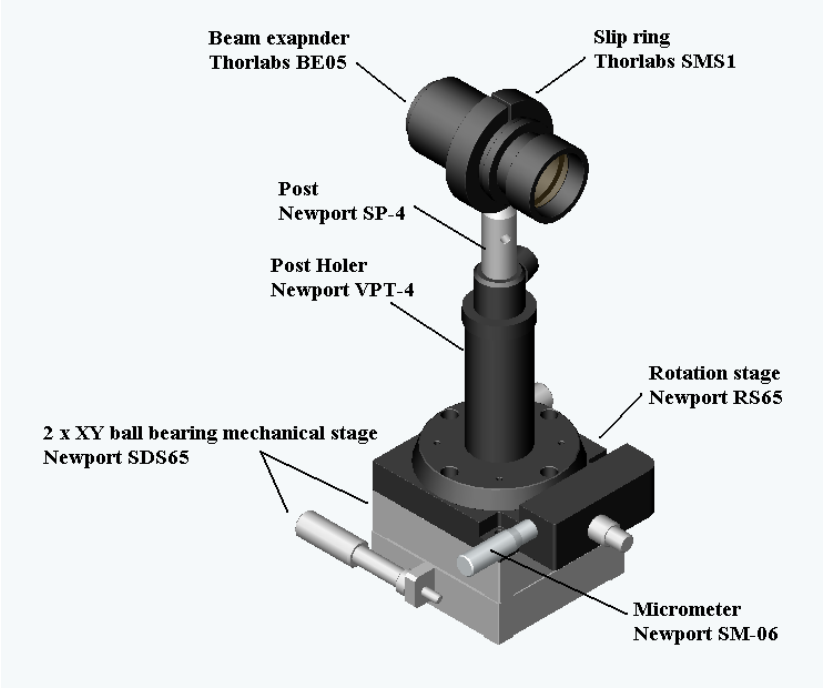

Figure A.13 Beam expander assembly

4—CCD video camera (Watec LCL-903k)

See the description in the 1064 nm laser tweezers system.

5a—Mechanical stage controller (ASI MS2000)

See the description in the 1064 nm laser tweezers system.

5b—XY mechanical stage (ASI MS2000)

See the description in the 1064 nm laser tweezers system.

5c—Z stage (ASI MS2000)

See the description in the 1064 nm laser tweezers system.

6—Air table (TMC 78-30885-01)

See the description in the 1064 nm laser tweezers system.

Appendix B
LabVIEW Program for Moving Neurons

An interface for communicating serially between the computer and the motorized stage controller was written in LabVIEW. Its main functions are to calculate the cage locations (16 cages) and bring trapped neurons automatically to their cages. LabVIEW has a front panel where users interact with the program and a block diagram panel where all the modules and functions are linked together to form the backbones of the program.

A. Program front panel

A user can input each cage location, set speed of the stage, and select cage for loading. In Figure B.1, each box labeled with a number will be described next.

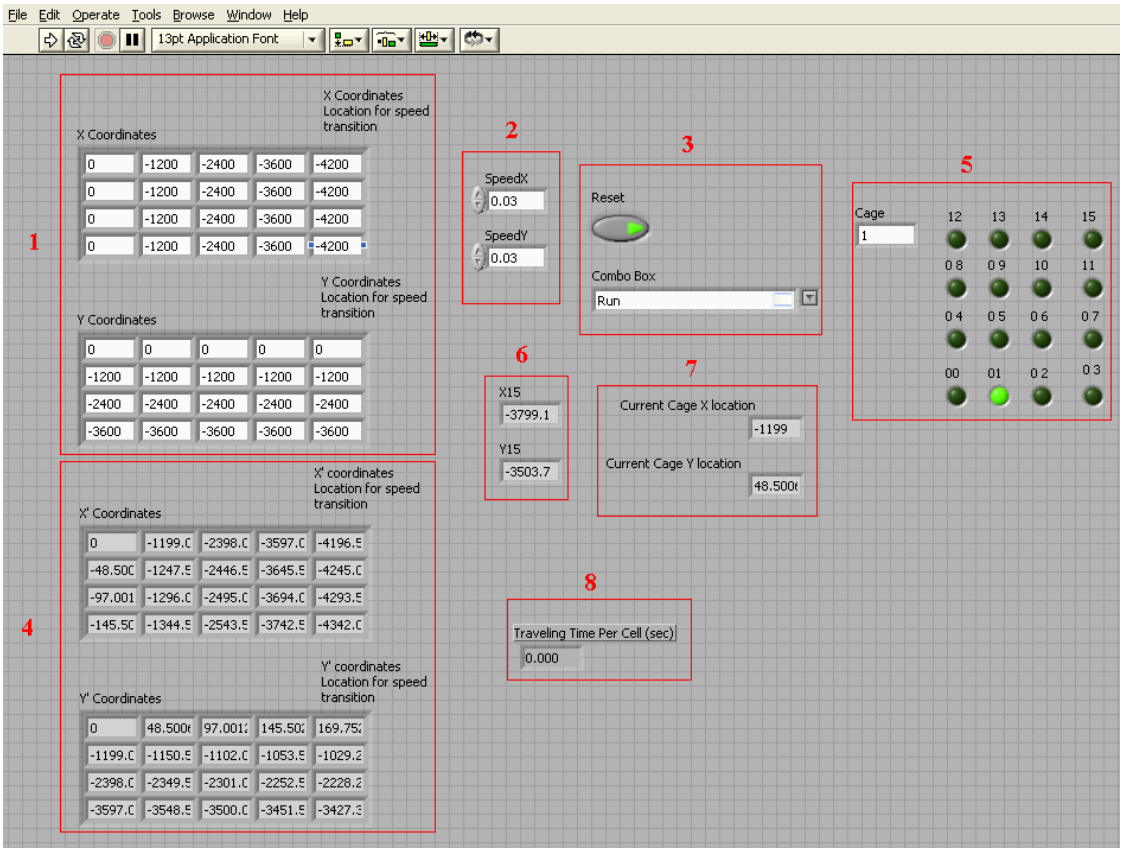

Figure B.1 Front panel of the program where user can set speed and select cage.

1. The layout of cages on a neurochip is known with (0,0) at the lower left corner. Input the cage locations into the first four columns of the X and Y arrays and save these values. The left box in Figure B.2 illustrates this for cages 120 um on centers. Input the locations where the XY stage changes its speed into the last column of the X and Y arrays, shown in the right box of Figure B.2, and save these values. They only have to be input once and the program will remember these values next time. Interger 1000 in the program is equivalent to 100 um in the real world.

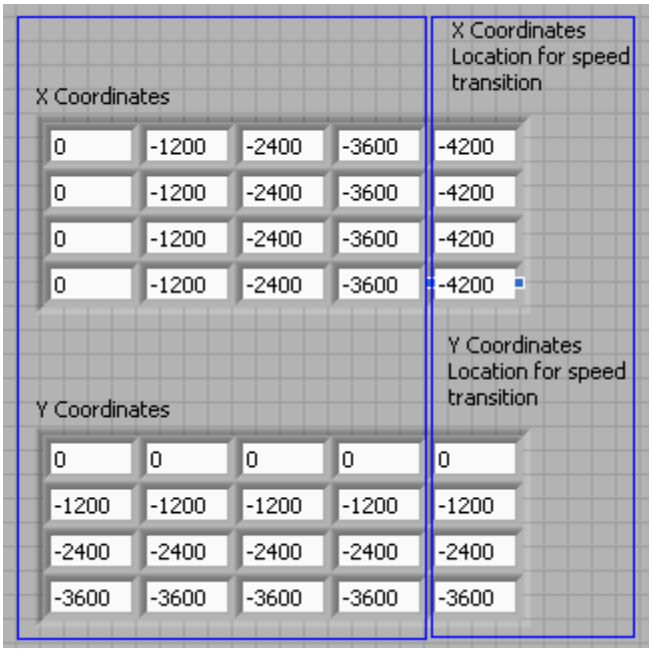

Figure B.2 Input cage locations and speed transition locations into these XY arrays

2. The program allows the user to set the speed of the stage. A user can set the speed according to the laser power at the specimen. Input the axis speed for X and Y in the boxes shown in Figure B.3. The speed for moving a neuron using the 980 nm laser is usually 60 to 80 um per second for X and Y directions.

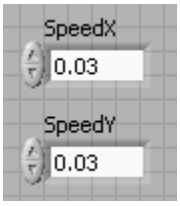

Figure B.3 Input axis speed for X and Y

3. This is a combo box, shown in Figure B.4, with a pull-down menu which is used to select the routine that you want to execute. These routines are Calibration point1, Calibration point2, and Run.

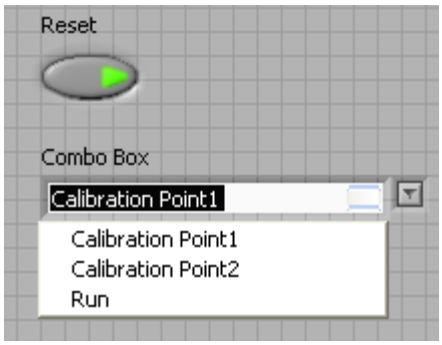

Figure B.4 Basic routines for loading neurons

Each chip needs to be calibrated before loading neurons. Two reference points from each chip are needed for computing the location of each cage. Place the center of cage00 at the laser spot, as shown in Figure B.5. Click the Reset oval button with the arrow and highlight the calibration point1 to execute the routine. This resets the stage, and the center of cage00 is at 0,0. Then, place the center of cage15 at the laser spot, and run the calibration2 routine. During this routine, each cage location in reference to the stage is computed and saved into a buffer.

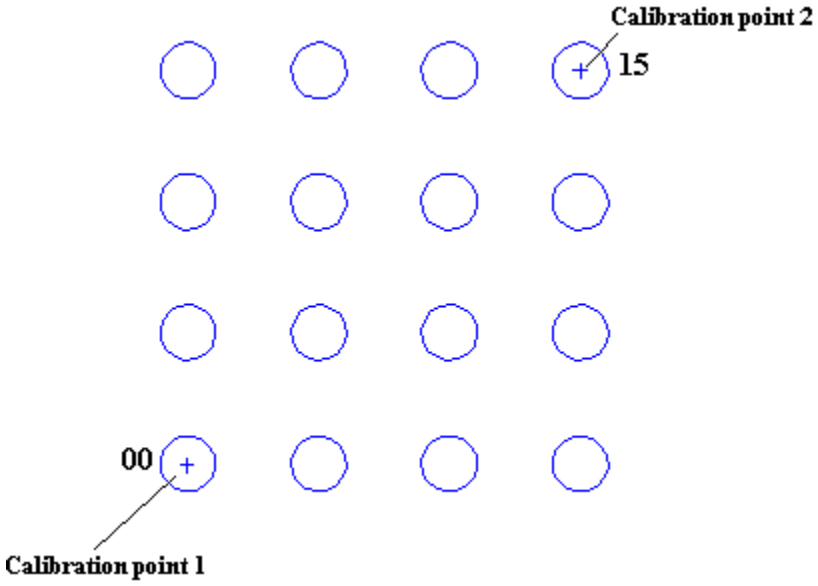

Figure B.5 Two calibration points are needed for calibrating the system.

4. The computed cage locations are shown in the first four columns of the X' and Y' arrarys, and the computed speed transition locations are shown in the last column of the X' and Y' arrays in Figure B.6.

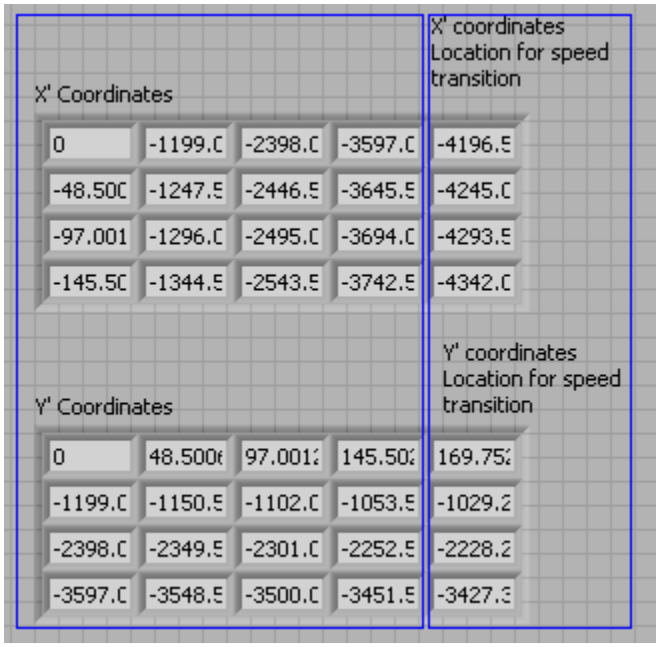

Figure B.6 The arrays display computed cage locations and speed transition locations.

5. A neuron is trapped and lifted 50 um above the polyHEMA surface using the laser tweezers before executing the run routine. Select a cage by entering the corresponding number in the cage box shown in Figure B.7; only 0 to 15 can be input into the box. Execute the run routine. The stage brings the neuron automatically over its cage during the run routine. The neuron is then manually lowered into the cage. The button that represents the cage turns green after the execution. This tells the user which cage has been loaded. To load the next neuron, input another cage number and execute the run routine.

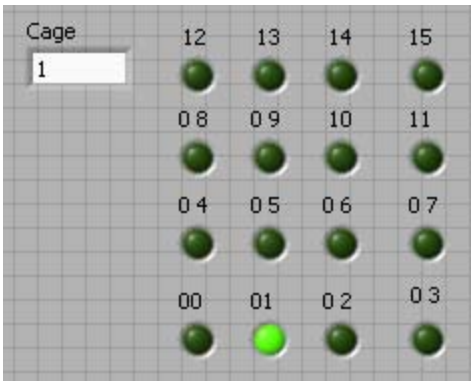

Figure B.7 Select cage number

6. In Figure B.8, the coordinates of cage15 are displayed in the X15 and Y15 boxes.

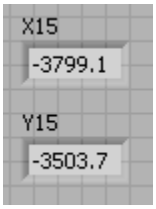

Figure B.8 Location of cage15

7. The coordinates of the current cage are shown in the current cage X and Y location boxes, as illustrated in Figure B.9.

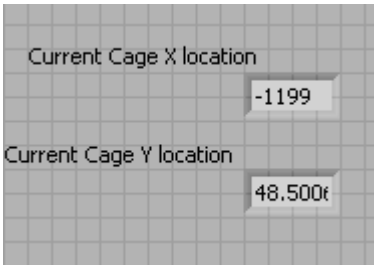

Figure B.9 Current cage location

8. The calculated time for a neuron to travel to its cage is shown in the time per cell box in Figure B.10.

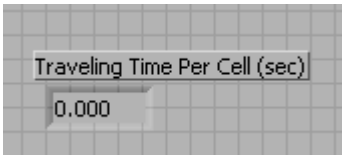

Figure B.10 The box displays traveling time for each neuron.

B. Program block diagram

Calibration point1

Calibration point1 is the default routine for the case structure. It calls out a reset subvi to reset the stage. The routine ends if the reset subvi does not execute within 5 seconds. (See Figure B.11.)

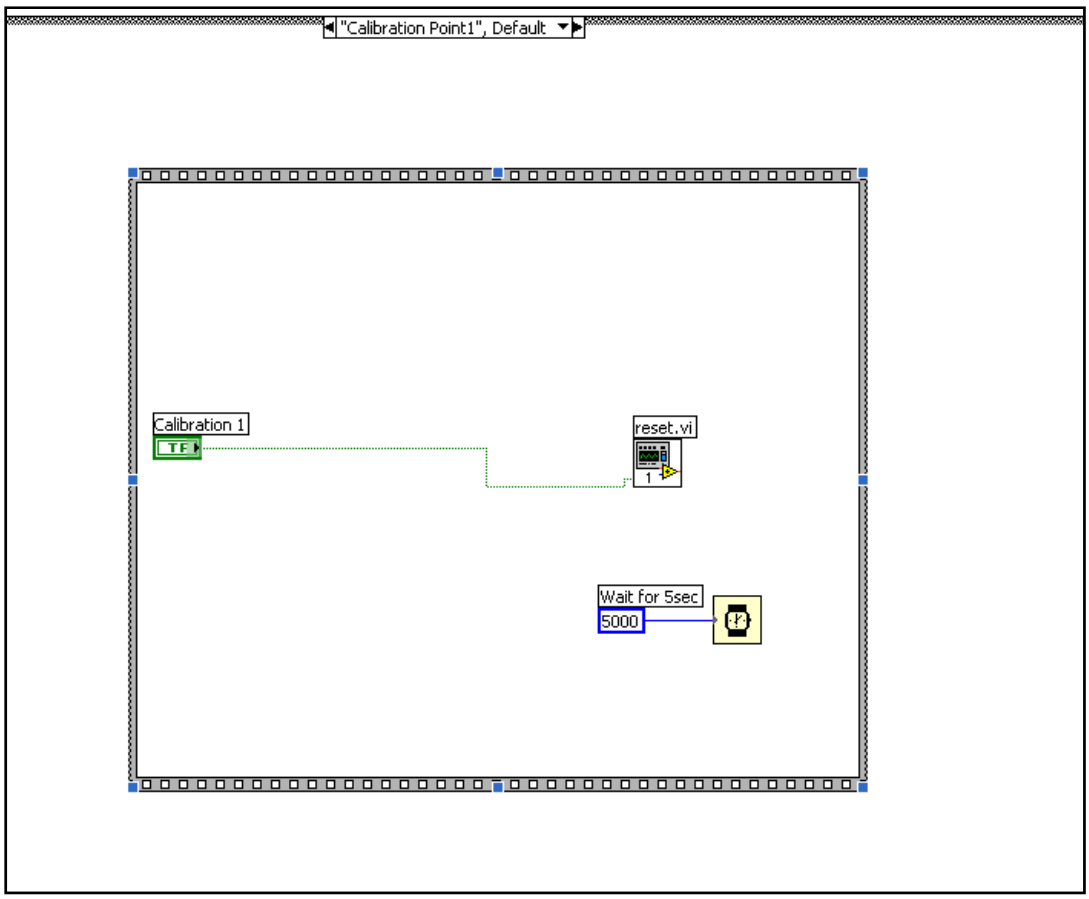

Figure B.11 Block diagram of calibration point1 routine

Reset subvi

Front panel

This subvi resets the stage. The user can adjust the time out value. (See Figure B.12.)

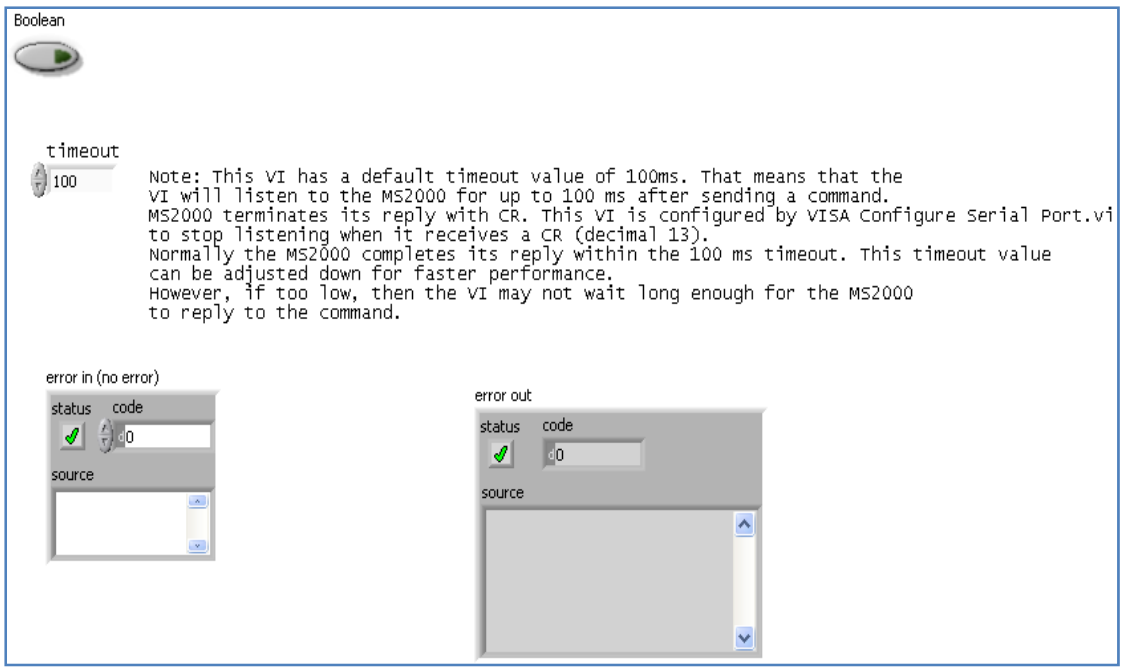

Figure B.12 Front panel of reset subvi

Block diagram

The reset subvi uses VISA to communicate with a serial port. VISA is a standard I/O language for instrumentation programming. It first configures and flushes the port. Then, the command "RESET" is sent to VISA write function to reset the stage. The error will be displayed if the stage is not reset properly. (See Figure B.13.)

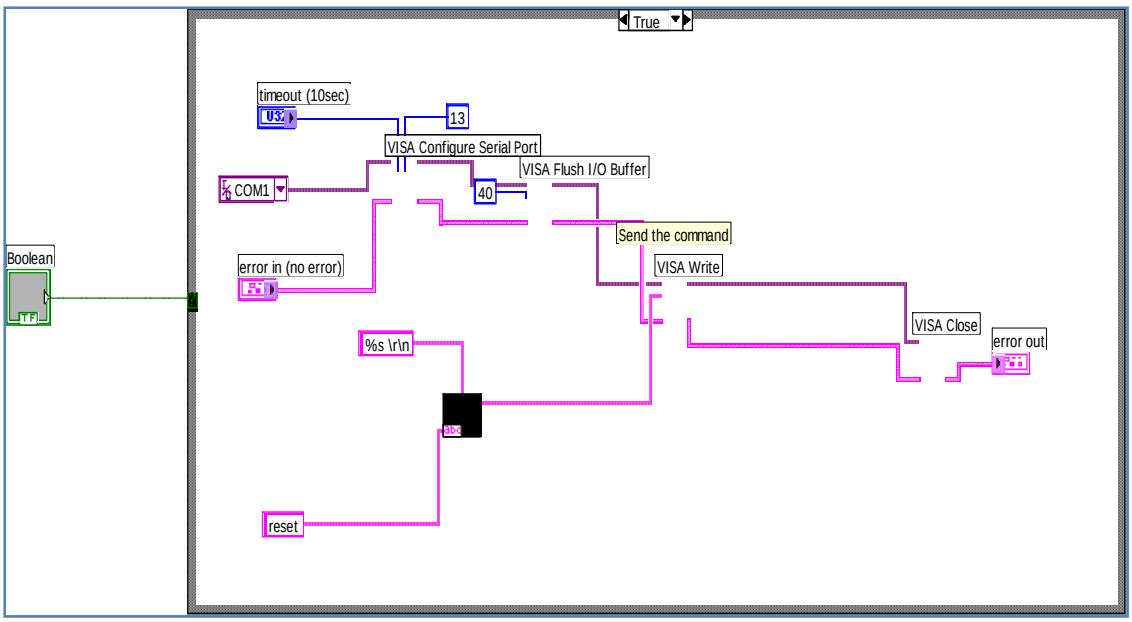

Figure B.13 Block diagram of reset subvi

Calibration Point2

The block diagram of this routine is broken into two pictures since it is too large to be shown in a single picture.

Part I—The whereXY subvi in Figure B.14 asks the controller where the current stage location is and outputs results into the buffers. A 200 ms delay is added to allow the controller to finish its previous task.

Part II—Then, calculations are performed to find cage locations, as shown in Figure B.15. The program first computes the theta and initializes a 4 by 5 array. Then, it calculates the sixteen cage locations and the four speed transition locations in a for_loop structure. The cage locations are input into the first four columns and the speed transition

locations are input into the last column of the X' and Y' arrays. Calculation details are explained in the next section.

Calculation of new coordinate system

Rotation of a vector is used to map out the new coordinates. If a neurochip is perfectly aligned with the mechanical stage, the vector pointing from the center of cage00 to the center of cage15 would be 45º from the stage X-axis. A neurochip can be placed somewhat precisely on the stage but requires calibration before using the software. Figure B.16 illustrates a neurochip that is not aligned with the stage and is rotated to the left by theta. This theta can be calculated using equation $\theta = \tan^{-1}\left(\frac{y}{x}\right) - 45°$, y and x are the coordinates of cage15. Then, one can multiply the known coordinates by the rotation matrix to get the new coordinates of each cage.

$$\begin{bmatrix} X' \\ Y' \end{bmatrix} = \begin{bmatrix} cos\theta & -sin\theta \\ sin\theta & cos\theta \end{bmatrix} \begin{bmatrix} X \\ Y \end{bmatrix}$$

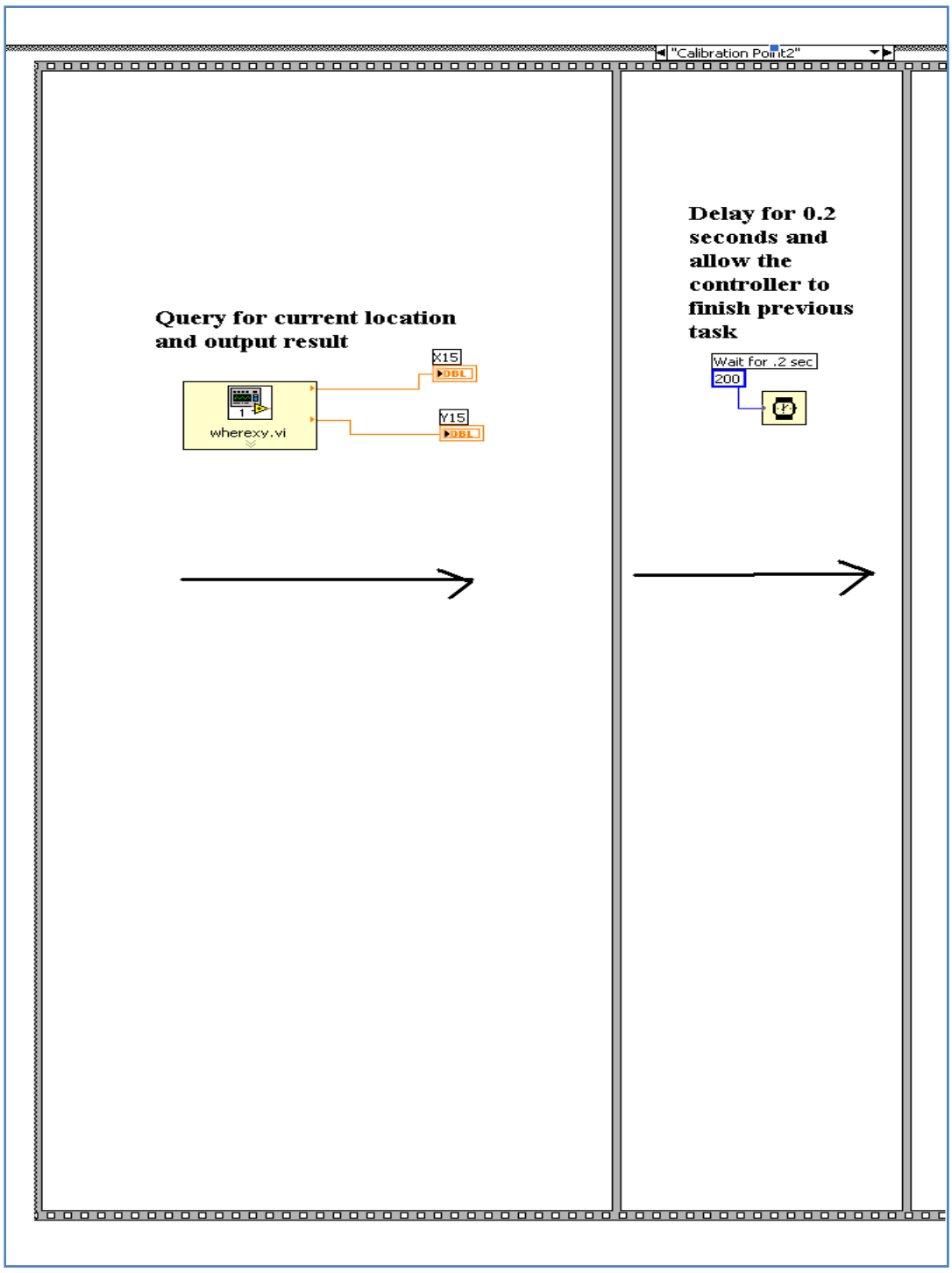

Figure B.14 Block diagram of calibration point2 routine, part 1

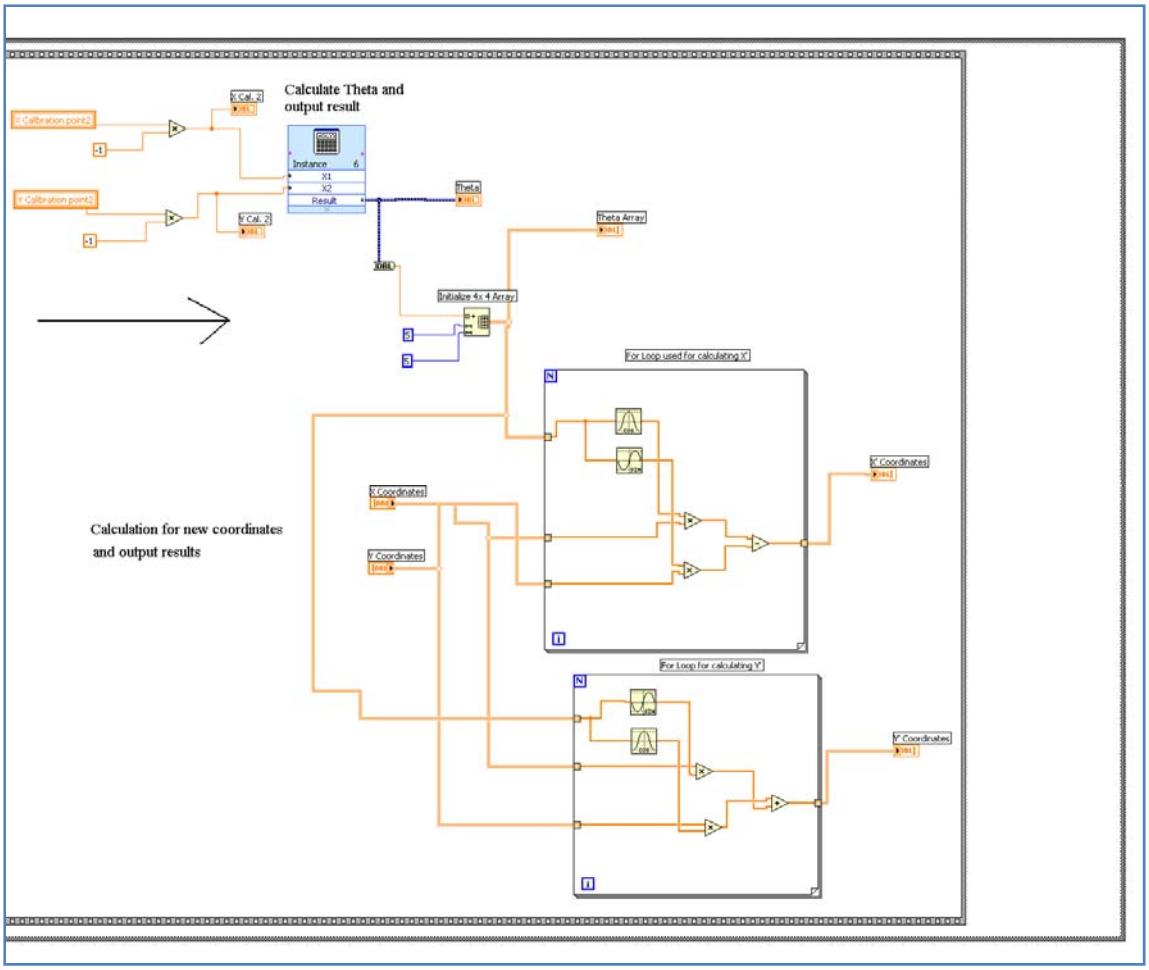

Figure B.15 Block diagram of calibration point2 routine, part 2

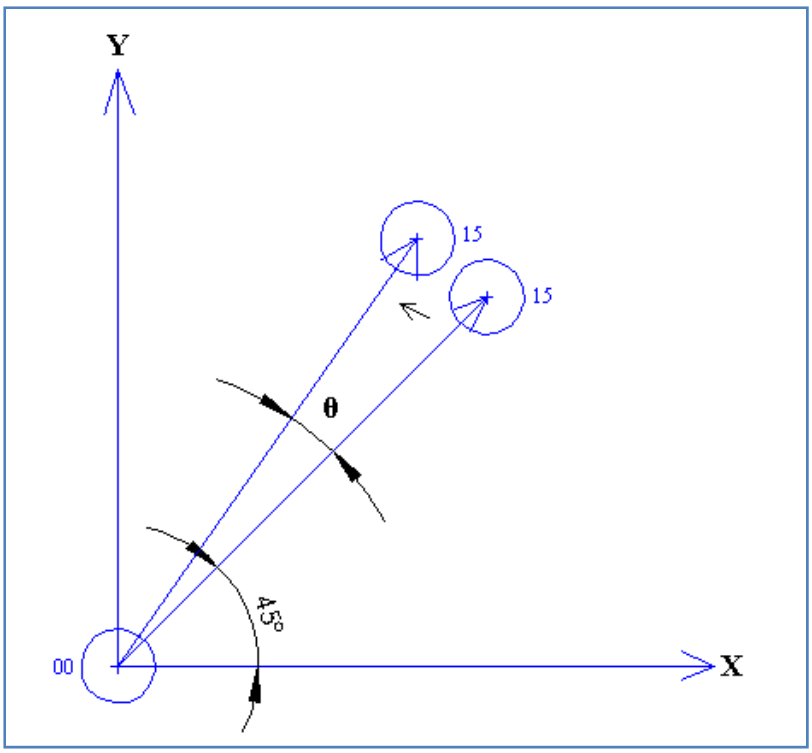

Figure B.16 The neurochip is rotated by θ.

WhereXY Subvi

Front panel

The subvi queries the current stage location and outputs the results into the buffers. The results are displayed in the X and Y box, as shown in Figure B.17. The timeout value can by adjusted by the user.

Block diagram

It first configures and flushes the port. It then sends "WHERE XY" to VISA Write to execute the command. Finally, VISA Read is used to get the coordinates of the current

stage position and the results are formatted to one decimal place and output to the front panel. The process flow is illustrated in Figure B.18.

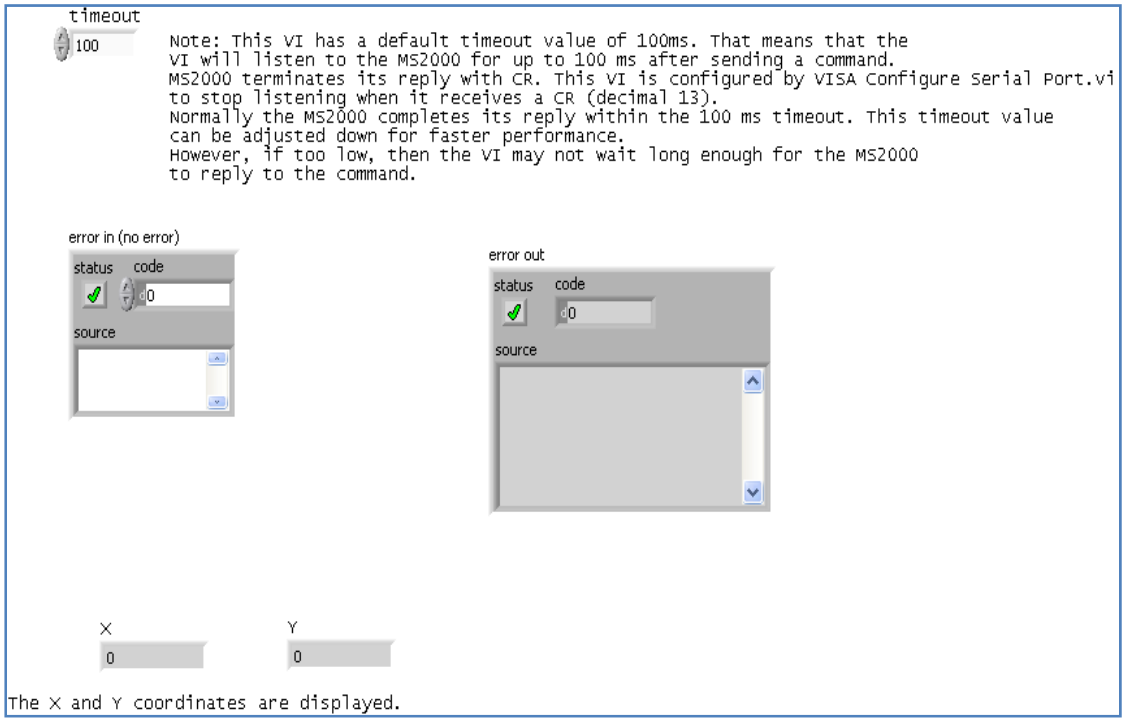

Figure B.17 Front panel of WhereXY subvi

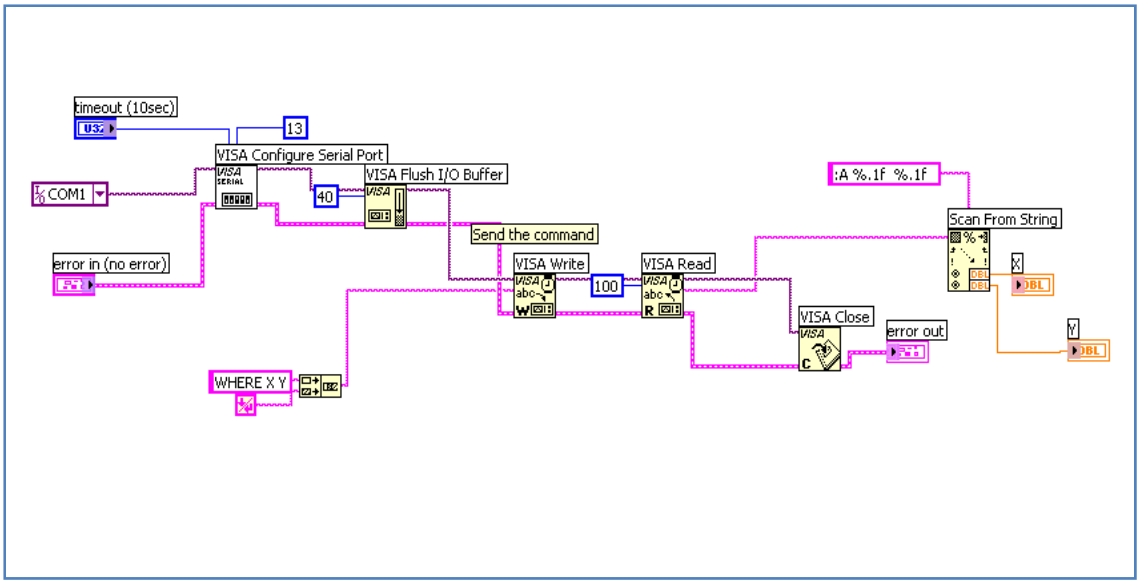

Figure B.18 Block diagram of WhereXY subvi

Run routine

The routine brings the neurons automatically to the cages. The block diagram is divided into two separate pictures.

Part I—It first sets the speed defined by the user using setspeed subvi before moving each neuron. Then, it waits for 200 ms for the controller to finish its previous task. Next, it uses a case structure to output the preselected cage number into an index array to retrieve the cage location. Finally, it brings the neuron along a direct line to a location near that cage (previously calculated) using the moveXY subvi. For example, the speed transition location for the first row of cages is about 120 um at the right of the last cage in the first row, as shown in Figure B.3. It waits another 200 ms before executing the next step. The process flow is shown in Figure B.19.

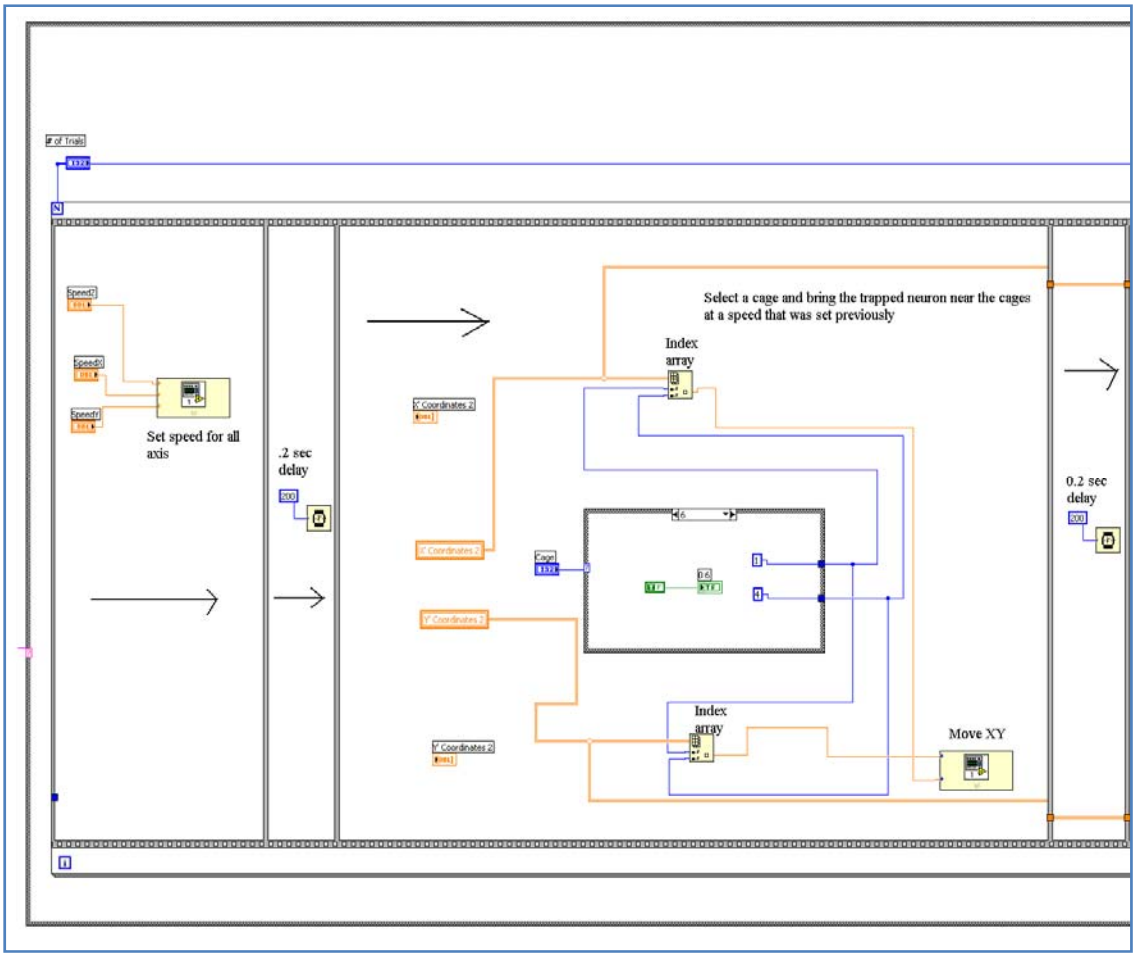

Figure B.19 Block diagram of Run routine, part I

Part II—The speed is set to 10 um/s for the X and Y axis by the setspeed subvi. The cage structures and electrodes reduce the light intensity significantly enough that a slower speed is needed for moving neurons. It waits for 200 ms. Then, it uses a case structure to output the preselected cage number into an index array to retrieve the cage location. Finally, the neuron is moved to the cage location using the moveXY subvi. (See Figure B.20.)

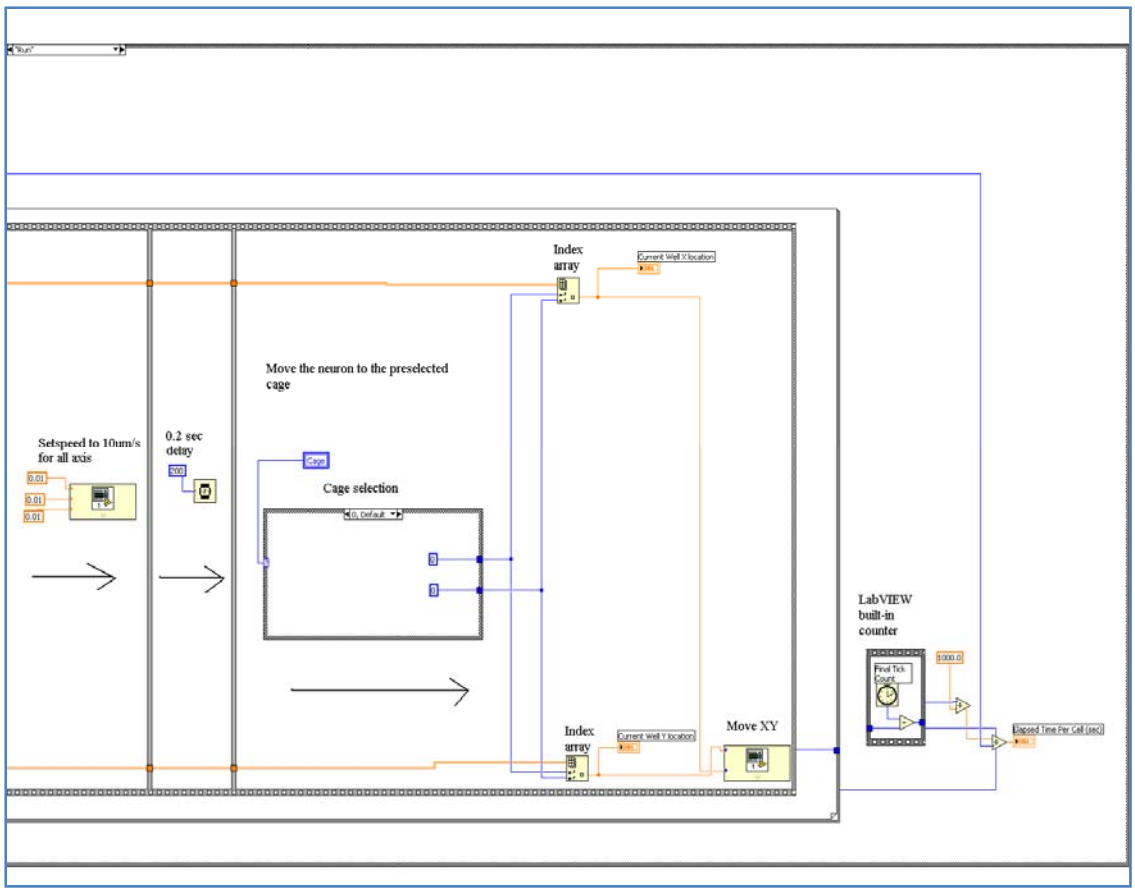

Figure B.20 Block diagram of Run routine, part II

Setspeed subvi

Front panel

The speed is input into Z, X, and Y boxes. The routine sets the speed of the stage according to these values. If the speed is set successfully, the success button turns green. If it is not, the error out box displays the error message, as shown in the bottom right of Figure B.21.

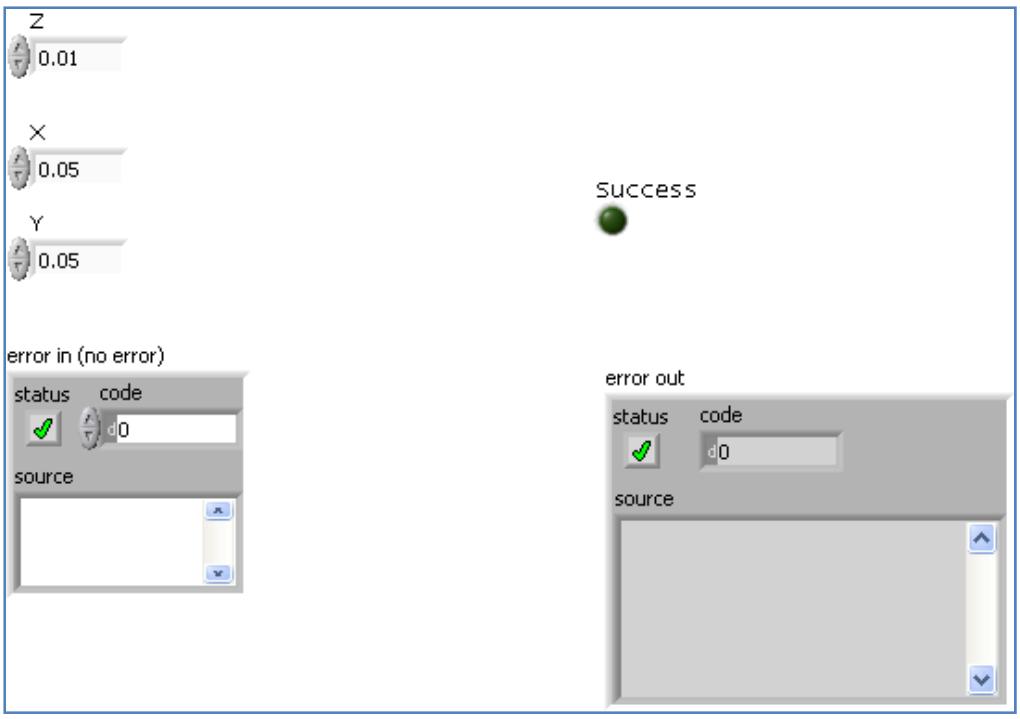

Figure B.21 Front panel of setspeed subvi

Block diagram

The block diagram is divided into two separate pictures.

Part I—In Figure B.22, it first configures and flushes the port. Then, it concatenates X, Y, and Z values into string and sends it to VISA Write to execute the command "SPEED X= Y= Z=". Then, it uses VISA Read to output its process.

Part II—In Figure B.23, it waits for the status of the controller. If the speed is successfully set to the input values, the success button turns green on the front panel. If it is not, the error message displays in the error out box on the front panel.

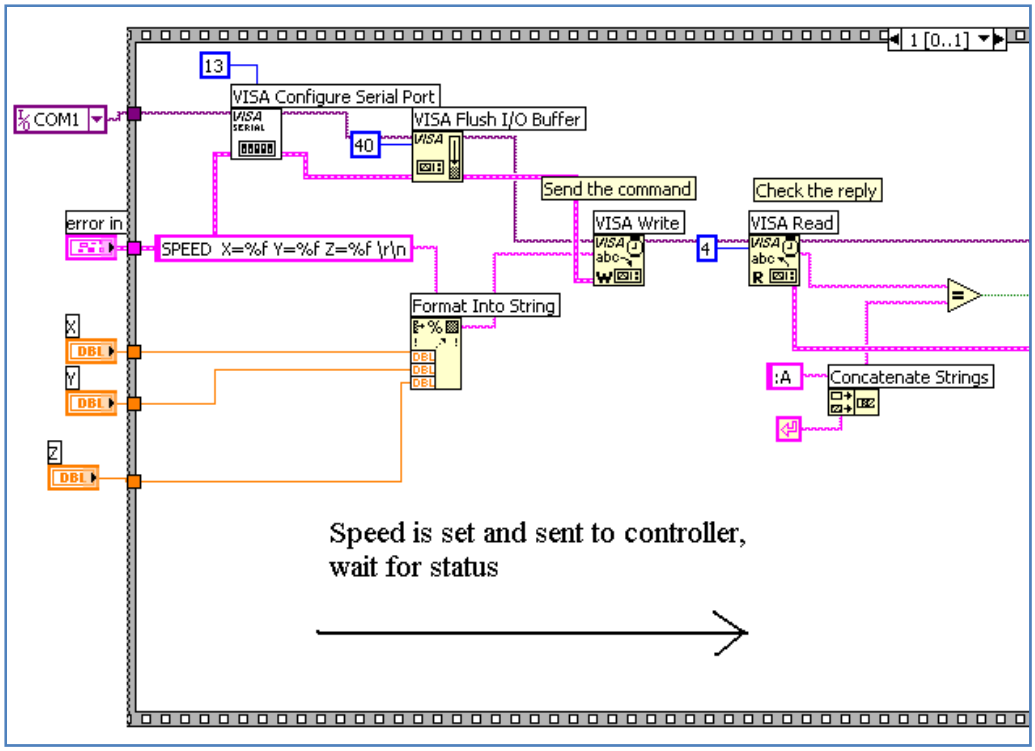

Figure B.22 Block diagram of setspeed subvi, part I

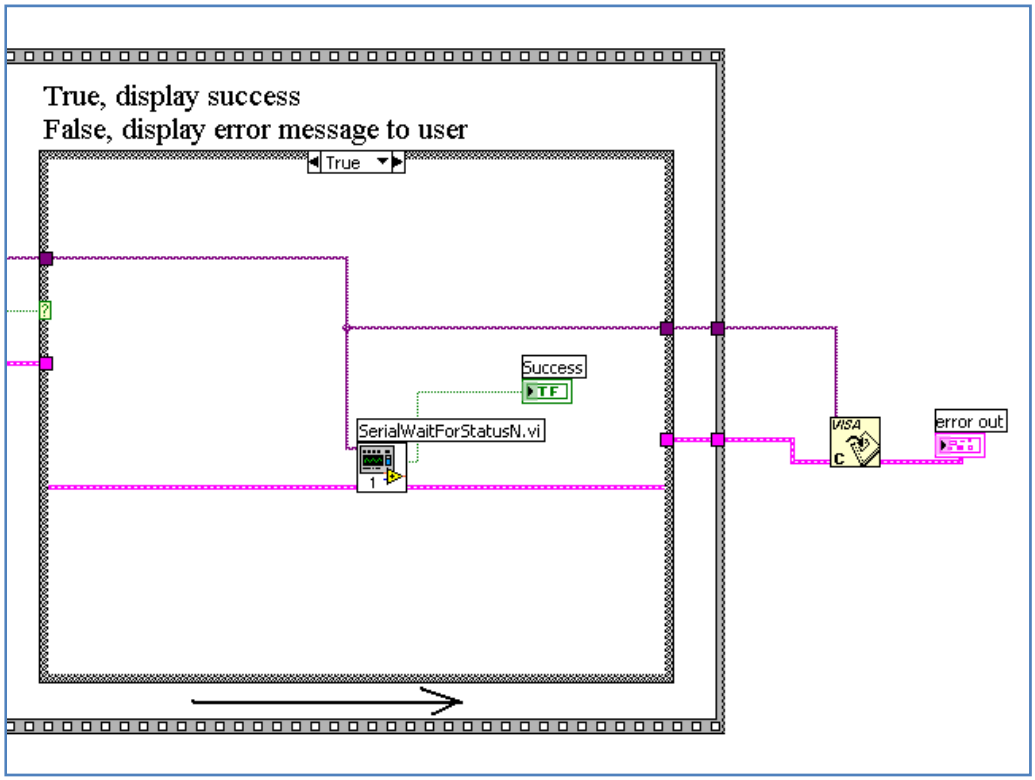

Figure B.23 Block diagram of setspeed subvi, part II

MoveXY subvi

Front panel

The X' and Y' coordinates of a cage are retrieved from the array buffers and input into the X and Y boxes. The routine moves the neuron to the cage location. If the move is successful, the success button turns green. If it is not, the error out box displays the error message. (See Figure B.24.)

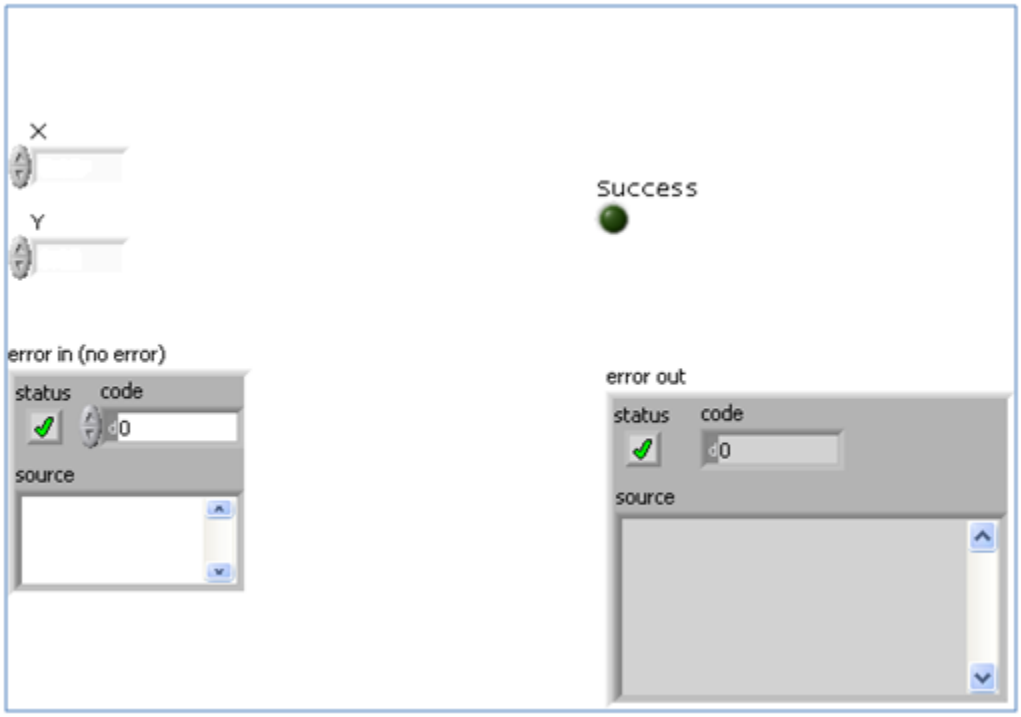

Figure B.24 Front panel of moveXY subvi

Block diagram

The block diagram is divided into two separate pictures.

Part I—In Figure B.25, it first configures and flushes the port. Then, it concatenates X, and Y values into string and sends it to VISA Write to execute the command "MOVE X= Y= Z=". Then, it uses VISA Read to output its process.

Part II—In Figure B.26, it waits for the status of the controller. If the stage is successfully moved to the specified location, the success button turns green on the front panel. If it is not, the error message displays in the error out box on the front panel.

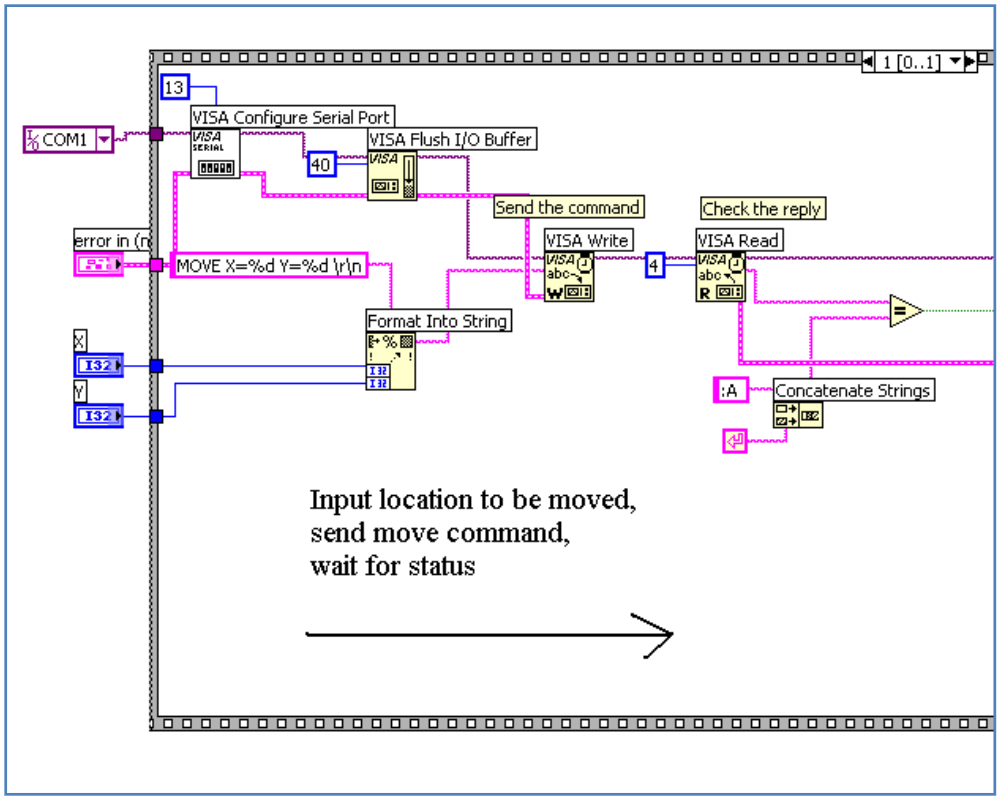

Figure B.25 Block diagram of moveXY subvi, part I

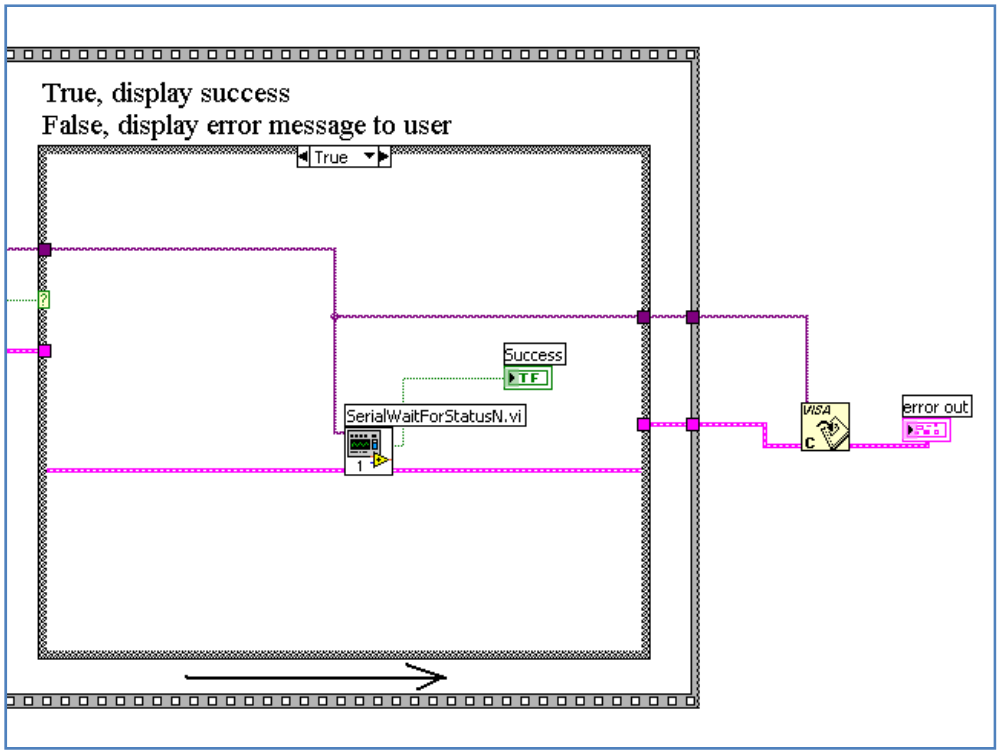

Figure B.26 Block diagram of moveXY subvi, part II

Appendix C
Laser Beam Alignment

A. 1064 nm System

Adjusting the beam outside the microscope. Measure the height between the top of the air table and the center of the microscope port. Adjust the beam steerer, beam expander, and beam reflector in z-direction to match this height along the entire beam path. Turn on the laser. Direct the beam through the beam expander by adjusting the beam steerer, and ensure that the beam is on center both coming in and going out. This is done by placing an IR viewing card at the entrance of the expander to see if the spot is at the center of the entrance. Measure the laser power before the expander and after the expander with a power meter and compare these powers. The power of the input beam should be nearly the same as that of the expanded beam. Then, adjust the beam reflector to reflect beam into the center of the fluorescent port on the microscope. Again, use the IR card to locate the laser spot. The beam path is shown in Figure C.1.

Adjusting the beam inside the microscope. Turn the microscope turret to a position that has no objective. Place the IR card on the stage at the specimen position. Adjust the beam reflector, so the beam is at the center of the turret hole and the laser spot appears circular on the IR card. Measure the laser power at the entrance of the fluorescent port and at the specimen position. These two powers should be nearly the same. Put a culture

dish with a cover slip on the stage. Turn the turret to a position that has the objective. A laser spot should appear in the viewing field of the CCD camera. Now, adjust the z-control to bring the laser spot to its focus near the specimen plane. Put a power meter after the objective, and adjust the beam reflector until the highest laser power (the beam is straight when entering the objective) is recorded. Now, the system is aligned and ready for lifting.

B. 980 nm System

Alignment of the 980 nm system is relatively easy due to its compactness. The collimator and beam expander can fit right behind the microscope, as illustrated in Figure C.2. The diode is remote and connects through the fiber.

Adjusting the beam outside the microscope. Position the collimator and the beam expander in a straight line with the center of the fluorescent port.

Adjusting the beam inside the microscope. The procedure used here is identical to that used with the 1064 nm system except one adjusts the collimator mount instead of the beam reflector to position the beam spot on the specimen plane.

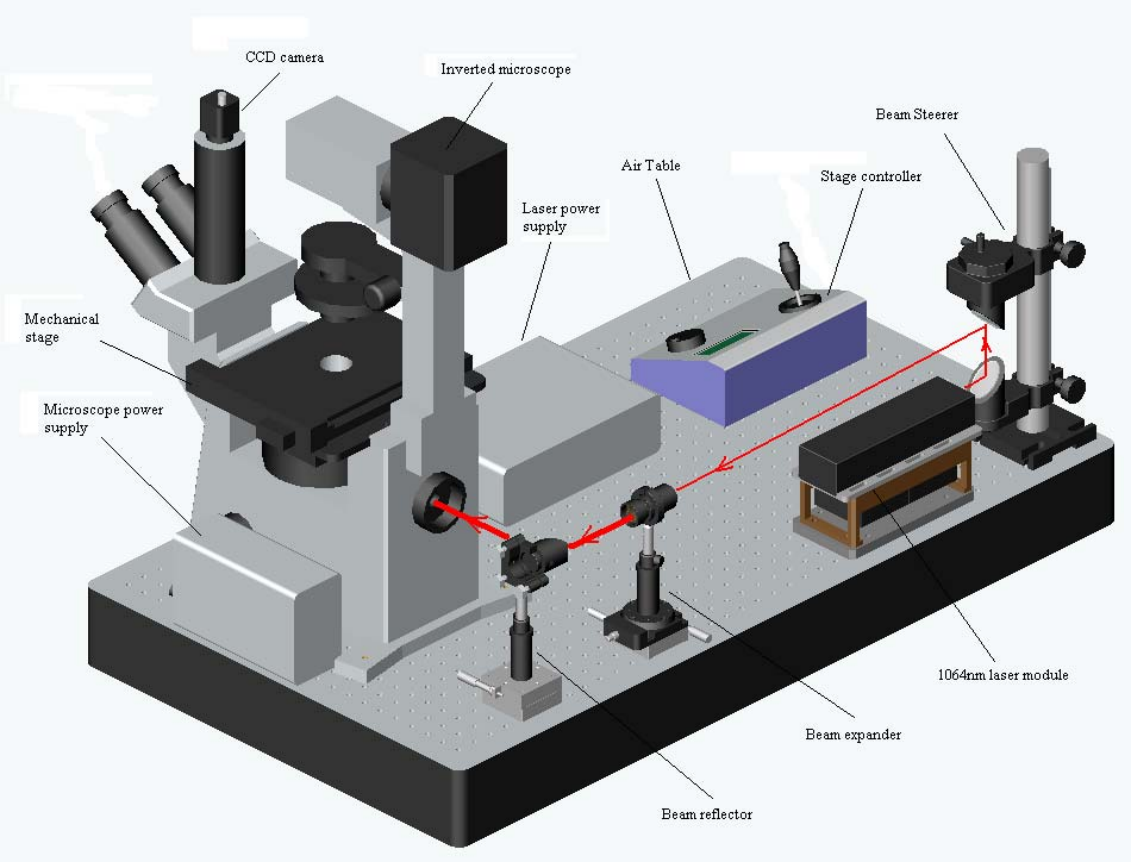

C.1 The beam path for the 1064 nm laser tweezers system

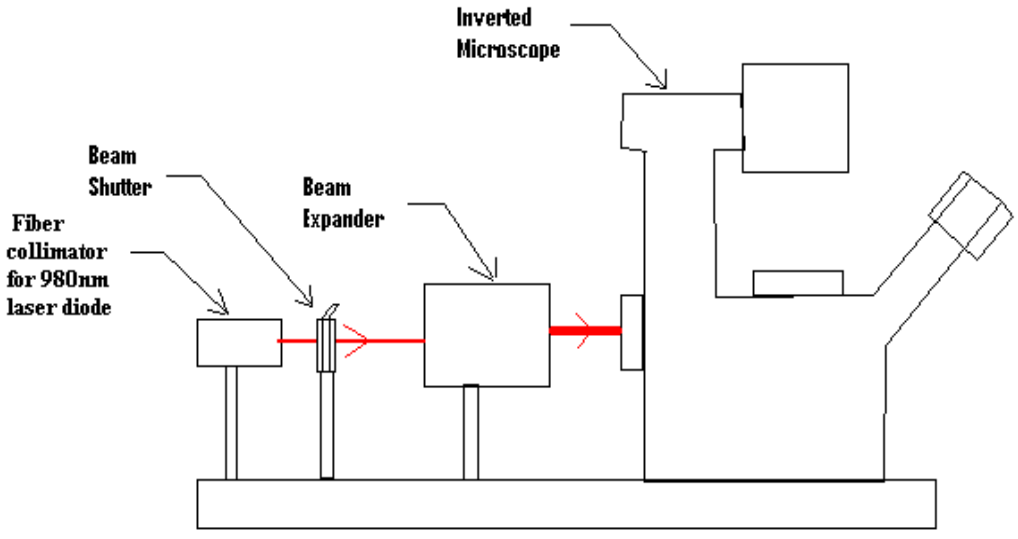

Figure C.2 980 nm beam path, not drawn to scale

Appendix D
Procedures

A. Preparing Cell Culturing Medium

1. Thaw the frozen B27 (Gibco 17504-044), the GlutaMAX (Gibco 35050-079), and the horse serum (HyClone SH.30074.03).
2. Transfer 47 ml of Neurobasal media (Gibco 21103-049) into a 50 ml vial.
3. Add 1 ml of B27, 0.125 ml of GlutaMAX, and 2.5 ml of horse serum.
4. Vortex the vial to mix it.
5. Label the vial, including date and initials.
6. Transfer the vial into a refrigerator for storage up to a month.

B. Preparing PolyHEMA Solution

1. Use a metal spatula to measure 40.0 mg of Poly-HEMA crystals (Sigma P3932) and transfer it to the vial.
2. Transfer 2 ml of 95% EtOH into the vial.
3. Cap the vial and place it on Vari-mix mixer at room temperature and mix it for more than 8 hours.
4. Store tightly closed.

C. Gluing Coverslips to Predrilled Dishes

1. Place a plastic weighing cup on a digital scale and tare it.
2. Add 3 g of Sylgard 184 base and 300 mg of 184 primer to the plastic cup.
3. Mix slowly with a Q-tip stick.
4. Wait for 10 minutes to allow bubbles to degas from the glue.
5. Flip the culture dish over, so the bottom side of the dish is up.
6. Clean the bottom side of the dish with ethanol.
7. Use a metal wire to apply a thin layer of glue on the area around the hole in the dish.
8. Place the coverslip face down and across the clearance hole of the dish.
9. Transfer the dish into 50 ºC oven and allow it to cure for 3 days.

D. Preparing Culture Dishes with PEI and Laminin

1. Place the dishes on a sterile metal tray.
2. Place a piece of tape on the tray and label it with date and initials.
3. Place the tray under a UV light source and take off the top of each dish.
4. Turn on the UV light for 20 minutes.
5. Turn off the UV light and close the top of each dish.
6. Transfer the tray to a laminar flow hood.

7. Deposit about 100 ul of 0.05% PEI into each dish and spread out the PEI drop with a pipette to cover the entire glass surface.
8. Transfer the dishes into a 37 ºC incubator and incubate overnight.
9. Transfer the tray to the laminar flow hood.
10. Place a 1 ml pipette tip on the hose of a vacuum pump and turn on the pump.
11. Siphon the PEI out of the dishes using the 1 ml pipette tip.
12. Add double de-ionized water and swirl the dishes.
13. Siphon the water out of dishes.
14. Repeat steps 12 & 13 for five more times.
15. Take out the top of each dish and allow the dishes to air dry in the laminar flow hood.
16. Transfer 20 ul of laminin (1 mg/ ml, Sigma L2020) and 10 ml of HBSS (Gibco 24020-117) into the test tube.
17. Vortex the test tube.
18. Add 1 ml of laminin solution into each dish.
19. Transfer the tray into the incubator and incubate for overnight.
20. Transfer the tray to the laminar flow hood.
21. Siphon the laminin out of the dishes.
22. Add double de-ionized water, and swirl the dishes.
23. Siphon the water out of the dishes.
24. Repeat steps 22 & 23 two more times.
25. Take out the top of each dish and allow the dishes to air dry in the laminar flow hood.

26. Transfer the tray into the incubator for storage.

E. Preparing Neurochips with PolyHEMA

1. Deposit 40 ul of PolyHEMA on the opposite side from the nuerocages in each dish after the PEI has been applied.
2. Spread the PolyHEMA drop carefully to cover half the surface evenly using a 200 ul pipette tip and make sure that the PolyHEMA does not get into the neurocages.
3. Close the top of each dish and allow the PolyHEMA to evaporate.
4. Repeat all the above steps five more times.
5. Transfer the tray under the UV light and open the top of each dish.
6. Turn on the UV light for 20 minutes.
7. Turn off the UV light and close the top of each dish.
8. Transfer the tray into the incubator for storage.

F. Cell Culturing

1. Vortex the cell suspension.
2. Transfer 60 k of neurons from the cell suspension into an empty 15 ml test tube.
3. Dilute the transferred cell suspension with the culture medium to make 20 k/100 ul for controls.
4. Vortex the tube to mix the solution.
5. Plate 100 ul of neurons onto each of three previously prepared Matek dishes.

6. Spread the drop to cover the entire area of the well.
7. Transfer 60 k of neurons from the cell suspension into another empty 15 ml test tube.
8. Dilute the transferred cell suspension with the culture medium to make 20 k/40 ul for the background neurons of neurochip dishes.
9. Vortex the tube to mix the solution.
10. Place 40 ul of neurons near the cages on the PEI side of each neruochip dish.
11. Transfer the tray into the incubator and incubate for half an hour.
12. Take out the tray and wet the neurocages with 40 ul of culture medium to fill them and allow bubbles to dissipate.
13. Transfer the tray back into incubator and incubate for half an hour.
14. Take out the tray and flood each control dish with 2 ml culture medium.
15. Transfer 20 k of neurons from the cell suspension into an empty 15 ml test tube.
16. Dilute the transferred cell suspension with the culture medium to make 2 k/100 ul for free neurons to load with the tweezers.
17. Vortex the tube to mix the solution.
18. Place the 50 to 60 ul of neurons onto the PolyHEMA side of a neurochip dish.
19. Allow these neurons to settle before moving the dish to the microscope stage for experiments.

G. Loading Neurons with 980 nm Laser Tweezers

1. Turn on the microscope illuminator, the stage controller, the CCD video camera, and the thermal electrical cooler (TEC) controller.
2. Turn the display mode knob on the TEC controller to SET R .
3. Use knob located at the upper right hand corner of the TEC controller to set R to a value of 10 kohms (the thermistor resistance value of 10 kohms is equivalent to an operating temperature of 25 ºC).
4. Press the output button located at the lower right hand corner of the TEC controller to receive temperature status from the laser diode (LD) .
5. Turn the display mode knob to ACTUAL R to see the temperature value.
6. Turn on the LD driver.
7. Turn the knob on the LD driver clockwise to increase the laser power to about 100 mW.
8. Run Ulead Video Studio.
9. Click on “Start Capturing” to capture the video.
10. Click on the video input option and set the video input to composite video, so the image from the microscope can appear on the computer screen.
11. Place a drop of oil on top of the objective.
12. Place the neurochip on the mechanical stage.
13. Raise the objective up slowly until the laser beam is focused to a fine point, and mark the beam position on the computer screen.
14. Shut off the fluorescence port shutter to block off the laser beam.

15. Use the joystick on the stage controller to move the stage until the mark is at the center of neurocage00.
16. Start the LabVIEW program called formula5.vi.
17. Run the Calibration point1 routine in formula5.vi to reset stage.
18. Move the stage until the mark is at the center of neurocage15.
19. Run the Calibration point2 routine in formula5.vi to calculate each cage location.
20. Use the joystick to search for a free neuron on the PolyHEMA side.
21. Open the fluorescent port shutter.
22. Bring the neuron to the laser spot for trapping.
23. Turn the Z-direction knob on the controller counter clockwise to lift the trapped neuron 40 to 50 um above the substrate.
24. Choose a cage and set XY stage speed in formula5.vi.
25. Execute the Run routine in formula5.vi to bring the neuron over the selected cage.
26. Lower the neuron into the bottom of the cage with laser tweezers once the neuron is over the center of the cage by visual observation.
27. Shut off the fluorescent port shutter.
28. Wait for about 30 seconds and allow the neuron to adhere to the PEI surface.
29. Repeat steps 20 through 28 until all cages are loaded with neurons.
30. Wipe off the oil from the bottom of the dish with Kimwipes.
31. Transfer the dish into the incubator.